



## Dissertation

# Adaptive assistance considering human factors for industrial carts

*Study programme:*

*Study branch:*

*Author:*

*Supervisor:*

*Consultant:*

N2612 – Electrical engineering and informatics

2612V045 – Technical cybernetics

**Ing. Dmitry Kochubey**

prof. Ing. Aleš Richter, CSc.

doc. Ing. Petr Tůma, CSc.

Liberec 2023

## Declaration

I hereby certify, I, myself, have written my dissertation as an original and primary work using the literature listed below and consulting it with my thesis supervisor and my thesis counsellor.

I acknowledge that my dissertation is fully governed by Act No. 121/2000 Coll., the Copyright Act, in particular Article 60 – School Work.

I acknowledge that the Technical University of Liberec does not infringe my copyrights by using my dissertation for internal purposes of the Technical University of Liberec.

I am aware of my obligation to inform the Technical University of Liberec on having used or granted license to use the results of my dissertation; in such a case the Technical University of Liberec may require reimbursement of the costs incurred for creating the result up to their actual amount.

At the same time, I honestly declare that the text of the printed version of my dissertation is identical with the text of the electronic version uploaded into the IS STAG.

I acknowledge that the Technical University of Liberec will make my dissertation public in accordance with paragraph 47b of Act No. 111/1998 Coll., on Higher Education Institutions and on Amendment to Other Acts (the Higher Education Act), as amended.

I am aware of the consequences which may under the Higher Education Act result from a breach of this declaration.

10. 12. 2023

Ing. Dmitry Kochubey

# Elektrická pomoc pro průmyslové vozíky

## Abstrakt

Tato výzkumná práce se zaměřuje na probádání fyzikální interakce, která vzniká mezi lidským operátorem a průmyslovým vozíkem s pohonem (IPAC). Cílem výzkumu je zlepšit spolupráci člověka a IPAC tím, že se nalezne správný mechanický design a způsob inteligentní kontroly za účelem dosažení takového stavu, ve kterém vozík umí rozpoznat záměr operátora a je schopen nastavit svoje parametry tak, aby došlo k lepší interakci vozíku s člověkem a bylo zajištěno pohodlí a celkový výkon.

V rámci této disertační práce byl vyvinut prototyp průmyslového vozíku, který byl vybaven sadou senzorů na měření parametrů interakce člověka s vozíkem. Tento vyvinutý průmyslový vozík je schopen rozpoznat záměr člověka na základě sledování parametrů procesu interakce. Na začátku této práce byla provedena analýza současného stavu techniky a byly vybrány nejslibnější kontrolní techniky. Analyzovali jsme součásti průmyslového vozíku a vytvořili jsme kinematický a dynamický popis modelu. Tento vyvinutý vozík má dva stupně volnosti a byly použity regulátory impedance tak, aby ovládaly oba stupně.

Přesto je však tato disertační práce hlavně zaměřena na zpětnou vazbu a pohodlí člověka. Proto byl proveden soubor experimentů s cílem odhadnout účinky parametrů proměnné impedance, co se týče regulátoru translačních a rotačních pohybů. Za účelem vyhodnocení emocionální zpětné vazby lidského operátora byl vyvinut objektivní párový dotazník. Ve výsledku jsme našli vztah mezi nezávislými proměnnými, jako jsou například parametry komfortu obsluhy. Pomocí regresivní analýzy jsme zjistili, že ne všechny parametry regulátoru impedance mají významný vliv na interakci. Také jsme zjistili, že parametry impedance pro pohodlnou interakci se liší u různých operátorů. Zjistili jsme, že existuje významná korelace mezi průměrnou a standardní odchylkou absolutní hodnoty interakční síly a rychlostí vozíku a pohodlím člověka.

Pomocí výsledků regresivní analýzy jsme použili algoritmus zesíleného učení, který mohl přepínat stavy regulátorů impedance podle záměrů operátora. V rámci této diplomové práce je představen proces vývoje vozíku a metodologie výzkumu.

**Klíčová slova:** Inteligentní elektrická vozidla, adaptivní mechatronika pro člověka, rozhraní člověk-vozidlo, řízení s posilovačem, řízení se snímáním síly, hodnocení lidského pohodlí, průmyslový vozík.

## Poděkování

Tento výsledek byl částečně finančně podpořen Ministerstvem školství, mládeže a tělovýchovy ČR a Evropskou unií (Evropské strukturální a investiční fondy - Operační program Výzkum, vývoj a vzdělávání) v rámci projektu „Modulární platforma pro autonomní podvozky specializovaných elektrovozidel pro dopravu nákladu a zařízení, reg. č. CZ.02.1.01/0.0/0.0/16 025/0007293.

# Adaptive assistance considering human factors for industrial carts

## Abstract

The research work is focused on the study of physical interaction between the human-operator and an industrial power-assisted cart (IPAC). The research goal is to improve the cooperation between human and IPAC by finding a proper mechanical design and methods of intelligent control in order to achieve a state in which the cart can recognize operator's intention and adjust its parameters for a better human-cart interaction, comfort and overall performance.

In the scope of the thesis a prototype of an industrial cart was developed and equipped with a set of sensors to measure the human-cart interaction parameters. Developed industrial cart could recognize human intention by observing interaction process parameters. In the beginning of the work the analysis of the state of art was performed and the most promising control techniques were selected. We analyzed the components of the industrial cart and created the kinematic and dynamic description of the model. The developed cart has two degrees of freedom and impedance controllers were implemented to manage both of these degrees.

Nevertheless, The thesis is mainly focused on human feedback and comfort. Therefore, a set of experiments was performed to estimate the effect of variable impedance parameters for the controller of translational and rotational motions. In order to evaluate emotional feedback of the human-operator an objective pair-based questionnaire was developed. As a result, we found a relationship between independent variables such as impedance control parameters and operator's comfort experience. Using regression analysis we found out that not all the parameters of the impedance controller have a significant effect on the interaction. We also learned that the impedance parameters for comfortable interaction are different for different operators. We learned that there is a strong correlation between the mean and the standard deviation of absolute value of interaction force and cart speed and human comfort.

Using the regression analysis results we implemented the reinforcement learning algorithm that could switch states of the impedance controllers according to the operator's intention. The process of cart development and the research methodology is presented in the scope of the thesis.

**Keywords:** Intelligent electric vehicles, human adaptive mecha-  
tronics, human-vehicle interface, power-assist control, force sensing  
control, human comfort evaluation, industrial cart.

## Acknowledgement

The result was partly supported by the Ministry of Education, Youth and Sports of the Czech Republic and the European Union (European Structural and Investment Funds - Operational Programme Research, Development and Education) in the frames of the project “Modular platform for autonomous chassis of specialized electric vehicles for freight and equipment transportation”, Reg. No. CZ.02.1.01/0.0/0.0/16\_025/0007293.

## Acknowledgements

I would like to express my gratitude to everyone who helped me in my studies leading to this dissertation. First and foremost, I offer my sincerest gratitude to my supervisors, prof. Ing. Aleš Richter and doc. Ing. Petr Tůma, CSc. (Department of Mechatronics and Technical Informatics (MTI)), who provided his supervision and valuable guidance through my research experience. I also thank doc. Dr. Mgr. Ing. Jaroslav Hlava (MTI) for his time and consultations in the field of adaptive control algorithms and simulation.

Additionally, I would like to extend my special thanks to doc. RNDr. Jaroslav Mlýnek, CSc., CSc. and Mgr. Václav Bittner for their support and advice related to human-oriented research and mathematical modeling. I appreciate support of Ing. Pavel Jandura, Ph.D. for his support in electrical wiring of the first platform prototype.

I have special acknowledgments to doc. Ing. Michal Petrů, Ph.D., Ing. Voženílek Robert, Ph.D. and Josef Stuchlik for their support in mechanical construction of the platform and data analysis. Further, I highly appreciate the effort of Professor Kouhei Ohnishi (Keio University, Japan), who has shared his extraordinary experience in the field of human-robot interaction and soft robotics.

I am deeply grateful to Dr. Fillia Makedon (Department of Computer Science and Engineering University of Texas at Arlington (UTA)) and her colleagues for the conference experience and cooperation. Moreover, I have greatly progressed in many areas thanks to my internship at Linz Center of Mechatronics (LCM GmbH). Close collaborations and discussions with the smart and cordial group of colleagues helped me to reach the level that would have been impossible to achieve on my own. There are too many to name all of them, but I would like to mention MSc. Kalus Pendl who was always incredibly helpful and supportive.

I would like to thank Phd. David Krcmarick as my office mate he was the first person to bounce my ideas off and to share the joy and sorrows of my research life. Last but not least, I would like to take the opportunity to express my gratitude to the Siemens colleagues in the name of MSc. Johannes Hofmann and Dr. Michael Fielder for their understanding and support. In the end I would like to express my deep gratitude and special thanks to whole my family for their support, patience and love throughout the years.

# Contents

List of Figures . . . . .	10
List of Tables . . . . .	13
List of abbreviations . . . . .	15
<b>1 Introduction</b>	<b>16</b>
<b>2 Problem statement</b>	<b>18</b>
2.1 Topic relevance . . . . .	20
<b>3 State of art</b>	<b>23</b>
3.1 Physical human-robot interaction . . . . .	24
3.2 Aspects of human comfort and expectations . . . . .	25
3.3 Impedance/Admittance control . . . . .	28
3.4 Compliance control . . . . .	29
3.5 Model Reference Adaptive Impedance Control (MRAIC) . . . . .	30
3.6 First order lag controller . . . . .	32
3.7 Alternative control strategies . . . . .	33
List of formulas . . . . .	37
<b>4 Motivation</b>	<b>40</b>
<b>5 Goal and Objectives</b>	<b>41</b>
<b>6 A Brief Summary of the Implemented Methods</b>	<b>43</b>
<b>7 Industrial cart concept evaluation</b>	<b>44</b>
7.1 A rationale for the current industrial cart . . . . .	44
7.2 Constructing the industrial cart . . . . .	45
<b>8 Test platform development</b>	<b>53</b>
8.1 Main requirements . . . . .	53
8.2 Hardware design . . . . .	53
8.3 Arduino ecosystem . . . . .	56
8.4 Software development . . . . .	62
8.5 Cart kinematics . . . . .	62
8.6 Human operator interface . . . . .	65
8.7 Impedance control . . . . .	67



List of formulas . . . . .	69
<b>9 Human operator study</b>	<b>71</b>
9.1 Research workflow development . . . . .	72
9.2 Human Factors, Hazards and Limitations . . . . .	77
9.3 Emotional feedback . . . . .	80
9.4 Physical feedback . . . . .	82
List of formulas . . . . .	85
<b>10 Human-cart interaction</b>	<b>87</b>
10.1 Procedure description . . . . .	87
10.2 Raw data analysis and feature detection . . . . .	88
10.3 Effect of the impedance control . . . . .	90
10.4 Experiment design . . . . .	97
<b>11 Evaluating comfort by means of the regression analysis</b>	<b>103</b>
<b>12 Q-Learning for human-cart interaction</b>	<b>109</b>
12.1 States . . . . .	112
12.2 Actions . . . . .	112
12.3 Rewards . . . . .	113
12.4 High-level control . . . . .	113
<b>13 Conclusion</b>	<b>119</b>
<b>14 Internship</b>	<b>122</b>
<b>15 Publications</b>	<b>124</b>
<b>References</b>	<b>137</b>
<b>A Appendix</b>	<b>138</b>
<b>B Mathematical Modeling of an Industrial Cart</b>	<b>142</b>
B.1 Caster wheel . . . . .	142
B.2 Numerical methods for solving ordinary differential equations (ODEs)	143
B.3 Direct current motor model . . . . .	145
B.4 Powered wheel . . . . .	146
B.5 Wheel suspension . . . . .	147
B.6 Load distribution . . . . .	148
B.7 Friction simulation . . . . .	149
B.8 Kinematics . . . . .	150
B.9 Dynamics . . . . .	151
List of formulas . . . . .	153

## List of Figures

2.1	Accidents at work by specific physical activity and economic activity, EU, 2020, per cent [4]	21
2.2	Non-fatal accidents at work by part of body injured and economic activity, EU, 2020 (per cent of non-fatal accidents for each activity) [4]	22
2.3	Employment by low job satisfaction for 15-74 year-olds, elementary occupations, thousand workers, in 2021, Eurostat (online data code: LFSO_21JSAT03) [4]	22
3.1	PHRI publications in web of science core collection [23]	23
3.2	Mechanical traction system for electrical load cart developed by Silva et al. [43]	26
3.3	Load cell mounting scheme for human force measurement [43]	27
3.4	Human force with 120kg total load over a non-inclined surface [43]	27
3.5	Example of a block diagram of an impedance controller form [36]	29
3.6	Block diagram of the compliant controller based on the applied force by Nagami et al [35]	30
3.7	The structure of the Model Reference Adaptive Impedance Controllers [37]	31
3.8	Block diagram of skill assist system by Terashima et al. [44]	32
3.9	Skill level estimation Terashima et al. [44]	33
8.1	Test platform [54]	54
8.2	Tensiometer location	55
8.3	Drive system overview	55
8.4	Single wheel drive system layout	56
8.5	Arduino Mega Board	59
8.6	Arduino Mini Pro Board	60
8.7	Raspberry Pi Board	60
8.8	Connection Block Diagram	61
8.9	Cart kinematics	63
8.10	Angular speed conversion	64
8.11	Handlebar for PHRI	66
8.12	Impedance controller representation	67
9.1	Process of the dynamic walking [70]	73
9.2	Model of an inverted pendulum with a fixed length [68]	74

9.3	Examples of human walking with different model parameters . . . . .	75
9.4	Myosin and actin filaments in a muscle [71] . . . . .	75
9.5	Maxwell (A) and Voight (B) muscle models . . . . .	76
9.6	Mechanical impedance of the human arm. Structural model [73]. Arm illustration is adopted from [71] . . . . .	77
9.7	A few possible poses of the human operator during manipulation with the cart . . . . .	78
9.8	Rating scale for the emotional feedback of the human . . . . .	81
9.9	No.1 F4 IP68 Waterproof Smartband . . . . .	84
10.1	Moving cargo task . . . . .	88
10.2	Raw data sample from pHRI handlebar . . . . .	89
10.3	Human gait feature . . . . .	90
10.4	Change of interaction force with different settings of the impedance controller [54] . . . . .	91
10.5	Change of interaction force with different settings of the impedance controller [54] $T_{samp} = 60s$ . . . . .	92
10.6	Change of interaction force with different settings of the impedance controller [54] $T_{samp} = 60s$ . . . . .	93
10.7	Change of interaction force with different settings of the impedance controller [54] $T_{samp} = 30s$ . . . . .	94
10.8	Change of interaction force with different settings of the impedance controller [54] $T_{samp} = 30s$ . . . . .	94
10.9	Mean value of absolute interaction force for different settings of impedance controller. Sample 1. $T_{samp} = 60s$ . . . . .	95
10.10	Mean value of absolute interaction force for different settings of impedance controller. Sample 2. $T_{samp} = 60s$ . . . . .	96
10.11	Mean value of absolute interaction force for different settings of impedance controller. Sample 3. $T_{samp} = 60s$ . . . . .	96
10.12	Operator's motion task . . . . .	97
10.13	Trajectory setups . . . . .	98
10.14	Load variation . . . . .	98
10.15	Predefined track. Setup for $m_{load+cart} = 103[kg]$ . . . . .	100
10.16	Linear track . . . . .	100
10.17	Circular track . . . . .	101
10.18	8-like track . . . . .	101
10.19	Free-run track . . . . .	102
12.1	Physical collaboration scenario . . . . .	109
12.2	Decision network representing a finite part of an MDP [14] . . . . .	110
12.3	Reinforcement learning flow diagram [18] . . . . .	111
12.4	Set of states . . . . .	112
12.5	Set of actions . . . . .	113
12.6	Rewards . . . . .	113
12.7	Q-learning process diagram . . . . .	115

12.8	Console output of the learning process . . . . .	117
12.9	Dynamic change of the Q-value during the learning process . . . . .	118
14.1	Linz Center of Mechatronics GmbH . . . . .	122
14.2	Developed indoor positioning system . . . . .	123
A.1	Standard deviation of absolute interaction force for different settings of impedance controller. Sample 1. . . . .	138
A.2	Standard deviation of absolute interaction force for different settings of impedance controller. Sample 2. . . . .	138
A.3	Standard deviation of absolute interaction force for different settings of impedance controller. Sample 3. . . . .	139
A.4	Mean value of absolute cart velocity for different settings of impedance controller. Sample 1. . . . .	139
A.5	Mean value of absolute cart velocity for different settings of impedance controller. Sample 2. . . . .	139
A.6	Mean value of absolute cart velocity for different settings of impedance controller. Sample 3. . . . .	140
A.7	Mean value of absolute cart velocity for different settings of impedance controller. Sample 1. . . . .	140
A.8	Mean value of absolute cart velocity for different settings of impedance controller. Sample 2. . . . .	140
A.9	Mean value of absolute cart velocity for different settings of impedance controller. Sample 3. . . . .	141

## List of Tables

2.1	Key Factors in Pushing/Pulling Tasks [7] . . . . .	19
3.1	Control Algorithms: Pros and Cons . . . . .	36
7.1	Review of available types of the wheels . . . . .	48
7.2	Review of available wheel configurations . . . . .	52
8.1	Cart parameters . . . . .	53
8.2	Motor parameters . . . . .	54
8.3	Tensiometer parameters . . . . .	54
8.4	Drive gearing parameters . . . . .	56
8.5	List of sensors with interfaces . . . . .	58
9.1	Recommended Upper Force Limits for Horizontal Pushing and Pulling [6] . . . . .	80
9.2	Comparison of Likert and Borg Scales . . . . .	83
9.3	Borg scale (rate per exertion) . . . . .	83
10.1	Operators parameters . . . . .	98
10.2	Tested impedance controller settings for translational and rotational motion . . . . .	99
11.1	Regression analysis for comfort of the operator 1 using impedance controller coefficients . . . . .	104
11.2	Regression analysis for operator 1 comfort using mean value and standard deviation of interaction force and cart velocity . . . . .	105
11.3	Regression analysis for operator 1 comfort using biological markers . . . . .	106
11.4	Regression analysis for comfort of all the operators using impedance controller coefficients . . . . .	106
11.5	Regression analysis for comfort of all the operators using mean value and standard deviation of interaction force and cart velocity . . . . .	107
11.6	Regression analysis for comfort of all the operators using biological markers . . . . .	107
12.1	Learn function of the Q-Learning algorithm presented in a pseudo-code	116
B.1	Coefficients of Friction for Material Handling Surfaces . . . . .	150

B.2 Coefficients of Friction for Material Handling Surfaces . . . . . 150

## List of abbreviations

<b>ADC</b>	Analog-Digital Converter
<b>AI</b>	Artificial Intelligence
<b>BLE</b>	Bluetooth Low Energy
<b>CNS</b>	Central Nervous System
<b>CRC</b>	Cyclic Redundancy Check
<b>CSV</b>	Comma-Separated Values
<b>DMA</b>	Direct Memory Access
<b>DOF</b>	Degrees of Freedom
<b>FM</b>	Faculty of Mechatronics Informatics and Interdisciplinary Studies
<b>HW</b>	Hardware
<b>IMU</b>	Inertia Measurement Unit
<b>IPAC</b>	Industrial power assisted cart
<b>MAFs</b>	Maximum acceptable interaction forces
<b>MDP</b>	Markov Decision Process
<b>MEMS</b>	Microelectromechanical systems
<b>MSD</b>	Mass-Spring-Damper
<b>PAV</b>	Power assisted vehicle
<b>PHRI</b>	Physical human – robot interaction
<b>PPG</b>	Photoplethysmography
<b>PWM</b>	Pulse-Width Modulation
<b>RL</b>	Reinforcement Learning
<b>RPE</b>	Rate Per Excretion
<b>SPI</b>	Serial Peripheral Interface
<b>SW</b>	Software
<b>SWI</b>	Size-Weight Illusion
<b>TD</b>	Temporal-Difference
<b>TUL</b>	Technical University of Liberec
<b>UART</b>	Universal Asynchronous Receiver-Transmitter

# 1 Introduction

In the rapidly developing landscape of industrial automation, the synergy between human operators and intelligent machines plays an important role in shaping the future of efficient and safe manufacturing environment [1].

According to a recent survey conducted by Fang et al. [2], a crucial aspect of this development is the physical collaboration between human operators and robots, which can be considered from two perspectives. On one side, human sensorimotor control models provide novel insights into the human response that robots can utilize to enhance human performance. On the other side, robots are becoming instrumental in quantifying the performance of the musculoskeletal system. Consequently, the combined use of human modeling and robotic methods in physical human-robot interaction (PHRI) [3] can lead to both improved understanding of human capabilities and functional assistance.

Within the context of this thesis, we consolidate and integrate the knowledge of physics, control theory, reinforcement learning and emotional side of human being, such as comfort, to improve process of physical interaction. Dissertation contributes to the topic of PHRI on various levels from information collection and statistical analysis to software development and hardware implementation.

The thesis consists of thirteen chapters. Chapter 1 provides the summary of the topics involved in the dissertation and explains how to navigate through the thesis's content. Chapter 2 contains problem definition, where risk factors in material handling process and their root causes were identified by evaluation of high-quality statistics and data provided by Eurostat [4], ergonomic manuals [5], [6], [7], risk assessment reports [8], [9] and epidemiological studies [10], [11].

Chapter 3 includes a critical review of existing control algorithms, considering classical techniques such as impedance and admittance control [12], [13], alongside contemporary machine learning-based methodologies [14] and model predictive control [15], suitable for power-assisted vehicles (PAV).

Chapter 4 derives motivation for conducted research, followed by chapter 5 that sets the goal and objectives of the project. In order to reach the research goal and fulfill the objectives, the description of used theoretical, mathematical and empirical research methods [16], [17] was combined in chapter 6. The concept of an industrial cart was evaluated in chapter 7.

Chapter 8 reviews the process of the test platform development including the main requirement hardware (HW) design, software (SW) implementation, the description of cart kinematics and dynamics. Appendix B contributes to the mathematical description of industrial carts, by providing the reader with step-by-step



explanation of the PAV model. Chapter 9 presents the workflow of the human-operator study starting with the description of the human motion and following description of applied methods to evaluate the operator's feedback.

Chapter 10 describes the process of human - industrial cart interaction. It includes the analysis of raw data and experiment design. In the chapter 11, the regression analysis of the experiment results is performed in order to reveal dependencies between measured physical values from industrial cart and emotional feedback from the operator.

Chapter 12 reinforcement learning [18] demonstrates the implemented algorithm that uses a rating system based on actions, states and rewards. Based on the rewards which are obtained for the actions by the learning system, the novel algorithm is able to change the system's state and adjust impedance controllers according to the intentions of the operator. Most chapters are concluded by a list of variables used in this particular chapter.

The thesis is concluded by the collection of outcomes and technical solutions, highlights of the thesis, as well as suggestions for possible future research opportunities and the area of human-industrial cart interaction.

## 2 Problem statement

“If you define the problem correctly, you almost have the solution.”

---

Steve Jobs

In this chapter the statement of the problem is formulated to be resolved in the later workflow of the thesis. Firstly, it is necessary to define the key components of the human-robot interaction process. Secondly, the main factors in pushing/pulling tasks are described and classified. It goes on to overview the latest statistics coming from Eurostat to uncover the roots of the human-cart interaction problem. The following pages summarise the information about the factors that could affect the interaction process and lead to injuries or hazards. Some of the main potential injuries and hazards are joined up in a system.

Human-robot interaction is a complex process that, in our view, should be addressed from the perspective of multiple disciplines, such as physiology, ergonomics, robotics and machine learning. In the framework of the current thesis, the main components are defined and referred to as follows: *Human-Robot Interaction (HRI)* includes both physical aspects of helping a human being with some tasks, and socio-emotional aspects, including but not limited to communication, social interaction, robot acceptance. *Haptic interaction* is based on studying the tactile interaction between a human and a robot. It can be viewed from two perspectives of a human and a robot, addressing the physical interaction feelings of the human, and the algorithms how a robot can define, classify, organise and apply the information about the surrounding environment. *Power-assisted system (support system)* is a system that allows to perform physical tasks. Examples of such systems include exoskeletons, manual vehicles (carts equipped with an electrical drive). *Material handling tasks* refer to logistical objectives of obtaining, moving, transporting, and handling materials and goods to ensure the consistent operation of supply chains within a factory or a warehouse. The definition of a *mobile robot* is generally broader than the one of a mobile platform, but for the sake of simplicity, in the framework of this thesis these two concepts will be used interchangeably. *Collaborative robotic environment* is the type of environment that allows robots and humans operate efficiently and with minimal failures. *Human operator* is an individual who manipulates a mobile platform and performs material handling tasks. *Mobile platform* is in this case a mobile robot which can move in Cartesian space equipped with sensors and actuators,

it can help an operator to perform material handling tasks. *Human-cart interaction* describes the relationship between an operator and a powered industrial cart. *Industrial cart* is a special type of a cart used at factories and warehouses which can carry large volumes of freight. *Manual pulling/pushing tasks* involve applying force by an operator to push the cart forward, backward, or to perform rotational movement. *Overexertion* is a phenomenon of applying more force than needed to perform a certain task. It may occur due to a fault in estimating the weight of a load.

Industrial cart manipulation is a physical activity of a human operator that involves exertion of considerable force in order to overcome the forces that resist motion and reach target position. When operators carry a loaded or empty industrial cart, they generate the force and transmit it to the cart through contact points. A few researchers [7] identified a number of key factors that have a considerable effect on the human – cart interaction process during manual pushing and pulling tasks. These key factors are organized into the table 2.1.

<b>Category</b>	<b>Factors</b>
<b>Human Factors</b>	Height Weight Size-weight Illusion (SWI) Age Gender Strength Posture Physiological Capacity
<b>Task Factors</b>	Distance Moved Movement Initiation Force Requirements Sustained Motion Force Requirements Direction and Nature of Movement Duration of Pushing/Pulling Task
<b>Cart/Equipment Factors</b>	Handhold Height Handhold Orientation Handhold Type Caster/Wheel Design Specifications Stability Size Weight
<b>Floor/Ground Factors</b>	Surface Characteristics (smooth, rough, inclined) Contaminants

Table 2.1: Key Factors in Pushing/Pulling Tasks [7]

However, there are certain material handling tasks performed with little assistance from PAVs, or without any assistance at all, which means that human operators tend to perform algorithms which might harm their physical health and

well-being. If such algorithms are continuously carried out, it can result in worsening physical conditions of human operators employed in various industrial fields. Several studies have reported a relationship between pushing/pulling and shoulder pain, such as increased shoulder pain from pushing/pulling wheeled equipment [9]; pushing/pulling heavy weights [19] and pushing against a high handle [20].

A review on pushing and pulling forces was carried out by Garg et al. [8], who provided definition and recommendations on maximum acceptable pushing and pulling forces applied by operators. Cross-sectional epidemiological studies often show that the cart manipulation activities are associated with the shoulder pain, low-back pain, and musculoskeletal disorders [21] and [10]. Pushing and pulling of carts and objects exposes workers to two types of hazards: stresses to the musculoskeletal system from applied hand force, and accidents due to slipping or tripping [11].

Pushing, pulling, and maneuvering industrial carts involves some common hazards, such as overexertion. According to Eurostat data (2020), the most common injuries that result from cart operations are:

- fingers and hands being caught in, on, or between the cart and other object
- toes, feet and lower legs being bumped into or crushed by the cart
- slips, trips, and falls, and strain injuries predominantly for the lower back, shoulder, and arm muscles and joints.

These problems might be resolved with the help of adequate power-assisted vehicles used to help operators perform material handling tasks.

## 2.1 Topic relevance

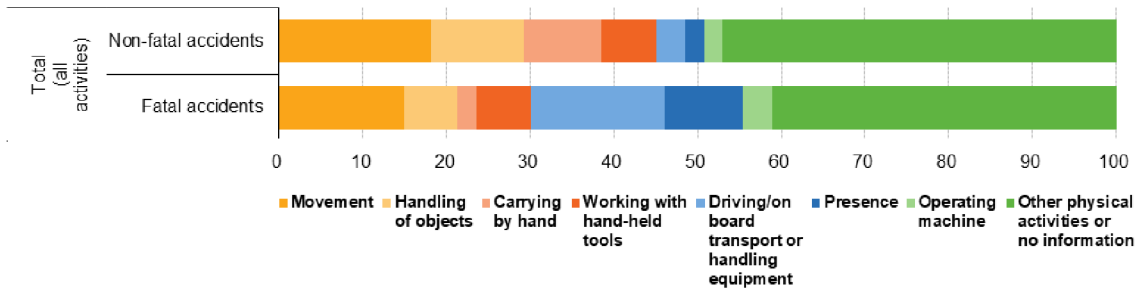
Manual cargo transportation tasks, many of which require pushing, pulling and rotating are common in almost all industrial and warehouse environments. Nearly half of all manual materials handling consists of pushing and pulling activities [22]. The current research thesis focuses specifically on carrying activities while using industrial power assisted carts. These tasks often expose workers to musculoskeletal stresses as well as other related injuries, slipping and tripping hazards.

Material handling exposes the worker to known risk factors for low-back disorder, such as lifting, bending, twisting, pulling, pushing and maintenance of static postures.

If we take a look at the fatal and non-fatal accidents statistics in Europe in 2020 according to the Eurostat data shown in the figure 2.1, it becomes clear what activities are the most dangerous. A share of 11.1% of all non-fatal accidents at work is strongly connected to the activity "handling of objects", and 9.1% of accidents happened when the workers were in process of carrying something by hand.

People who work in construction, transportation and manufacturing suffer from many injuries. Nearly 40% of all non fatal injuries come from these three fields. Nearly 54% all deaths during working hours also happen in construction, transportation and

**Accidents at work by specific physical activity and economic activity, EU, 2020**  
(%)



Note: all accidents for Belgium, Czechia, Denmark, Germany, Ireland, Greece, Cyprus, Malta and Sweden are included in the heading for no information.

Source: Eurostat (online data code: hsw\_ph3\_04)



Figure 2.1: Accidents at work by specific physical activity and economic activity, EU, 2020, per cent [4]

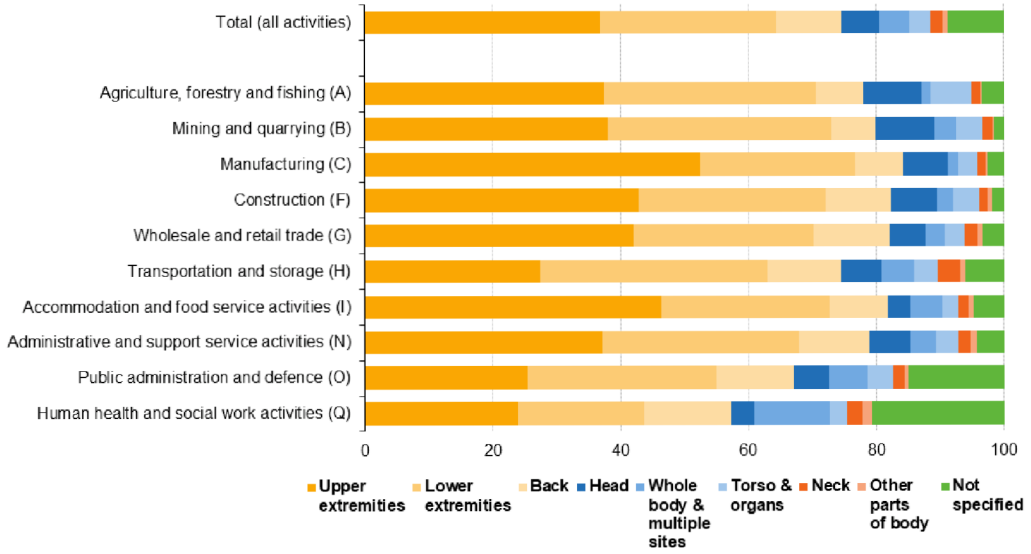
manufacturing. Risk factors related to transportation and manual handling tasks are placed second in the graph 2.2 of accidents at work by the injured body part for the individual economic activities. In 2020, non-fatal accidents at work that resulted in injuries of the upper extremities were particularly common in the EU within manufacturing (52.5%). For injuries of the lower extremities, there were few variations by activity, with the highest shares of injuries occurring in transportation and storage (35.7%), and mining and quarrying (34.9%).

By analysing the job satisfaction level it was illustrated in figure 2.3 that people in the countries that may have more production and therefore, have more elementary occupation positions tend to be less satisfied with their jobs and lives.

However, the existing statistics do not reflect the importance of maneuvering with industrial carts as potential risk factors causing injury at work in the full scope, because the injuries may often fall into different categories making them difficult to analyze. To conclude, human operators often do not obtain enough support from a cart and may suffer from a number of injuries at their working place. The imperfections of human-cart interactions may often put human operators at risk of compromising their physical health and overall well-being, thus leading to fatigue of their fellow colleagues. This results in a vicious circle of fatal and non-fatal accidents which occur in material handling in various industries.

**Non-fatal accidents at work by part of body injured and economic activity, EU, 2020**

(% of non-fatal accidents for each activity)



Note: non-fatal accidents reported in the framework of ESAW are accidents that imply at least four full calendar days of absence from work (serious accidents).  
 Source: Eurostat (online data code: hsw\_n2\_06)



Figure 2.2: Non-fatal accidents at work by part of body injured and economic activity, EU, 2020 (per cent of non-fatal accidents for each activity) [4]

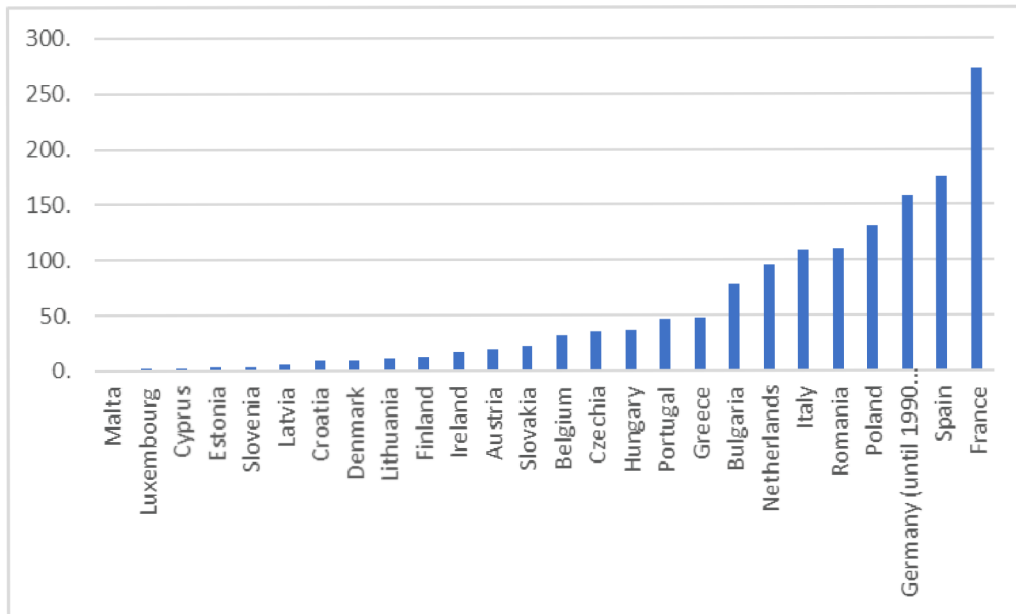


Figure 2.3: Employment by low job satisfaction for 15-74 year-olds, elementary occupations, thousand workers, in 2021, Eurostat (online data code: LFSO\_21JSAT03) [4]

### 3 State of art

“A state-of-the-art calculation requires 100 hours of CPU time on the state-of-the-art computer, independent of the decade.”

---

Edward Teller

The objective of this chapter is to review the existing information on human – mobile robot physical interaction including hazards, problems and existing solutions in the area of physics, automation control theory, machine learning and psychology, namely, emotional feedback. This chapter is aimed to demonstrate the existing theories and approaches in the field of power-assisted vehicles. This topic is quite relevant nowadays, as over the last few decades there have been a large number of studies related to the physical human-robot interaction (between a man and a machine), see Figure 3.1.

When analyzing the state of the art in the field of human – robot physical interaction, it is necessary to consider the problem from two perspectives, such as the point of physical interaction between the human operator and the industrial cart, and methods of emotional feedback evaluation during their interaction with the cart. This chapter describes the most promising power assisted techniques developed by previous researchers, as well as the works related to the evaluation of operator’s characteristics.

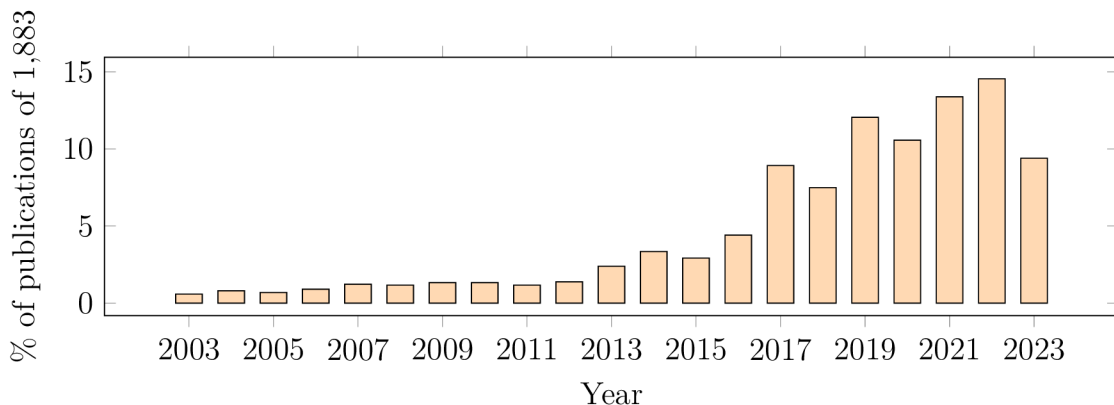


Figure 3.1: PHRI publications in web of science core collection [23]

### 3.1 Physical human-robot interaction

In order to enable humans and robots to work together in close proximity, a learning framework was developed by Dinh et al. (2019) [24] that incorporates real-time obstacle avoidance. As a result, both legibility and safety issues are addressed within this framework. This implies that the task generalization strategy helps the robot adapt to new tasks more quickly, which cuts down on training time. The method was tested using both a real robot and an articulated KUKA IIWA robot in virtual reality (VR) and human operators. According to Wang et al. (2019) [25], utilizing robots' ability to learn by demonstrating examples increased the quality of collaboration between humans and robots. In this paper, techniques on human teaching and robot learning have been examined together with the relevant applications. The researchers created two comparison charts of human teaching approaches and robot learning approaches, from which kinaesthetic-based teaching was applied in the current research. A method for postural optimization that considers task limits and acceptability while reducing the risk of MSDs was introduced in Busch et al. (2017) [5] who evaluated the operators' posture during the interaction process with 39 participants with the help of a motion tracking technology. A comprehensive study by Muller et al. (2018) [26] investigated differences between variable impedance controller and admittance controller finding that the participants improved their problem-solving time using the variable impedance controller. Another study (Kang et al., 2019) [27] confirmed that variable admittance control improves run time, accuracy, and operators' comfort.

However, the success of HRI in material handling tasks depends on a number of factors, including the design of the robot and its user interface, the layout and organization of the work environment, and the level of training and support provided to human workers. Studies have also shown that the effectiveness of HRI in material handling tasks is influenced by the level of collaboration and communication between humans and robots, as well as the level of trust that humans have in the robot's abilities. Namely, Capdepuy et al. (2015) [28] demonstrated that inversed kinematics approach (IK) improves interaction comfort. The results obtained by Herrera et al. (2016) [29] suggest that the system can overcome many common disturbance situations and adapt its behavior to different disturbance events over time using fuzzy logic methods. HRI has the potential to improve the efficiency and productivity of material handling tasks, while also reducing the risk of injury and fatigue for human workers. However, it is important to carefully consider the design and implementation of HRI systems in order to ensure that they are safe, reliable, and effective. A journal of HRI (vol.4) published in 2015 precisely focused on the ways in which haptic interaction can be used to enable cooperation and communication between humans and robots, considering both the human perspective and the engineering challenges involved. The introduction made by its editors MacLean and Frisoli [30] stated that the development of robots that could potentially share physical space and work cooperatively with humans will require the use of haptic technology to facilitate communication and interaction during physical contact.

The article published in 2019 by Oltean [31] describes a mobile robot platform



that has a fixed four-wheel chassis and is equipped with an electronic system based on Raspberry Pi and Arduino Uno interfaces. The platform is designed to be low-cost, reliable, and flexible, making it suitable for use in teaching and research. Potential applications for this platform include serving as an autonomous guide robot for indoor environments, assisting patients in a medical setting, military use, organizing and transporting materials in warehouses, and transporting waste, laundry, food, pharmaceuticals, or mail.

A great deal of research has been done on physiological and psychophysical aspects of materials handling. Ciriello and Snook [32],[33] have published a large data base for designing lifting, lowering, pushing, pulling and carrying tasks. Ciriello's [34] study the maximum comfortable forces for pushing and pulling a cart. In addition, there have been many contributions to the human-robot physical interaction area related to impedance and compliance control [35], [12], force/motion impedance control [36], model reference adaptive impedance control [37]. In parallel, adaptive control of robotic manipulators has advanced considerably in recent decades to reduce dependency on a precise knowledge of the dynamics of the robot and the environment. It resulted in the increased interest in adaptive impedance control [38], [39].

These studies focused on design factors of carriers and their effects through kinematic and biomechanical models. Despite researchers' effort on the carrier design improvement in terms of human factors, there are still various injuries because users' preferences and reactions were not considered in the studies.

This dissertation proposes a systematic approach in development of a unified, flexible and inexpensive device developed for comfortable human-robot interaction that responds to the human operator expectations. The use of hand carts to transport loads instead of carrying them saves workers a lot of effort. It decreases the risk of overexertion injuries at work that include manual materials handling.

## 3.2 Aspects of human comfort and expectations

Within the topic of measuring comfort in human-robot interaction (HRI), user comfort in material handling tasks can be measured through a variety of methods, including self-report surveys, physiological measures (such as heart rate and sweat gland activity), and behavioral observations. These techniques are described in the following paragraphs to reveal the research gap.

Self-report surveys are a common method to assess user comfort, as they allow individuals to describe their experiences and perceptions directly. Surveys can include questions about the overall comfort level with the task, the perceived level of physical strain, and the ease of the robot's use. Physiological measures can provide objective data on the body's response to the task and can be used to indicate levels of stress or discomfort. For example, an increase in heart rate or sweat gland activity may indicate that the user is experiencing discomfort or strain during the task. In the study by Widdowson et al. (2017) [40] a multi-method approach incorporating behavioural measurements, self-report questionnaires, and physiological data to

detect human arousal in a variety of predefined real-time scenarios and settings was applied.

Behavioral observations involve observing and recording the actions and behaviors of the user during the task. This can include measures such as the speed and smoothness of movements, the frequency of breaks or pauses, and the overall performance on the task. In the article published in 2021 by Liu et al. [41], a human-robot handover system was proposed based on human behaviour patterns. The results showed that the model can predict an object's transmission points that conform to human handling habits. It can potentially provide a more natural and smoother transmission experience with human operators.

The choice of method to measure user comfort depends on the specific goals of the study and the resources available. It is important to use a combination of methods to obtain a comprehensive understanding of user comfort in material handling tasks. For this reason in the framework of this research, operator's comfort estimation methods are described in Chapter 9.

To our knowledge, the aspects of human comfort and expectations during human – industrial cart interaction appear to be understudied. There are no studies related to the human comfort estimation during goods transportation process with help of industrial power-assisted cart (IPAC). However, Silva et al. present a cart built to move 500 kg net loads with friendly human perception [42]. The complete system is shown in the figure 3.2.



Figure 3.2: Mechanical traction system for electrical load cart developed by Silva et al. [43]

In their study, the mechanical structure and power elements were designed to aid in translational displacements of 500kg net load. The human command were measured by a 1300N side effort compensated load cell. The control system developed by Silva et al. is based on emulated mechanical impedance that generates the speed setpoint.

In order to evaluate the force controller performance, the authors compared the human force necessary to move the vehicle when the human aid system was enabled or disabled. As shown in figure 3.4, the average human force necessary to move the cart without help from the cooperative system is about 3.5 times greater than that

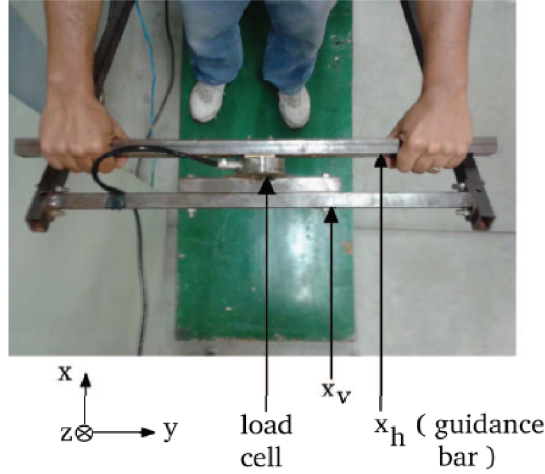


Figure 3.3: Load cell mounting scheme for human force measurement [43]

observed when the system is enabled. In order to summarise the algorithms that could be used to create a cooperative system, we will briefly describe the capabilities of each control algorithm to rationalise the choice of impedance control.

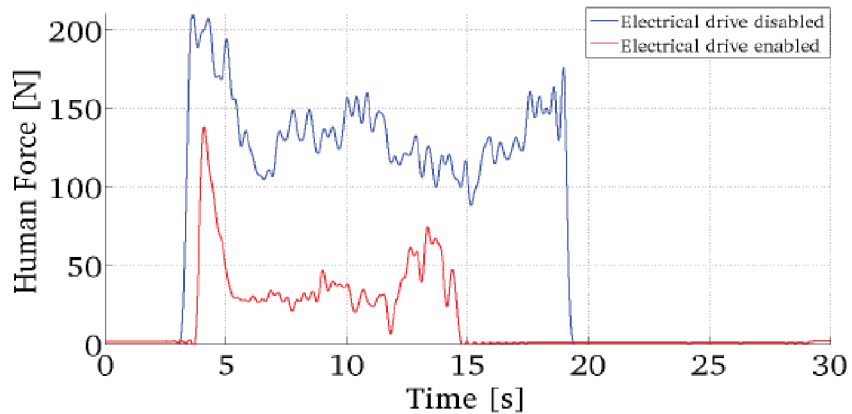


Figure 3.4: Human force with 120kg total load over a non-inclined surface [43]

Impedance control focuses on controlling the stiffness and damping properties of a system. In the context of a powered cart, this would mean controlling how the cart responds to external forces. Admittance control is essentially the inverse of impedance control, emphasizing the relationship between the cart's motion and the applied force. Both the impedance and the admittance control can be effective for applications where the cart needs to interact with its environment in a compliant manner, adapting to varying conditions. This appears to be suitable in our case when the cart needs to navigate through environments with uncertainties and obstacles.

Compliance control approach aims to make the system compliant or flexible, allowing it to absorb external disturbances without significant disruption. It might be

beneficial when the cart needs to handle dynamic and unpredictable environments, providing a level of flexibility to navigate through obstacles without causing damage.

Model Reference Adaptive Impedance Control (MRAIC) combines the adaptability of model reference control with the impedance control strategy. It adjusts the impedance parameters based on the difference between the actual and desired system behavior. This type of control is suitable for systems with varying dynamics or environments. It can be effective in industrial applications where the cart may encounter different loads or operating conditions.

First Order Lag controller introduces a time delay in the system's response to changes, providing a simple form of dynamic behavior. Such controllers are often used in systems where a gradual response to changes is acceptable. However, for applications like powered carts that require more sophisticated and adaptable control, other methods like impedance control or compliance control may be more suitable.

The most suitable control algorithm for an industrial powered cart depends on the specific requirements of the application. If the cart needs to navigate through dynamic and uncertain environments, impedance control, compliance control, or MRAIC may be more appropriate due to their adaptability. On the other hand, if a simpler response is acceptable, a first-order lag controller could be considered. The choice ultimately depends on factors such as the desired level of adaptability, precision, and response time in the given industrial context. In the case of the current research, we opted for the impedance control as we work with uncertain environment, which in this case, depends on the behaviour of the human operator.

### 3.3 Impedance/Admittance control

Theoretical concept of Impedance control was introduced in 1985 by Professor Neville Hogan from Massachusetts Institute of Technology (MIT) [12]. The objective of impedance control is not to directly control position or force, but the relationship between them. This allows to reduce or increase apparent stiffness, damping, or mass depending on the task. The overall purpose of the impedance control creation was to develop an approach to control a manipulated object that would be suitable for a broad range of applications. General impedance control scheme is shown in the figure 3.5.

Manipulation with the object of interest requires a physical interaction. In order to fulfill the task requirements, the user chooses a desired impedance that could be expressed by the following general equation 3.1:

$$M_d(\ddot{x} - \ddot{x}_d) + B_d(\dot{x} - \dot{x}_d) + K_d(x - x_d) = f_e \quad (3.1)$$

Where  $M_d$ ,  $B_d$  and  $D_d$  are positive constants that represent the desired inertia, damping and stiffness, respectively. From the equation 3.1 we could find the acceleration reference described by 3.2:

$$\ddot{x}_r = \ddot{x}_d + M_d^{-1}[-f_e + B_d(\dot{x} - \dot{x}_d) + K_d(x - x_d)] \quad (3.2)$$

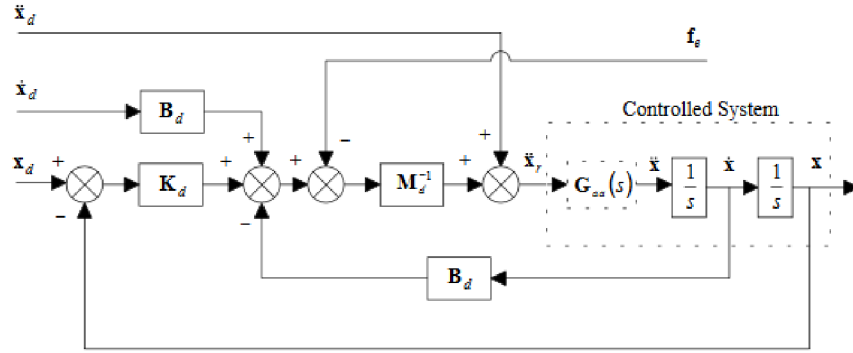


Figure 3.5: Example of a block diagram of an impedance controller form [36]

For admittance control, the control force is a position-controller designed to track the trajectory  $x = x_d$ . Trajectory tracking is implemented using a PD controller with positive gains  $K_p$  and  $K_d$ :

$$f_r = K_p(x_d - x) + K_d\dot{x} \quad (3.3)$$

The simplified impedance controller could be written in the following form:

$$M_d(\ddot{x} - \ddot{x}_d) + B_d(\dot{x} - \dot{x}_d) = f_e \quad (3.4)$$

It was proved by previous researchers [39] that the spring component of the impedance controller does not have a significant impact on the process of interaction.

The impedance controller is a virtual dynamic system. Along with the compliance controller it allows to set any desired system dynamics. By changing the settings of the virtual mass (Mass), a virtual damper (Damp) and virtual spring component we can obtain the desired system response to the control impact. In our work we will use two controllers. One controller will be used for translation motion in support of pushing and pulling tasks. The second controller will be used for rotational motion in order to support the human operator in the task of rotation.

### 3.4 Compliance control

The example of power – assisted control based on compliance controller was proposed by Nagami et al [35]. The author expresses his opinion regarding the conditions that should be taken into account by the operator when moving loads. The main idea of his work is the implementation of the operator’s desired movement without the influence of external disturbances.

Compliance controller makes it possible to perform the assist motion for the cart operator smoothly and improve the stability of the cart motion. The compliant controller with variable gain is shown in figure 3.6.

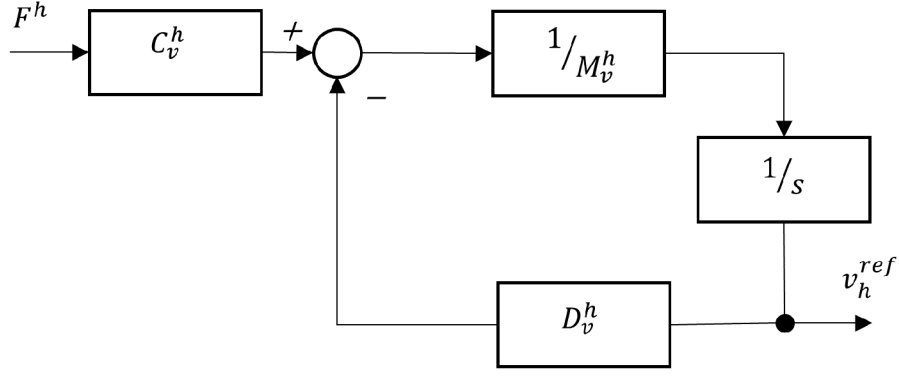


Figure 3.6: Block diagram of the compliant controller based on the applied force by Nagami et al [35]

The variable compliant gain, and is adjusted so that the cart operator can move the platform smoothly independently of the loaded object. The variable compliant gain formula is expressed by the equation 3.5:

$$C_v^h = \tan(a_v^h F^h) \quad (3.5)$$

where  $F^h$  - human force,  $a_v^h$  - adjustable coefficient.

Compliance controller speed reference is listed in 3.6:

$$\dot{v}_h^{ref} = \frac{1}{M_v^h} (C_v^h F^h - D_v^h v^h) \quad (3.6)$$

The parameters of the compliance controller are chosen empirically, which does not allow to apply the developed solution for mobile carts with modified parameters without prior resetting.

### 3.5 Model Reference Adaptive Impedance Control (MRAIC)

Model Reference Adaptive Impedance Control (MRAIC) allows not only to track the response of the reference model but also to make the dynamics of the closed-loop system similar to the reference impedance model.

The desired reference impedance model for the robot end-effector in Cartesian coordinates is generally defined by the equation 3.7. The reference model has two poles in each Cartesian coordinate direction as:

$$r_1 = -\lambda_1 + i\lambda_3 \quad (3.7)$$

$$r_2 = -\lambda_2 + i\lambda_3 \quad (3.8)$$

where for the reference model stability, constants  $\lambda_1$  and  $\lambda_2$  should be positive.

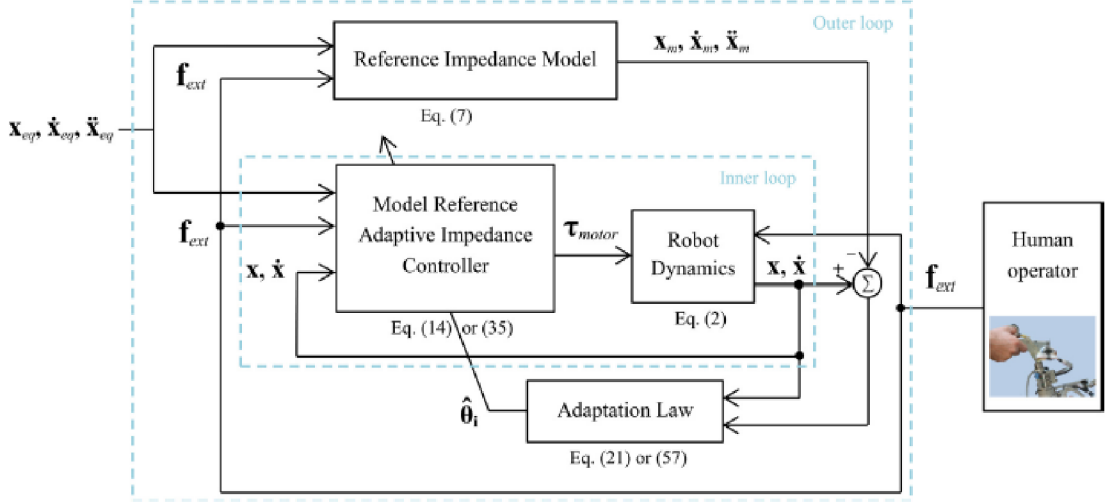


Figure 3.7: The structure of the Model Reference Adaptive Impedance Controllers [37]

The model reference adaptive impedance controller for motor torque could be written in the following form:

$$\tau_{motor} = \hat{M}_q v_1 + \hat{C}_q v_2 + \hat{G}_q + \hat{F}_q - J^T f_{ext} \quad (3.9)$$

where  $v_1$  and  $v_2$  are known vectors that do not contain any estimated parameters of the robot's dynamics.

$$v_1 = J^{-1} \left( \ddot{x}_{eq} - \frac{c}{m}(\dot{x} - \dot{x}_{eq}) - \frac{k}{m}(\dot{x} - \dot{x}_{eq}) + \frac{1}{m}f_{ext} + \lambda_3^2 \tilde{x} - \dot{J}J^{-1}\dot{x}_r \right) \quad (3.10)$$

$$v_2 = J^{-1}\dot{x}_r \quad (3.11)$$

Linearly parameterized equation in joint space has the following formula:

$$\tau_{motor} = Y_1 \hat{\theta}_1 - J^T f_{ext} \quad (3.12)$$

where  $\hat{\theta}_1$  - estimation of actual parameters vector,  $Y_1$  - regressors matrix in joint space.

$$Y_1 \hat{\theta}_1 = M_q v_1 + C_q v_2 + G_q + F_q \quad (3.13)$$

The adaptation law is expressed by the equation 3.14:

$$\dot{\hat{\theta}}_1 = -\Gamma Y_1^T J^{-1} s_1 \quad (3.14)$$

where  $\Gamma$  is symmetric positive definite matrix.  $s_1$  is error dynamics.

$$s_1 = \dot{x} - \dot{x}_{eq} \quad (3.15)$$

where  $\dot{x}_{eq}$  is the reference velocity.

$$\dot{x}_r = x_m - \lambda_1 \tilde{x} \quad (3.16)$$

$\tilde{x}$  is the reference model position error. This method gives very promising results. However, it requires reference impedance model that is not available in our case due to the human factor.

### 3.6 First order lag controller

Power-assisted control based on the first order lag controller and fuzzy logic was introduced in the work of authors led by Terashima [44]. They introduced the methodology which allowed to estimate the operators' skill level and adjusted the controllers' parameters accordingly to influence the cart dynamics. Block diagram of skill assist system is shown in the figure 3.8.

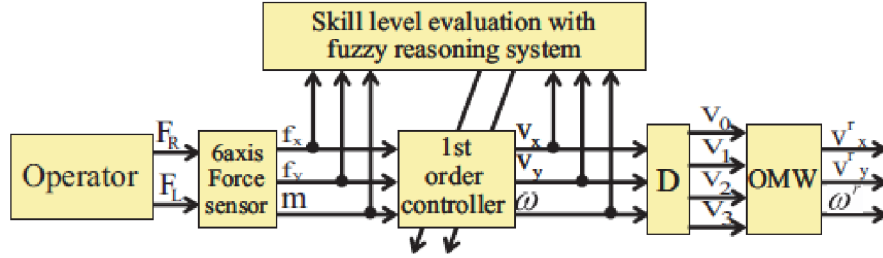


Figure 3.8: Block diagram of skill assist system by Terashima et al. [44]

In this work the author demonstrates his own developed methods to assess the level of operator's competence and configuration of a power – assisted controller using fuzzy logic. It is demonstrated in the figure 3.9.

The author mentions that the developed system has a difficulty with adding support in rotational motion. Operator feels uncomfortable during the manipulation and fluctuations in the support system when vibration is caused by the operator force. For this reason, this paper considers the support for the backward and forward movement. First-order lag controller is used in order to convert the force applied by the operator's into the motor speed setpoint. The controller formula is provided in 3.17.

$$\begin{bmatrix} v_x \\ v_y \\ w \end{bmatrix} = \begin{bmatrix} \frac{k_{vx}}{T_{vx}s+1} & 0 & 0 \\ 0 & \frac{k_{vy}}{T_{vy}s+1} & 0 \\ 0 & 0 & \frac{k_{vz}}{T_{vz}s+1} \end{bmatrix} \begin{bmatrix} f_x \\ f_y \\ m \end{bmatrix} \quad (3.17)$$

Performance index evaluating operator's skill degree:

$$\sigma_{vx} = \sqrt{\frac{1}{n} \sum_{i=1}^n (v_{xi} - \bar{v}_x)^2} \quad (3.18)$$



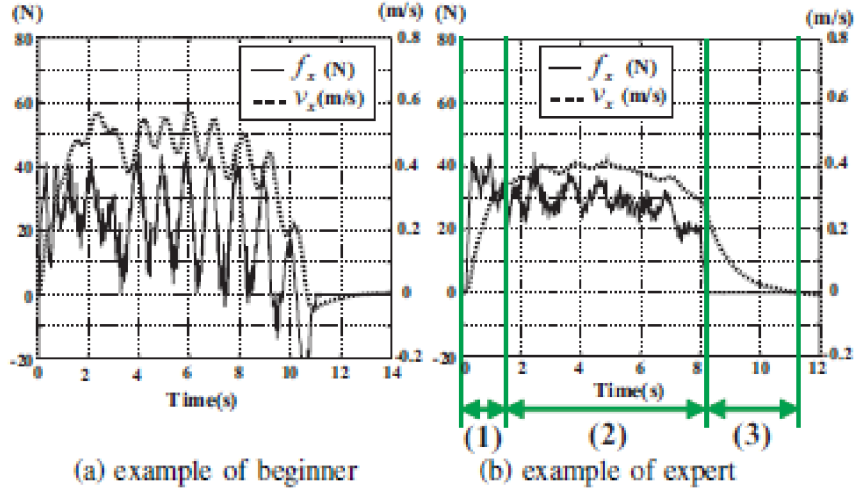


Figure 3.9: Skill level estimation Terashima et al. [44]

Skill level index:

$$S_{vx(t)} = S_{vx(t-1)} + \frac{\sigma_{vxs}}{T_s} \quad (3.19)$$

where  $T_s$  – forgettable time.

The author conducted a comparative experiment for two people and has proposed a formula to evaluate the skill of the operator. Later he conducted another experiment for four people and confirmed the correct operation methods for the operator's evaluation and the regulator setting when moving backward and forward. The implementation of presented methods for lateral, rotational and slant movement was suggested for further research.

### 3.7 Alternative control strategies

In the framework of the current research we have opted for impedance control as its suitability fits the specific requirements and constraints of the application, as well as the hardware and software available in the project. Additionally, we have considered safety, human-robot interaction, and real-time performance when selecting and implementing a control algorithm. However, we acknowledge that alternative control strategies exist, they were described in Kouro et al. [45], Blaya and Herr [46], Beltran et al. [47], Dayan and Balleine [48], Guo et al. [49], Guerrero et al. [50], Sciarretta et al. [51], and Kiguchi et al. [52]. We attempted to summarize the literature in the following table 3.1.

Algorithm	Description	Advantages	Drawbacks
Model Predictive Control (MPC)	MPC is a popular control strategy for systems with non-linear dynamics and constraints. It involves formulating a predictive model of the system dynamics and using an optimization algorithm to compute the optimal control inputs over a finite horizon.	Can handle non-linear dynamics and constraints. Provides good performance and robustness in the presence of disturbances and uncertainties.	Computationally intensive. Requires a good model of the system dynamics. Sensitive to modeling errors and parameter uncertainties.
Adaptive Control	Adaptive control is a family of control algorithms that adjust the control gains online based on the observed system response. This can improve the robustness and stability of the control system in the face of uncertainties and disturbances.	Adjusts control gains online. Provides good performance and robustness in the face of uncertainties and disturbances.	May require a large number of tuning parameters. Sensitive to measurement noise and model uncertainties. May suffer from slow convergence and stability issues.
Sliding Mode Control (SMC)	SMC can provide robustness to disturbances and uncertainties, and can be used for systems with nonlinearities or uncertainties. It is also relatively simple to implement and requires little tuning.	Provides robustness to disturbances and uncertainties. Can be used for systems with nonlinearities or uncertainties. Relatively simple to implement, requires little tuning.	Generates high-frequency control inputs, which can be difficult to implement. May suffer from chattering and high sensitivity to modeling errors.

<b>Algorithm</b>	<b>Description</b>	<b>Advantages</b>	<b>Drawbacks</b>
Reinforcement Learning (RL)	RL can learn optimal control policies through trial-and-error interactions with the environment, without the need for a model of the system dynamics. It can also adapt to changes in the environment and disturbances.	Learns optimal control policies through trial-and-error interactions. Adapts to changes in the environment and disturbances.	Computationally intensive, may require a large amount of training data. May suffer from exploration-exploitation trade-offs and overfitting.
Fuzzy Control	Fuzzy control can handle uncertainties and nonlinearities in the system, and can generate interpretable control rules. It can also be robust to measurement noise and model uncertainties.	Handles uncertainties and nonlinearities. Generates interpretable control rules. Robust to measurement noise and model uncertainties.	Difficult to tune, may require a large number of fuzzy rules. Sensitivity to the choice of membership functions and rule aggregation methods.
Neural Network Control	Neural network control can learn the system dynamics and control policy from data, and can handle nonlinearities and uncertainties in the system. It can also provide good performance and robustness in the face of disturbances and uncertainties.	Learns system dynamics and control policy from data. Handles nonlinearities and uncertainties. Provides good performance and robustness.	Computationally intensive, may require a large amount of training data. May suffer from overfitting and sensitivity to the choice of network architecture and training algorithm.

<b>Algorithm</b>	<b>Description</b>	<b>Advantages</b>	<b>Drawbacks</b>
Optimal Control	Optimal control can minimize a given cost function subject to system constraints, and can generate optimal control inputs. It can also provide good performance and energy efficiency.	Minimizes a given cost function subject to system constraints. Generates optimal control inputs. Provides good performance and energy efficiency.	Computationally intensive, may require a good model of the system dynamics. Sensitivity to modeling errors and parameter uncertainties.
Robust Control	Robust control can provide performance and stability guarantees in the presence of uncertainties and disturbances. It can also be used for systems with nonlinearities or time-varying dynamics.	Provides performance and stability guarantees in the presence of uncertainties. Can be used for systems with nonlinearities or time-varying dynamics.	Computationally intensive, may require a good model of the system uncertainties. Conservatism and limited performance in the absence of disturbances.
Decentralized Control	Decentralized control can distribute the control task among multiple agents, providing scalability and fault tolerance. It can also be used for systems with complex interactions and dependencies.	Distributes the control task among multiple agents. Provides scalability and fault tolerance. Can be used for systems with complex interactions and dependencies.	Difficult to design, may require coordination among the agents. Limited performance compared to centralized control.

Table 3.1: Control Algorithms: Pros and Cons

## List of variables

### Impedance/Admittance control

$M_d$	Positive constant representing the desired inertia of the impedance controller
$B_d$	Positive constant representing the desired damping of the impedance controller
$K_d$	Positive constant representing the desired stiffness of the impedance controller
$x$	Current position of the system
$\dot{x}$	Current velocity of the system
$\ddot{x}$	Current acceleration of the system
$x_d$	Desired position of the system
$\dot{x}_d$	Desired velocity of the system
$\ddot{x}_d$	Desired acceleration of the system
$f_e$	External force acting on the system
$K_p$	Positive gain of the proportional (P) controller in trajectory tracking
$K_d$	Positive gain of the derivative (D) controller in trajectory tracking
$f_r$	Control force in trajectory tracking

### First order lag controller

$v_x$	Velocity component in the $x$ direction.
$v_y$	Velocity component in the $y$ direction.
$w$	Angular velocity (rotation around the $z$ axis).
$k_{vx}$	Controller gain for converting force to velocity in the $x$ direction.
$k_{vy}$	Controller gain for converting force to velocity in the $y$ direction.
$k_{vz}$	Controller gain for converting force to angular velocity.
$T_{vx}$	Time constant for the first-order lag controller in the $x$ direction.
$T_{vy}$	Time constant for the first-order lag controller in the $y$ direction.
$T_{vz}$	Time constant for the first-order lag controller in the angular direction.
$f_x$	Force component applied by the operator in the $x$ direction.
$f_y$	Force component applied by the operator in the $y$ direction.
$m$	Moment (torque) applied by the operator (around the $z$ axis).
$\sigma_{vx}$	Skill degree evaluation performance index for operator's velocity in the $x$ direction.
$v_{xi}$	Instantaneous velocity in the $x$ direction.
$\bar{v}_x$	Mean velocity in the $x$ direction.
$S_{vx(t)}$	Skill level index at time $t$ in the $x$ direction.
$S_{vx(t-1)}$	Skill level index at time $t - 1$ in the $x$ direction.
$\sigma_{vxs}$	Standard deviation of skill degree.
$T_s$	Forgettable time.

### Compliance control

$C_v^h$	Compliant gain adjusted for smooth movement of the platform by the cart operator
$F^h$	Human force applied to the system
$a_v^h$	Adjustable coefficient for the compliant gain
$\dot{v}_h^{ref}$	Speed reference for the compliance controller
$M_v^h$	Mass of the platform
$D_v^h$	Damping coefficient of the platform
$v^h$	Velocity of the platform

### Model Reference Adaptive Impedance Control (MRAIC)

$r_1$	First pole of the reference model in Cartesian coordinate direction
$r_2$	Second pole of the reference model in Cartesian coordinate direction
$\lambda_1, \lambda_2$	Positive constants for stability of the reference model. Real parts of the complex poles $r_1$ and $r_2$ of the reference mode
$\lambda_3$	Positive constants for stability of the reference model. Imaginary part of the complex poles $r_1$ and $r_2$ of the reference model
$\tau_{motor}$	Motor torque
$\hat{M}_q$	Estimated inertia matrix of the robot. Represents the resistance to changes in the robot's state of motion, influenced by the distribution of masses in its links.
$\hat{C}_q$	Estimated Coriolis and centrifugal effects matrix. Accounts for the forces and torques associated with motion and rotation, providing a more accurate representation of dynamic behavior.
$\hat{G}_q$	Estimated gravitational torque vector. Describes the torques induced by gravity on each joint, influenced by the mass distribution and geometry of the robot.
$\hat{F}_q$	Estimated additional external forces or torques. Accounts for external factors or disturbances not covered by inertia, Coriolis, centrifugal, or gravitational effects, such as friction or unknown external forces.
$v_1, v_2$	Known vectors not containing estimated parameters of the robot's dynamics
$\tau_{motor}$	Calculated motor torque.
$J$	Jacobian matrix.
$\ddot{x}_{eq}$	Desired acceleration.
$\dot{x}$	Actual velocity.
$\dot{x}_{eq}$	Reference velocity.
$f_{ext}$	External force.
$\tilde{x}$	Position error.
$\dot{x}_r$	Reference velocity.
$m$	Mass coefficient.
$c$	Damping coefficient.

$k$	Stiffness coefficient.
$Y_1$	Regressors matrix in joint space.
$\hat{\theta}_1$	Estimation of the actual parameters vector.
$s_1$	Error dynamics, calculated as $\dot{x} - \dot{x}_{eq}$ .
$\Gamma$	Symmetric positive definite matrix.
$x_m$	Measurement of the position.

## 4 Motivation

In our work we would like to evaluate a new power assistance system with human comfort estimation, which sets up operator's pushing, pulling and rotational force to the comfortable level and decreases the risk of injury. One of the highlighted specific challenges of the research was to develop a cart that responds more flexibly, robustly and efficiently to the everyday needs of workers and citizens in professional or domestic environments.

The motivation for this research is to reduce the number of injuries of people who work in the area of material handling by solving the problem of faulty interaction between human-operator and industrial cart. It is proposed to establish the system that recognizes and adapts to the human-operator intentions based on rewards and losses received for the quality of interaction process.

One significant part of the research is to specify the requirements for the industrial cart, develop the proper mechanical design and equip the cart with required set of sensors. Another important part is to design the architecture of the control system and implement the elements of artificial intelligence that affect the interaction process.

The objective is to establish a state in which the industrial cart seamlessly responds to the intentions of the human operator, exhibiting the necessary dynamics for a harmonious and efficient interaction. As a result, human oriented study has to be performed. It is necessary to find the correlation between emotional feedback of the human operator and physical measures that could be obtained using sensors of industrial cart.

In order to have a good overview on independent variables that affect human-operator comfort, interaction process parameters have to be collected and evaluated using regression analysis. Using a questionnaire-based technique the emotional feedback of the human operator will be obtained. The effect of found variables will be evaluated with the group of experienced and inexperienced human-operators.

Based on this dependency the reward system will be defined. Using the methods of artificial intelligence, the support system will adapt to the human operator intention by switching between different states and getting rewards for each single action. Finally, the set of impedance controller parameters will be selected based on the highest value of the interaction process quality for particular operator. It leads to adaptation of industrial cart dynamics according to the intention of the human operator.



## 5 Goal and Objectives

The key point of the comfortable human – industrial cart physical interaction is the question how to include physiological and psychophysical aspects of the human operator in to the control system. Furthermore, as far as the author is concerned, no estimation criteria which would address both the operator’s comfort level, and their subjective expectations from the interaction process have been developed to this day.

The research goal is to employ artificial intelligence (AI) methods to adjust the controller settings in order to achieve a state where an operator can manipulate a heavy loaded industrial cart with minimum physical effort and ultimate comfort. Once the proper mechanical design and methods of intelligent control are discovered, the processing of measured forces at the human-cart interface with recognition of the desired behavior and following calculation of the control impact for electric drives is assumed.

In order to achieve the goal, the following objectives are outlined as follows:

1. Collect the state of art information in the area of physical human-robot interaction and the most promising existing algorithm that can be adapted to deliver a new human-powered cart interaction control technique through literature analysis and practical investigations.
2. Prepare a mathematical description for dynamics and kinematics of the human – cart physical interaction model.
3. Develop and assemble an experimental model of an industrial cart.
4. Perform a set of experiments including real people and estimate the human feedback during the interaction process.
5. Analyze dynamic characteristics in order to search for criteria that directly or indirectly determine a physical feeling of human comfort and his expectations during the interaction with IPAC.
6. Synthesize the human estimation criteria that characterize the satisfaction and comfort from the human-powered cart interaction process.
7. Develop the human – powered cart interaction control algorithm based on the synthesized criteria using AI methods (Q-learning).
8. Test and verify the work of proposed solution for the developed industrial cart.

In the framework of the current research, it is important to contribute the following theoretical input into the field of technical cybernetics - the use of Q-learning algorithm in adjusting controller settings so that the mobile platform adapts to the unique gait and tasks of any operator it assists. To comply with this task, the models from Chapters 8 and 9 will be derived and the model could be used in the future to estimate the quality of control with the help of Markov processes. Markov processes are utilized to make decisions on regulating the impedance control settings.

## 6 A Brief Summary of the Implemented Methods

In this chapter we describe the way we would like to reach the goal and meet objectives defined in the beginning of the research. Theoretical, empirical and mathematical research methods are combined in this work in order to reach the goal formulated in chapter 5. The methods and objectives sorted by the research type and addressed by the current study are listed below.

### **Theoretical methods:**

- Analysis and synthesis of existing information was performed to determine the state of the art and current research gaps.
- Modeling was used for industrial cart simulation and development of kinematic and dynamic models.

### **Mathematical methods:**

- Statistics method - regression analysis was performed to evaluate the experimental data and determine the dependency between human operator feedback and measured parameters of the interaction process.
- Programming was used to implement control algorithm.

### **Empirical methods:**

- Observation was used to detect interaction states and conditions that could have a positive or negative effect on the feelings of the cart operator.
- Survey was used to collect the feedback from human operators after the interaction process.
- Experiment was used to collect the data of the interaction process with changing conditions such as impedance controller settings, loads and operators.

## 7 Industrial cart concept evaluation

### 7.1 A rationale for the current industrial cart

An industrial cart is a useful and popular tool for transporting goods and freight. Strong and reliable carts may increase the efficiency of the workers, protect their health and the integrity of the load. The rationale for a specific design is described in this chapter. Such criteria as price (affordability), design simplicity, reliability go in line with the state-of-the-art research described in 8.6. This chapter addresses the design of carts, their types and functional features, the correct choice of a model for specific needs. There are many research groups and organizations that have worked on the problem of evaluating and selecting mobile platforms for material handling tasks. These organizations also addressed the issue of occupational safety in various industries. Therefore, a few notable organizations are worth mentioning:

1. The National Institute for Occupational Safety and Health (NIOSH) in the United States, which conducts research and provides guidelines on the safe design and use of mobile platforms in the workplace.
2. The European Agency for Safety and Health at Work (EU-OSHA), which provides information and guidance on the safe use of mobile platforms in the European Union.
3. The International Organization for Standardization (ISO), which develops and publishes international standards for the design and use of mobile platforms, including ISO 3691-4:2015 for mobile elevating work platforms and ISO 3691-5:2015 for self-propelled industrial trucks.
4. The Industrial Truck Standards Development Foundation (ITSDF), which develops and publishes safety standards for industrial trucks in North America.
5. The Center for Compact and Efficient Fluid Power (CCEFP), which conducts research on the development of advanced power systems for mobile platforms.
6. The Robotics and Mechatronics Laboratory (RoMeLa) at Virginia Tech, which conducts research on the development of advanced mobile platforms for various applications, such as search and rescue, mining, and construction.

When evaluating construction and selecting a type of a mobile platform for material handling tasks, several criteria should be considered. These may include:

1. Load capacity: The maximum weight the platform can safely carry, as well as its weight distribution capabilities. This factor was chosen to be one of the most important ones for the current research as the platform is intended for carrying weight up to 500kg.
2. Mobility: The platform's maneuverability, stability, and ability to navigate through the work environment. This factor was chosen to be one of the most important ones for the current research as the same mobile platform is intended to be used by multiple operators.
3. Reach: The maximum height and distance the platform can reach, as well as its ability to rotate and pivot. We describe the specific configurations in the table 7.2.
4. Speed: The platform's maximum and minimum speeds, as well as its acceleration and braking capabilities. In the current case, the maximum velocity of the cart was limited 5 km/h to suit the gait of a human operator.
5. Durability: The platform's ability to withstand heavy use and harsh environments, as well as its ease of maintenance and repair. The test platform was built to be easily maintained and repairable.
6. Safety: The platform's ability to protect operators and other personnel from injury, as well as its compliance with relevant safety regulations. In our case the mobile platform is equipped with emergency stop button to ensure an immediate cut of the power supply to the drives.
7. Power source: The platform's energy source, such as electric, hydraulic, or combustion, and the compatibility with the available power supply. To power the cart, 24V Lithium batteries were used.
8. Ergonomics: The platform's design and features that can make the operator's task easier, more comfortable and less fatiguing. This factor was chosen to be one of the most important ones for the current research as the platform is intended for wider audiences of users.
9. Compatibility: The platform's ability to work with other equipment and tools that are already in use in the facility. The prototype is equipped with wired and wireless interfaces suitable for Operation technologies(OT)/Information technologies (IT) integration.

## 7.2 Constructing the industrial cart

Creating collaborative robotic environment for safe human robot interaction was covered in multiple articles, including e.g. Pozo, Patel and Schroedel (2022) [53]. The researchers pointed out at the importance of creating safe environment to work

with robots for inexperienced users. Collaborative industrial robot safety requirements are defined in ISO/TS 15066:2016 ISO (2016). Engineering of industrial cart is a complicated process. During the development phase it is necessary to estimate the required modifications to improve functionality for a specific task. Design process of any industrial cart considers the following requirements: cargo format (type of the load), ease of storage, carrying capacity, necessary ergonomics, safety margin, potential risk factors. The following basic points form the structure of a typical industrial cart:

- Chassis (wheels). The most important elements, supporting parts of the trolley. They consist of the wheel itself and the coating (tires). They could be fixed positioned or rotary.
- Platform. The working surface, which is made in the form of a grid, a solid structure, a base with a flooring of metal, plywood sheets or rubber-plastic.
- Handlebar (Control element). It can be single, double, folding, removable. Mainly made from metal pipes. In heavy-duty platform models that require a tractor for operation, the handle is replaced by the draw-bar.

The existing cart models could be classified according to the specific parameters:

- Platform layout;
- Wheels configuration;
- Maximum carrying capacity;
- Extra features and options (Power assistance, height regulation, color options, etc.)

The total lifting capacity of industrial carts depends on the configuration, model, type of structure and wheels, materials. The average load capacity of different carts is from 60 to 900 kg (heavy-duty carts carry up to 3 tons).

The wheel configuration as a base has a considerable impact on the load capacity and the amount of force exerted to move the cart. The most common configurations for traditional rectangular cart are collected in the table 7.2. Each layout has its own benefits and drawbacks.





Type, position and quantity of wheels impacts load capacity and maneuverability of the industrial cart. The industrial application adds a specific constraint on quantity and position of movable and fixed wheels of industrial cart. Each wheel needs to be as lightweight as possible compared to the weight of the cart, so that the kinetic energy goes into forward motion of the cart, not into the rotary motion of the wheels. That is an argument why fewer wheels are used in the current prototype. At the same time, larger wheels will have less rolling friction than smaller ones. The reason carts for heavy loads which travel on hard surfaces have more than four wheels to distribute the weight over six axles rather than just four. As a result, maneuvering with the cart becomes easier because of the reduced pressure on

the surface. A six wheel option has improved mobility when maneuvering in tight and confined spaces with the heavy load. The two center rigid casters and swivels on the end provide a tighter turning radius than the standard caster configuration. This configuration ensures the cart can pivot on its own axis and provides zero-turn maneuverability.

The frictional force has three components:

1. rolling resistance
2. friction at the axles
3. wind resistance

We assume that wind resistance is not changed very much by a 4-wheel versus 6-wheel design for indoor application, when the cart transportation speed is less than 5km/h. In addition, friction at the axles is probably not as big as rolling resistance. Therefore, we will now focus on the types of wheels which are described in the following table 7.1.

Symbol	Image	Description
		Rotatable supporting wheel (swivel caster) – wheel that automatically aligns itself to the direction of travel. One major disadvantage of casters is a flutter. A common example of a caster flutter is in a supermarket shopping cart, when one caster rapidly swings side-to-side. This oscillation, which is also known as shimmy, occurs naturally at certain speeds, and is similar to speed wobble that occurs in other wheeled vehicles. The speed at which caster flutter occurs is based on the weight borne by the caster and the distance between the wheel axle and steering axis. This distance is known as trailing distance, and increasing this distance can eliminate flutter at moderate speeds. Generally, flutter occurs at high speeds.
		Fixed/Rigid supporting wheel (caster) – rigid casters are casters that remain in one position. They tend to restrict vehicle motion so that the vehicle travels along a straight line. For improved results, it is common to use a combination of swivel and rigid casters to achieve the most favorable mix of stability and maneuverability.






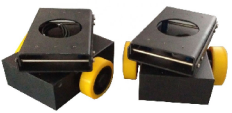
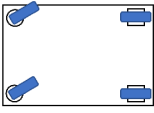

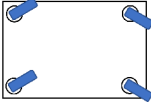

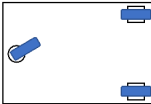

Symbol	Image	Description
		Mecanum wheel – the wheel consists of two rims and multiple free-running rollers, which are mounted at a 45 degree angle. The wheels move independently of each other, which means that the vehicle can move not only forwards and sideways, but also diagonally and in a circle. The entire wheel is driven by an electric motor.
		Omni wheel (poly wheel) – wheels with small discs (called rollers) around the circumference which are perpendicular to the turning direction. The effect is that the wheel can be driven with full force, but will also slide laterally with great ease. These wheels are often applied in holonomic drive systems.
		Differential wheel unit – here are two main wheels, each of which is attached to its own motor. High precision servo control. Precise angle control (absolute position detection). Low center of gravity. Strong ground adaptability.

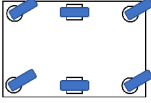

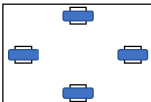

Table 7.1: Review of available types of the wheels

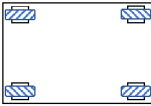
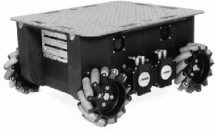
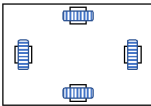
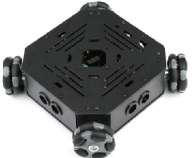
The following table 7.2 describes possible constructions of mobile platforms with our own analysis of their benefits and drawbacks.

Wheels' configuration	Application example	DoF	Application description
		2	Platform with two rotatable supporting wheels and two fixed supporting wheels. In case of powered industrial cart application fixed supporting could be equipped with the drives. This configuration is suitable for driving in a straight line with occasional turns (warehouse, shop, workshop). <b>Benefit:</b> This configuration turns easily and tracks very well when towed. Most popular configuration for casters on carts and trucks. <b>Drawback:</b> The cart cannot freely move in any direction. To make a 90° turn, the cart must be pulled around on a pivot of the rigid casters.



Wheels' configuration	Application example	DoF	Application description
		3	<p>Platform with four rotatable supporting wheels. In case of powered industrial cart application all wheels should be equipped with fraction and steering drives. This configuration is suitable for fast and short operations with a constant change of course/direction of motion, work with goods near the shelves (retail areas, shopping malls).</p> <p><b>Benefit:</b> The cart can be moved in any direction without the need for turning around.</p> <p><b>Drawback:</b> The cart can be hard to control when moving in a straight line. Easy fix: Equip the casters with swivel locks.</p>
		2	<p>Platform with one rotatable supporting wheel and two fixed supporting wheels. In case of powered industrial cart application there are two possibilities exist. One option is to add fraction and steering drives to rotatable supporting wheel. Alternative option is extending of the functionality of fixed supporting wheels in a way of differential drive. This configuration is suitable for driving in a straight line with occasional turns (warehouse, shop, workshop, assembly line). Straight forward motion. Turning about rear axle. Preferred direction of motion is forward.</p> <p><b>Benefit:</b> This is the lowest cost configuration for carts with very good maneuverability.</p> <p><b>Drawback:</b> It cannot carry heavy loads, because only three casters are in contact with the floor at one time and it cannot be pushed sideways. It is inconvenient to move the cart in a strait line with higher velocity because of the castor wheel shimmy vibration.</p>

Wheels' configuration	Application example	DoF	Application description
		2	<p>Platform with four rotatable supporting wheel and two fixed supporting wheels. In case of powered industrial cart application fixed supporting wheels are equipped with the drives. This configuration is suitable for transportation of heavy loads in a straight line with rare changes of direction (airport, station buildings, postal terminals).</p> <p><b>Benefit:</b> Similar to the 4-wheel diamond caster patterns but can carry heavier loads and are better suited for very long carts. This caster pattern allows the cart to turn in its own length and the cart style can either by tilt type or non-tilt for even greater load capacity.</p> <p><b>Drawback:</b> The cart cannot freely move in any direction. To make a 90° turn, the cart must be pulled around on a pivot of the rigid casters.</p>
		1	<p>Platform with four fixed supporting wheels. In case of powered industrial cart application fixed supporting wheels could be connected to the drive. This configuration is suitable for direct "runs" in a large area (shop, assembly line).</p> <p><b>Benefit:</b> This is the lowest cost configuration for carts and trucks. It can also pivot on the center wheels to turn or do complete 360° rotations.</p> <p><b>Drawback:</b> It cannot carry heavy loads, because only three casters are in contact with the floor at one time (tilt type cart) and it cannot be pushed sideways.</p>

Wheels' configuration	Application example	DoF	Application description
		3	<p>Platform with four mecanum wheels. Each wheel is connected to a separate motor with independent control. This configuration is suitable for maneuvers in a limited space. Motion in every direction on a surface.</p> <p><b>Benefit:</b> The cart could freely and instantly move in any direction and turn in its own length.</p> <p><b>Drawback:</b> Construction is complex in maintenance and expensive.</p>
		3	<p>Omni-directional robotic platforms have vast advantages over a conventional design in terms of mobility in congested environments. They are capable of easily performing tasks in environments congested with static and dynamic obstacles and narrow aisles. These environments are commonly found in factory workshops offices, warehouses, hospitals and elderly care facilities. Motion in every direction on a surface. Install on the heavy-duty Omni moving platform to make the platform rotate to Omni directions. And it is mainly used in industry, workshops, AGV, and so on. It can even be used on stage show equipment.</p> <p><b>Benefit:</b> The cart could freely and instantly move in any direction and turn in its own length.</p> <p><b>Drawback:</b> Construction is complex in maintenance and expensive.</p>

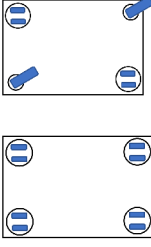

Wheels' configuration	Application example	DoF	Application description
		3	<p>Omnidirectional driving system can effortlessly move through very narrow aisles. With four driving units, the platform is based on an omnidirectional driving concept that allows unrestricted freedom of movement. This enables standardized forward and backwards movements, as well as parallel, diagonal, and rotary movements around its own axis. Motion in every direction on a surface.</p> <p><b>Benefit:</b> The cart could freely move in any direction and turn in its own length. However, the cart needs an extra time to make 90° turn, because the change of wheel unit orientation cannot be done immediately.</p> <p><b>Drawback:</b> Construction is complex in maintenance and expensive, because each wheel is a separate drive unit which is equipped with two servomotors.</p>

Table 7.2: Review of available wheel configurations

The configuration selected for the experimental platform corresponds to a platform with four tilt wheels and two fixed supporting wheels. This construction is capable of handling heavy loads and allows the cart to turn within its own length. The fixed supporting wheels are suitable for the implementation of electrical drives, as they are more cost-effective than in the case of implementing active steering for the tilt wheels. This construction is more complex, less robust and more expensive. Of course, the proposed construction has only two degrees of freedom, however, it is believed to be a robust and cost-effective solution.

## 8 Test platform development

### 8.1 Main requirements

This section describes the main requirements for a mobile platform that was created for testing and verification of operator's comfort. This developed model consists of aluminum profile, the basis of the platform is set on the four cluster wheels. In the center of the platform there are two leading wheels that function according to the principle of a differentiated drive.

The vehicle has been constructed to satisfy the following requirements:

- to be easy-assembled, cheap, rapid prototyping oriented
- to allow measurement of human-vehicle interaction characteristics
- to hold the maximum load mass in the range of 500 kg
- to attain the speed of a walking individual in a range of 5 km/h

### 8.2 Hardware design

The developed platform has the characteristics shown in the table 8.1.

N	Parameter	Value
1	Length	1.255 [m]
2	Width	0.8 [m]
3	Height	1.275 [m]
4	Mass	53.535 [kg]
5	Max. Load	500 [kg]
4	Max. Speed	5 [km/h]

Table 8.1: Cart parameters

System actuators are presented by two 350W motors MY1016Z connected to the wheels via chain belts. The drive is shown in the figure 8.3.

In the back of the cart there is a handle for the operator. The handle is connected to the body of the cart through the tensiometers which are located on the right and left side of the cart. The two tensiometers were selected as an optimal solution because more tensiometers may not guarantee considerable enhancement



Figure 8.1: Test platform [54]

N	Parameter	Value
1	Power	350 [W]
2	Voltage	24 [V]
3	Current	18 [A]
4	Rotor Resistance	1.3 [Ohm]
5	Rotor Inductance	0.001 [H]
6	kV	500 [kg]
7	Max. Speed	5 [km/h]

Table 8.2: Motor parameters

N	Parameter	Value
1	Excitation	10 [Vdc]
2	Load	$\pm 100$ [KgF]
3	In Resist	378.3 [Ohm]
4	Out Resist	351.9 [Ohm]
5	Sensitivity	2.9994 [mV/V]

Table 8.3: Tensiometer parameters

in the learning process to an extent to which the costs of construction and design may rise to. The accelerometer is located on the platform's body in a significant distance from drives and motor driver in order to avoid possible disturbances that might be caused by the effect of the electromagnetic field. For detailed information please see the visual 8.2.

The leading wheels are connected to the drives by a chain belt. The drives are accommodated with encoders. In the chain of anchors of each drive there is a current sensor.

The motors were selected based on reliability, price and low complexity criteria

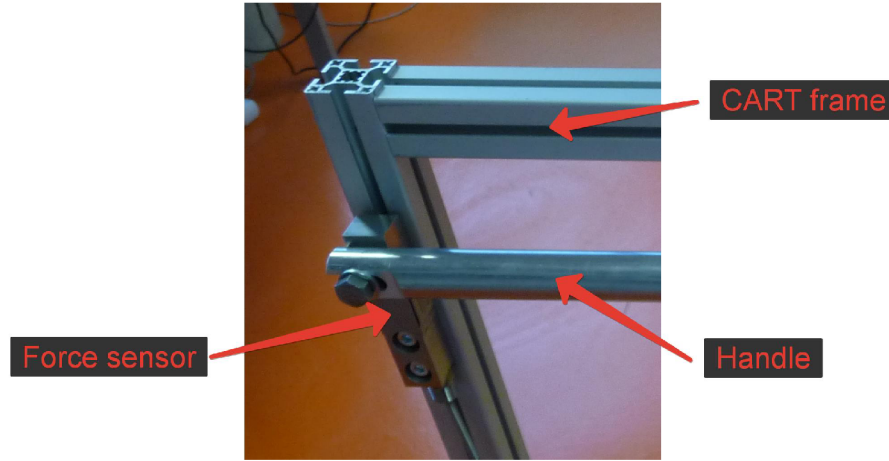


Figure 8.2: Tensiometer location

and are equipped with  $z_m = 9$  teeth pitch 12.7 roller. The motors have to satisfy the dynamic parameters of the cart (mass and damping, see section 8.7). The desired linear speed of the powered cart  $v_d = 5[km/h] = 1.389[m/s]$ . Powered wheel diameter  $D_w = 200[mm] = 0.2[m]$ . Desired wheel rotational speed [rpm]:

$$n_w = \frac{60 v_d}{\pi D_w} = (60 \cdot 1.389)/(3.14 \cdot 0.2) = 132.696 \quad (8.1)$$

Gear ratio:

$$G_r = \frac{n_m}{n_w} = 353/132.696 = 2.66 \quad (8.2)$$

Teeth number of the wheel gear:

$$z_w = G_r \cdot z_m = 2.66 \cdot 9 \approx 24 \quad (8.3)$$

The final overview of the developed drive system is shown in the figure 8.3.

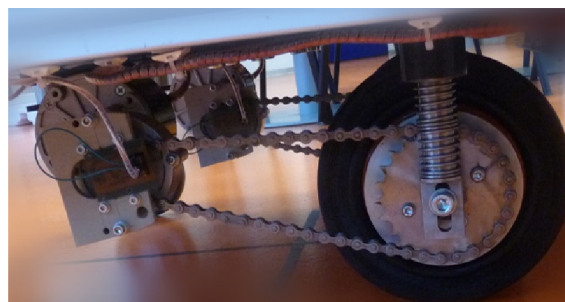


Figure 8.3: Drive system overview

Figure 8.4 demonstrate the layout of the drive system for a single wheel. The cart has two powered wheels. Each wheel is connected to the motor by means of spur and sprockets gears.

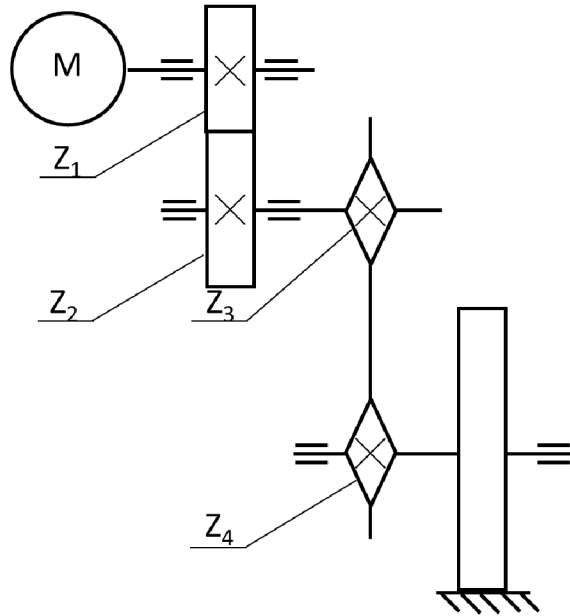


Figure 8.4: Single wheel drive system layout

N	Gears	Gear ratio
1	Z1:Z2	9.78:1
2	Z3:Z4	1:2.66

Table 8.4: Drive gearing parameters

Motor control is carried out with the help of a driver. The driver is controlled by a controller of a lower level. The controller of a lower level collects and partly processes the signals from peripheral areas (encoders, current sensors, tensiometers). The lower level controller is also connected to the extra controller that is responsible for collecting and processing the data from the inertia motion unit (IMU) that typically includes a magnetometer, an accelerometer and a gyroscope.

Detailed description of the technical characteristics could be found in the technical specifications [55], [56], [57], [58].

The second revision of the hardware consisted of HX711. Tensiometers are processed by a pair of 24bit analog-to-digital converters HX711.

Inertia measurement unit is presented by HMC5983 and MPU6050 modules. The module HMC5983 is a temperature compensated three-axis integrated circuit magnetometer and MPU6050 is combining a MEMS 3-axis gyroscope and a 3-axis accelerometer. As for the lower-level controller, prototyping boards from the ARDUINO ecosystem were used.

### 8.3 Arduino ecosystem

Arduino board provides a set of significant benefits. Firstly, it has the minimum required amount of peripheral components such as frequency oscillator, capacitors,



resistors, transistors, a DC-DC converter, the USB-UART ttl converter and the USB port. The board should be selected based on system requirements. We define these requirements based on the amount, type and interface of sensors and actuators that we would like to connect to the control system. The equipment we used for the interfaces is presented in the Table 8.5.

The Arduino Mega 2560 shown in Figure 8.5 is a microcontroller board based on the ATmega2560 (8-bit AVR Microcontroller). It has 54 digital input/output pins (of which 15 can be used as PWM outputs), 16 analog inputs, 4 UARTs (hardware serial ports), a 16 MHz crystal oscillator, a USB connection, a power jack, an ICSP header, and a reset button. It contains the compulsory components needed to support the microcontroller. It is possible to connect it to a computer with a USB cable or power it with a AC-to-DC adapter or battery. The Mega 2560 board is compatible with most shields designed for the Uno and the former boards Duemilanove or Diecimila.

The high-performance, low-power Microchip 8-bit AVR® RISC-based microcontroller combines 256 KB ISP flash memory, 8 KB SRAM, 4 KB EEPROM, 86 general purpose I/O lines, 32 general purpose working registers, real-time counter, six flexible timer/counters with compare modes, PWM, four USARTs, byte-oriented Two-Wire serial interface, 16-channel 10-bit A/D converter, and a JTAG interface for on-chip debugging. The device achieves a throughput of 16 MIPS at 16 MHz and operates between 4.5-5.5 volts. By executing powerful instructions in a single clock cycle, the device achieves a throughput approaching one MIPS per MHz, balancing power consumption and processing speed.

Another microcontroller board used in the project was the Arduino Pro Mini. This board is shown in the figure 8.6 based on the ATmega328P. It has 14 digital input/output pins (of which 6 can be used as PWM outputs), 6 analog inputs, an on-board resonator, a reset button, and holes for mounting pin headers. A six pin header can be connected to an FTDI cable breakout board to provide USB power and UART communication to the board.

The board has a number of facilities for communicating with a computer, another Arduino, or other microcontrollers. The ATmega328P provides UART TTL serial communication, which is available on digital pins 0 (RX) and 1 (TX). The Arduino software includes a serial monitor which allows simple textual data to be sent to and from the Arduino board via a USB connection.

Third important component of the platform control system was Raspberry Pi 4 Model B featured with high-performance 64-bit quad-core processor, dual-display support at resolutions up to 4K via a pair of micro HDMI ports, up to 8GB of RAM, dual-band 2.4/5.0 GHz wireless LAN, Bluetooth 5.0, Gigabit Ethernet, USB 3.0, and PoE capability (via a separate PoE HAT add-on).

This compact single-board computer is suitable for space-constrained environments in mobile robots. Its small form factor allows for easy integration into robotic systems without taking up much space. Raspberry PI provides sufficient computing power for various robotic tasks such as image processing, sensor data fusion, and control algorithms. It can handle real-time processing demands of mobile robots effectively.

In our application shown in connection block diagram 8.8, interaction forces between human operator and industrial cart are measured by two load cells. Analog values of the forces are converted to the digital format using HX711 24-bit ADCs and sent to the low-level controller (Arduino Mega board) over SPI. Using equations 8.18 and 8.19, the translation force and rotational torque are calculated based on the forces measured from the right and left side of the handle bar. These calculated values are supplied to the corresponding input of transnational and rotational impedance controller. The setpoints for linear and angular velocities of the cart were obtained at the outputs of impedance controllers. Based on the linear and angular velocities, the values for angular velocities of the left and right wheels were calculated using equations 8.16 and 8.17. At the final stage, the setpoints were processed by the PID controllers of the corresponding wheels. Motors are controlled by the drive unit (MOD-035) using PWM and direction control. Information about the actual position and the current velocity of the wheels is received from the magnetic rotary encoders (AS5040). The parameters of impedance controllers 8.22 and 8.23 could be changed remotely over the serial port of Arduino Mega board.

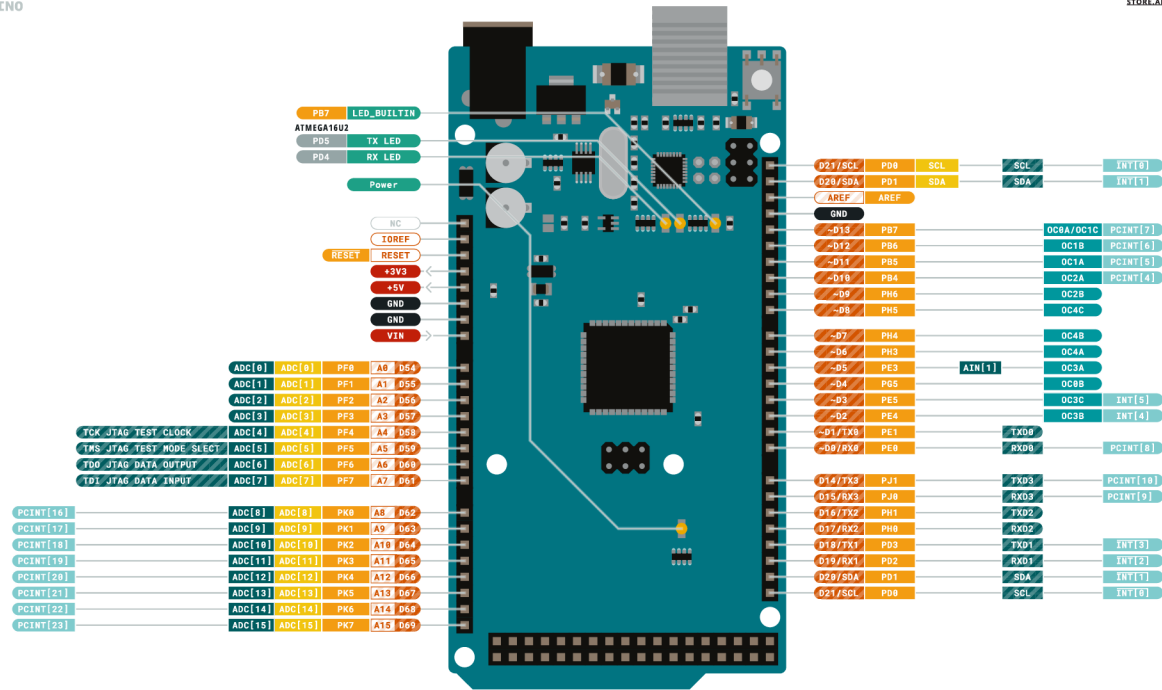
Additionally, we installed one more micro-controller (Arduino Pro Mini) that was connected to IMU. Using the serial port the IMU controller passed the data through the low-level controller to the high-level controller. Actual information about the interaction process was recorded to an SD card with the time stamp.

Device	Qty.	Description	Interface
HX711	2	ADC	SPI
HMC5883L	1	Magnetometer	I2C
MPU-6050	1	Accelerometer/Gyroscope	I2C
AS5040	2	Incremental encoder	Digital inputs (SPI optional)
MOD-035	1	Motor driver	Digital Inputs/Outputs
ACS712	2	Current measurement sensor	Analog Inputs

Table 8.5: List of sensors with interfaces



ARDUINO  
MEGA 2560 REV3  
STORE.ARDUINO.CC/MEGA-2560-REV3



<ul style="list-style-type: none"> <li><span style="display: inline-block; width: 10px; height: 10px; background-color: black; margin-right: 5px;"></span> Ground</li> <li><span style="display: inline-block; width: 10px; height: 10px; background-color: red; margin-right: 5px;"></span> Power</li> <li><span style="display: inline-block; width: 10px; height: 10px; background-color: #008000; margin-right: 5px;"></span> LED</li> <li><span style="display: inline-block; width: 10px; height: 10px; background-color: #cccccc; margin-right: 5px;"></span> Internal Pin</li> <li><span style="display: inline-block; width: 10px; height: 10px; background-color: #808080; margin-right: 5px;"></span> SWD Pin</li> </ul>	<ul style="list-style-type: none"> <li><span style="display: inline-block; width: 10px; height: 10px; border: 1px solid orange; margin-right: 5px;"></span> Digital Pin</li> <li><span style="display: inline-block; width: 10px; height: 10px; border: 1px solid #ccc; margin-right: 5px;"></span> Analog Pin</li> <li><span style="display: inline-block; width: 10px; height: 10px; border: 1px solid #ccc; margin-right: 5px;"></span> Other Pin</li> <li><span style="display: inline-block; width: 10px; height: 10px; border: 1px solid orange; margin-right: 5px;"></span> Microcontroller's Port</li> <li><span style="display: inline-block; width: 10px; height: 10px; border: 1px solid yellow; margin-right: 5px;"></span> Default</li> </ul>	<ul style="list-style-type: none"> <li><span style="display: inline-block; width: 10px; height: 10px; background-color: #008000; margin-right: 5px;"></span> Analog</li> <li><span style="display: inline-block; width: 10px; height: 10px; background-color: #008000; margin-right: 5px;"></span> Communication</li> <li><span style="display: inline-block; width: 10px; height: 10px; background-color: #008000; margin-right: 5px;"></span> Timer</li> <li><span style="display: inline-block; width: 10px; height: 10px; background-color: #008000; margin-right: 5px;"></span> Interrupt</li> <li><span style="display: inline-block; width: 10px; height: 10px; background-color: #008000; margin-right: 5px;"></span> Sercom</li> </ul>	<ul style="list-style-type: none"> <li><span style="display: inline-block; width: 10px; height: 10px; border: 1px solid red; margin-right: 5px;"></span> <b>MAXIMUM</b> current per I/O pin is 20mA</li> <li><span style="display: inline-block; width: 10px; height: 10px; border: 1px solid red; margin-right: 5px;"></span> <b>MAXIMUM</b> current per +3.3V pin is 50mA</li> </ul>	<p>VIN 6-20 V input to the board.</p>	<p>ARDUINO.CC Last update: 16/12/2020</p> <p>This work is licensed under the Creative Commons Attribution-ShareAlike 4.0 International License. To view a copy of this license, visit <a href="http://creativecommons.org/licenses/by-sa/4.0/">http://creativecommons.org/licenses/by-sa/4.0/</a> or send a letter to Creative Commons, PO Box 1866, Mountain View, CA 94042, USA.</p>
---	--	---	--	---------------------------------------	--

Figure 8.5: Arduino Mega Board



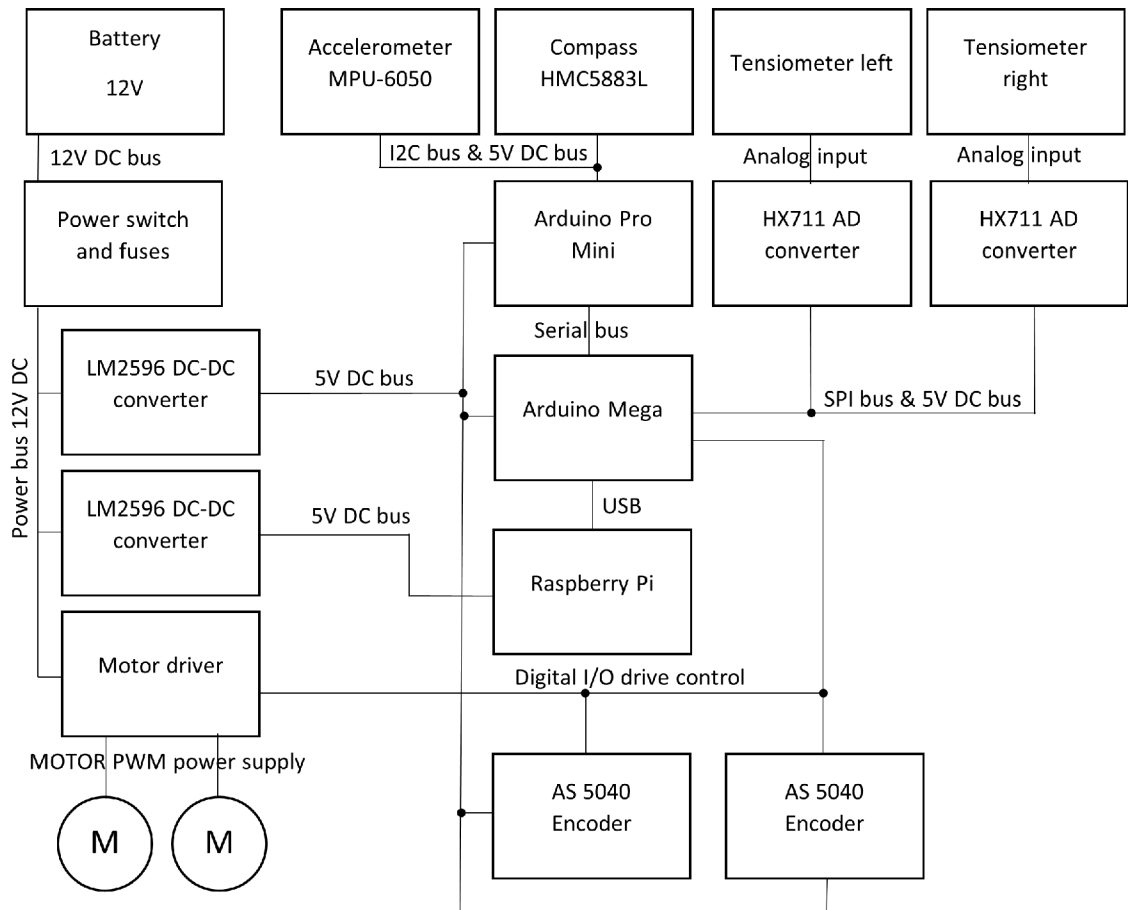


Figure 8.8: Connection Block Diagram

## 8.4 Software development

In order to extend the number of ready-made modules and to decrease the time spent on programming and manuals, it was decided to merge libraries from ARDUINO open-source community with Matlab Simulink. To use the original Wiring language of ARDUINO with RPi, the Wiring Pi library was developed. Wiring is an open-source electronics prototyping platform composed of a programming language, an integrated development environment (IDE), and a single-board microcontroller. It was developed starting in 2003 by Hernando Barragán.

The Wiring IDE is a cross-platform application written in Java which is derived from the IDE made for the Processing programming language. It is designed to introduce programming and sketching with electronics to artists and designers. It includes a code editor with features such as syntax highlighting, brace matching, and automatic indentation capable of compiling and uploading programs to the board with a single click. The Wiring IDE includes a C/C++ library called "Wiring", which makes common input/output operations much easier. Wiring programs are written in C++. A minimal program requires only two functions:

*setup()*: a function run once at the start of a program which can be used to define initial environment settings.

*loop()*: a function called repeatedly until the board is powered off or reset.

Project experts, intermediate developers, and beginners from around the world share ideas, knowledge and their collective experience as a project community. Wiring makes it easy to create software for controlling devices attached to the electronics board to create various interactive devices. The concept of software development implies writing a few lines of code, connecting a few electronic components to the Wiring hardware. This process is called sketching with hardware.

## 8.5 Cart kinematics

In the framework of this study, we conducted experiments on a range of motors utilizing various kinematic configurations. The results revealed that the controller settings varied depending on the type of the motor employed (e.g. brushless DC motors, DC motors with gearbox). To facilitate the experimental setup, specialized software was employed for each driver, incorporating automatic identification capabilities. Additionally, we utilized the System Identification Toolbox for data analysis. A visual representation of the experimental setup is available upon request. The vehicle described in this thesis has two driving wheels and four passive casters. The IPAC model used in this paper is shown in the figure 8.9. To simplify the kinematics model of the vehicle, it is assumed that casters are not active.

Parameters shown in the figure 8.9 have the following description:  $W_s$  – distance between two sensors;  $W_w$  – distance between two wheels;  $L_{sv}$  – distance between sensors installation line and wheels installation line;  $\theta_w L$ ,  $\theta_w R$  – wheels rotation angles;  $\alpha$  – direction angle;  $x_0$ ,  $y_0$  – position of the vehicle in the world coordinates;  $C_0$  – the middle point between the two powered wheels. Mathematical description

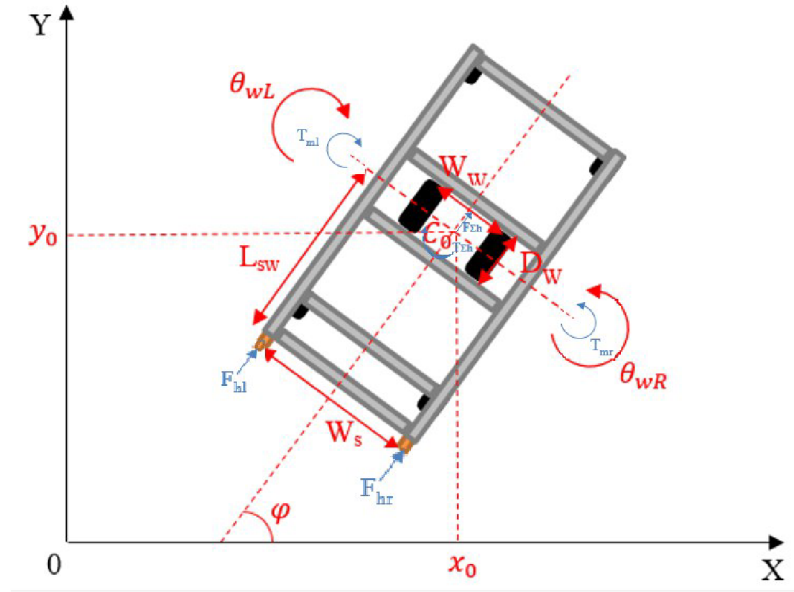


Figure 8.9: Cart kinematics

of the control object is presented below.

Relation for linear and angular velocity:

$$v = wR \quad (8.4)$$

where  $R$  is radius (distance between the point for which linear speed is calculated and rotation axis).

The relation for linear and angular velocity is described by the following equation 8.5:

$$v_{\Sigma cart} = \frac{D_w}{4} (w_{wheel\_left} + w_{wheel\_right}) \quad (8.5)$$

Velocity at  $C_0(x_0, y_0)$  point is described by the equations 8.6 and 8.7 (Conversion from polar to Cartesian coordinate system).

$$\dot{x}_0 = v_{\Sigma cart} \cos(\phi) \quad (8.6)$$

$$\dot{y}_0 = v_{\Sigma cart} \sin(\phi) \quad (8.7)$$

Dependency of powered cart angular velocity from angular velocity of the wheel:

Wheel linear velocity:

$$v = w_{cart}L = w_{wheel}R \quad (8.8)$$

where  $L$  is the distance depicted in figure 8.9.

Cart angular velocity generated by one wheel:

$$w_{cart} = w_{wheel} \frac{R}{L} \quad (8.9)$$

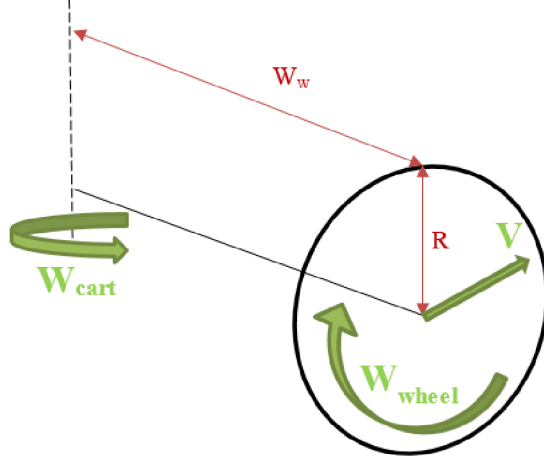


Figure 8.10: Angular speed conversion

Cart angular velocity at the point  $C_0$ :

$$w_{\Sigma cart} = \frac{D_w}{2W_w} \cdot (w_{wheel\_left} - w_{wheel\_right}) \quad (8.10)$$

Matrix form of the equations 8.5 and 8.9 is shown in 8.10. Control vector is defined as  $\dot{X} = [v_{cart\_sum}, w_{cart\_sum}]^T$ , rotational speeds vector is defined as  $\dot{\theta} = [w_{wheel\_left}, w_{wheel\_right}]^T$ .

$$\dot{X} = \begin{bmatrix} v_{\Sigma cart} \\ w_{\Sigma cart} \end{bmatrix} = \begin{bmatrix} \frac{D_w}{2W_w} & -\frac{D_w}{2W_w} \\ \frac{D_w}{4W_w} & -\frac{D_w}{4W_w} \end{bmatrix} \times \begin{bmatrix} w_{wheel\_left} \\ w_{wheel\_right} \end{bmatrix} = J_{aco} \cdot \dot{\theta} \quad (8.11)$$

By differentiating the equation 8.11 we obtain an equation for the total linear and angular acceleration:

$$\ddot{X} = J_{aco} \cdot \ddot{\theta} + \dot{J}_{aco} \cdot \dot{\theta} \quad (8.12)$$

where  $J_{aco}$  is a Jacobian matrix which describes cart kinematics sized  $R^{2 \times 2}$ .

The second term on the right side has a insignificant impact on the acceleration value compared to the first term and could be neglected.

$$\ddot{X} = J_{aco} \cdot \ddot{\theta} \quad (8.13)$$

In order to obtain equation for calculating the wheel angular accelerations, we need to find the pseudo-inverse matrix  $J_{aco}^{-1*}$ .

$$\ddot{\theta} = J_{aco}^{-1*} \cdot \ddot{X} \quad (8.14)$$

$$\begin{bmatrix} \varepsilon_{wheel\_left} \\ \varepsilon_{wheel\_right} \end{bmatrix} = \frac{D_w}{4} \cdot \begin{bmatrix} 1 & \frac{W_w}{2} \\ 1 & -\frac{W_w}{2} \end{bmatrix} \begin{bmatrix} a_{cart\_sum} \\ \varepsilon_{cart\_sum} \end{bmatrix} \quad (8.15)$$

Based on the kinematic model, we can determine the position and direction of movement of the industrial cart from the rotation speed of the left and right wheels.



The angular velocity of the wheels could be calculated based on the linear and angular velocity of the cart, according to the equations 8.16 and 8.17.

$$w_{wheel\_left} = \frac{2v_{cart} + W_w w_{cart}}{D_w} \quad (8.16)$$

$$w_{wheel\_right} = \frac{2v_{cart} - W_w w_{cart}}{D_w} \quad (8.17)$$

## 8.6 Human operator interface

In case of controlling remote robots, the use of haptic technology can create a sense of telepresence for the human operator and allow the performance of physical tasks from a distance. This type of human-robot interactions presents complex and interdisciplinary challenges, such as the need for a robot to be physically capable of performing a task and safe for close proximity with humans while also being practical in size, and the need for both the human and robot to be able to communicate, plan, and make decisions based on uncertain information. The current example of this is the problem of a human and a robot working together to move objects up to 500 kg, which has been partially solved but still requires further advancement in the various aspects of human-robot interaction.

According to Okamura (2018) [59], haptic devices have the potential to facilitate touch-based communication between humans and robots, allowing people to communicate in a noticeable but private way while leaving other senses free for other purposes. Haptic communication can be achieved through direct physical interaction between humans and robots, or through the use of specialized haptic devices that allow for communication without requiring physical contact. In this latter case, control interfaces and interactions based on touchless gesture tracking devices allow users to interact with computers or other devices using hand gestures or other types of body movements, rather than through physical touch.

These devices typically use sensors such as cameras or depth sensors to track the user's movements and interpret them as input commands. They can be used to control a wide variety of applications, such as controlling the cursor on a computer screen, navigating through menus or other user interfaces, and interacting with virtual or augmented reality environments. Some touchless gesture tracking devices are designed to be worn on the body, while others are stationary and designed to be used in a fixed location. They can be used in a variety of settings, including in homes, offices, classrooms, and public spaces. Touchless gesture tracking devices have the potential to provide a more natural and intuitive way for users to interact with technology, and can be particularly useful for people who may have difficulty using traditional input methods such as a keyboard or mouse. An example of such studies might be the research work carried by Giordano et al. in 2018 [60]. In order for haptic devices to become widely used for this purpose, they must be easy to use, not disruptive or obtrusive, able to be used comfortably, and socially acceptable. Okamura's criteria for successful application of haptic devices go in line with

the criteria used in this thesis, namely, price (affordability), reliability, operator's comfort and relative incomplexity of the decision.

In case of the current test vehicle, the cart is equipped with two tensiometers (see chapter 8.2). They are shown in the figure 8.11. They connect the handle to the cart body and are used to measure interaction forces and torques for transnational and rotational motions correspondingly. They can measure the force along one axis (push and pull motions), but it allows the operator to control all degrees of freedom (DOFs) because the cart has only two DOF (one rotational and one translational degree). The operator plans a handling task based on his own desires and expectations as well as information from his sense organs (vestibular and vision systems), and provides the information about the motion to the cart by acting on the handle. Forces detected on the left and right sensors are resolved into translational force and rotational torque in the cart coordinates.



Figure 8.11: Handlebar for PHRI

Transnational force for the motion in linear direction could be written as a simple sum of the measured force values as described by the equation 8.18.

$$F_{\sum h} = F_{hr} + F_{hl} \quad (8.18)$$

Equation 8.19 presents a rotational torque for the motion around the axis that goes vertically through the central point  $C_0$ . See figure 8.9 for more details.

$$T_{\sum h} = (F_{hr} - F_{hl}) \cdot W/2 \quad (8.19)$$

where  $W$  is the width of the cart. According to the mechanical configuration, the cart is equipped with tensiometers which measure two forces in the direction  $x$ , perpendicular to the handle. The distance between two sensors equals to the width of the cart. The values for cart width could be found in table 8.1. As the result, the input for the controller of rotational motion is approximately two times higher, however, it is compensated by the dynamics of impedance controller in order to obtain the desired response.

## 8.7 Impedance control

Impedance control (or admittance control) was developed by N. Hogan [12]. It uses two basic laws of physics such as Newton's second law (see eq. 8.20) and D'Alembert's law (see eq. 8.21). It can be described as a second order dynamic system. Figure 8.12 represents the impedance control scheme using a mass-damper-spring system. In this relationship, impedance is the passive reaction that a robot performs when it is disturbed by external forces. In contrast, admittance control is the active reaction of the robot to such external forces. The "spring coefficient" or stiffness parameter  $K$  defines the force output for a tension or compression of the spring produced by a force  $F$ , its value is taken as 0 in order to eliminate fluctuations and abrupt and unexpected stops of the platform to ensure safety for the operators; and the "damping coefficient"  $D$  is the force output for a velocity input of the displacement  $x$ , "mass coefficient" describing the inertia of the system. The rationale for choosing this controller for the purpose of this research is that this approach allows to control not only separate variables like force or position, but changes the dynamics of the system.

$$\sum F_{ext} = ma \quad (8.20)$$

$$\sum F = 0 \quad (8.21)$$

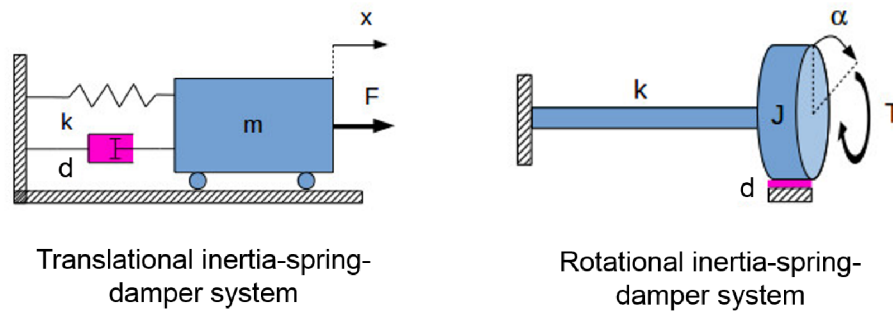


Figure 8.12: Impedance controller representation

Equation 8.22 describes the impedance controller output for translational motion.

$$M\ddot{x}(t) + D\dot{x}(t) + Kx(t) = F(t) \quad (8.22)$$

Equation 8.23 describes the impedance controller output for rotational motion.

$$J\ddot{\alpha}(t) + D\dot{\alpha}(t) + K\alpha(t) = T(t) \quad (8.23)$$

In current application the  $\dot{x}(t)$  and  $\dot{\alpha}(t)$  velocity outputs of the impedance controller are in focus. The parameter  $K$  is used to denote stiffness. In the context of ideal position control, an infinite value of stiffness is desired, whereas in force control, zero stiffness is desired. However, as stated by Katsura and Ohnishi (2006) [61], the use

of  $K$  is not recommended as it does not have a positive impact on the interaction experience. Furthermore, the use of this parameter has been observed to result in undesirable outcomes such as an abrupt stop of the platform. The force applied to the handle bar is fed to the input of the impedance controller. If this force is constant and  $K$  does not equal to 0 (if  $M > 0$  and  $D > 0$ ), it could cause the cart to stop at some point  $x > 0$ . This behavior is not desirable, therefore, the value of  $K$  should equal to 0. Impedance control methods comparison is provided below. There are several different methods of implementing impedance control for manipulators or other mechanical systems. Some of the most commonly used methods include the following:

1. Voltage-controlled impedance was introduced in 1964 by Moog [62]. Their work has been continued in many fields, particularly by Herr et al. [63] in 2009. In this method, the impedance of the system is controlled by modulating the voltage applied to the actuators. It can be suggested that the method is fast and easy to implement, but it is sensitive to changes in the load and the environment and may not provide consistent performance.

2. Current-controlled impedance was proposed by Marshak [64]. This method involves modulating the current supplied to the actuators to control the impedance of the system. It is generally more robust than voltage-controlled impedance, but it requires more complex hardware and may be slower to implement.

3. Hybrid impedance control was mentioned in the research paper by e.g. Sartori [65] in 1968. This method combines passive impedance control with active control to provide a more flexible and robust system. The passive compliance of the system is used to provide a baseline impedance, while active control is used to adjust the impedance in response to changes in the load or the environment. This method can provide good performance, but it may be more complex to implement and require more computational resources.

4. Inverse dynamics impedance control was described in Petrov and Yuchanov in 1980 [66]. This method involves estimating the forces and torques acting on the system and using these estimates to compute the desired impedance. It is a model-based approach that can provide good performance, but it requires accurate models and may be sensitive to model errors.

5. Computed torque impedance control referred to by [67]. This method involves estimating the desired torque at each joint and using this estimate to compute the desired impedance. It is a model-based control method that requires an accurate model of the manipulator dynamics and kinematics. It is useful for controlling manipulators with high precision and stability, but it may be sensitive to model errors and require more computational resources. Computed torque impedance control is often used in conjunction with impedance control methods such as hybrid impedance control or inverse dynamics impedance control to improve the performance of the manipulator. It is commonly used in robotic applications such as assembly, inspection, and medical procedures.

For the case of this research, inverse dynamics impedance control was selected because it is generally believed to provide a reliable performance and does not require extensive computational resources.

## List of variables

### Hardware design

$n_w$	Desired wheel rotational speed in revolutions per minute (rpm).
$v_d$	Desired linear velocity of the wheel.
$D_w$	Diameter of the wheel.
$G_r$	Gear ratio between motor and wheel.
$n_m$	Rotational speed of the motor.
$z_w$	Number of teeth on the wheel gear.
$z_m$	Number of teeth on the motor gear.

### Cart kinematics

$v$	Linear velocity.
$w$	Angular velocity.
$R$	Radius (distance between the point for which linear speed is calculated and rotation axis).
$v_{\Sigma cart}$	Total linear velocity of the cart.
$D_w$	Diameter of the wheel.
$\phi$	Angular orientation.
$x_0, y_0$	Coordinates of point $C_0$ .
$\dot{x}_0, \dot{y}_0$	Derivatives of $x_0$ and $y_0$ with respect to time.
$w_{cart}$	Angular velocities of the cart.
$w_{wheel}$	Angular velocities of the wheel.
$L$	Distance in the kinematic diagram.
$w_{\Sigma cart}$	Total angular velocity of the cart.
$D_w, W_w$	Diameter and width of the powered wheel.
$v_{cart\_sum}$	Total linear velocity of the cart.
$w_{cart\_sum}$	Total angular velocity of the cart.
$w_{wheel\_left}$	Angular velocities of the left wheel.
$w_{wheel\_right}$	Angular velocities of the right wheel.
$\dot{X}$	Control vector.
$\dot{\theta}$	Rotational speeds vector.
$J_{aco}$	Jacobian matrix for cart kinematics.
$\ddot{X}$	Total linear and angular acceleration.
$J_{aco}^{-1*}$	Pseudo-inverse matrix of $J_{aco}$ .
$\ddot{\theta}$	Angular accelerations of the wheels.
$\epsilon_{wheel\_left}$	Angular accelerations of the left wheel.
$\epsilon_{wheel\_right}$	Angular accelerations of the right wheel.
$a_{cart\_sum}$	Total linear acceleration of the cart.
$\epsilon_{cart\_sum}$	Total angular acceleration of the cart.

### Human operator interface

$\mathbf{F}_{\Sigma h}$	Total horizontal force.
$\mathbf{F}_{hr}$	Horizontal force applied to the right side.
$\mathbf{F}_{hl}$	Horizontal force applied to the left side.
$\mathbf{T}_{\Sigma h}$	Total rotational torque for the motion around the axis that goes vertically through the central point $C_0$ .
$\mathbf{W}$	Width of the system.

## 9 Human operator study

In the dynamic realm of industrial automation, the design and control of mobile platforms play an important role in achieving efficient and seamless material transportation. The accurate representation of these systems through mathematical models is necessary to analyze their behavior, predicting their performance, and ultimately optimizing their operation. The development of a comprehensive mathematical model for an industrial cart can be found in the appendix B. There we aim to provide a framework to understand cart's dynamics, control strategies, and system optimization.

In this chapter we design a mathematical model of a human operator who is pushing a cart with two hands. This model involves several factors, including the mechanics of the human body, the dynamics of pushing, and the human-cart interaction. We will use the following steps in order to implement the model:

- Identify the variables involved in the system. For example, we might consider the position, velocity, and acceleration of the cart, as well as the angles, forces, and torques applied by each hand.
- Define the coordinate system that describes the position and orientation of the cart and the human. This could be a 2D system for the sake of simplicity.
- Create a model of a human body using rigid segments, such as the torso, upper arms, lower arms, and hands. Each segment can be represented as a mass with inertia and connected by joints that allow movement. We use simplified assumptions, such as assuming the arms are straight or including joint constraints to limit their range of motion.
- Determine the forces and torques applied by each hand to push the cart. This could involve considering factors like the grip force, body weight distribution, and the interaction between the human's hands and the cart's handles. The frictional forces between the cart and the ground were considered.
- Apply Newton's laws to derive the equations of motion for the cart and the human segments. This involves considering the forces and torques acting on each body segment and integrating them over time.
- Use numerical methods or simulation software to solve the equations of motion. This allows to simulate the system's behavior and observe how the human's actions affect the cart's motion.

The concept of emotional and physical feedback in human-robot interaction (HRI) was developed and studied by researchers in the fields of robotics, psychology, and human-computer interaction and are described below. These researchers set an example of recognising the importance of emotional and physical feedback in HRI and conducted research to understand how these types of feedback can affect a person's overall experience of interacting with a robot in various disciplines. These are just a few research papers published to date by researchers who have worked on the concept of emotional and physical feedback in human-robot interaction (HRI). The use of haptic feedback in HRI was discussed in Chotiprayanakul et al., [86], social and emotional feedback was covered in e.g. Breazeal [87], Greczek et al. [88], and Dautenhahn [89], and ethical implications were covered in e.g. Bröhl et al. [90], affective and multimodal feedback in HRI was described in e.g. Moubayed et al. [91] and Boudoin et al. [92].

The two types of feedback - emotional and physical - are considered in the current research work because they are believed to be two of the main factors that influence the feedback of an individual. There are various methods that can be used to evaluate emotional and physical feedback in response to interaction with a robot, for example:

1. Self-report measures, which are often subjective measures that rely on individuals to report their own emotional and physical responses. The examples of self-report measures include surveys, questionnaires, and interviews.
2. Behavioral measures involve observing and recording an individual's behavior during interaction with a robot. The examples of behavioral measures include facial expression, body posture, and gestures.
3. Physiological measures involve collecting data on physiological responses to interaction with a robot, such as heart rate, skin conductance, and blood pressure.
4. Neural measures involve collecting data on brain activity during interaction with a robot, such as using electroencephalography (EEG) or functional magnetic resonance imaging (fMRI). In the case of the current research, we consider physical impact as an influence of various factors on our neural system. Emotional feedback is referred to as how this influence is evaluated by an individual.

## 9.1 Research workflow development

“That’s one small step for man,  
one giant leap for mankind”

---

Neil Armstrong

In order to find a reliable solution for human-robot interaction we should understand the nature of human motion, individual motivation and stimulus. This chapter starts with the explanation of the human step nature.

Several studies have been conducted to understand the methods and techniques behind human locomotion. In order to study and investigate human locomotion,



researchers propose modeling human locomotion as an easy and simple way to get a clear picture of how human locomotion is performed. Modeling in terms of masses, links, and joints could demonstrate the characteristics of human motion. Moreover, modeling could provide theories and techniques for locomotion. The general method for modeling the human walking gait is the inverted pendulum. The body is supported by the leg and rotated around the ankle joint 9.2. This modeled system is considered to be a passive system, whereby the dynamic motion depends upon the gravitational force and the body's momentum. In order to complete a one-step cycle, the momentum has to be sufficient to provide forward motion. Moreover, the velocity must not be too large, because the normal acceleration could become greater than the gravitational acceleration that acts in the opposite direction [68].

Two of the most commonly presented theories that address the nature of human gait popular in our time. The first theory proposed by Saunders et al. defines six major determinants of gait [69]. It states that the six major determinants are pelvic rotation, pelvic tilt, knee and hip flexion, knee and ankle interaction, and lateral pelvic displacement. The serial observations of irregularities in these determinants provide insight into the individual variation and a dynamic assessment of normal and pathological step.

The second theory of human walking describes the locomotion by using an inverted pendulum model. It states that the stance leg behaves like an inverted pendulum, allowing for economical gait. The advantage of a pendulum is that it conserves mechanical energy and thus requires no mechanical work to produce motion along an arc. Observations of mechanical energy exchange and leg-length change during a single-limb support provide a strong indication of pendulum-like behavior. The figure 9.1 depicts the process of human walking.

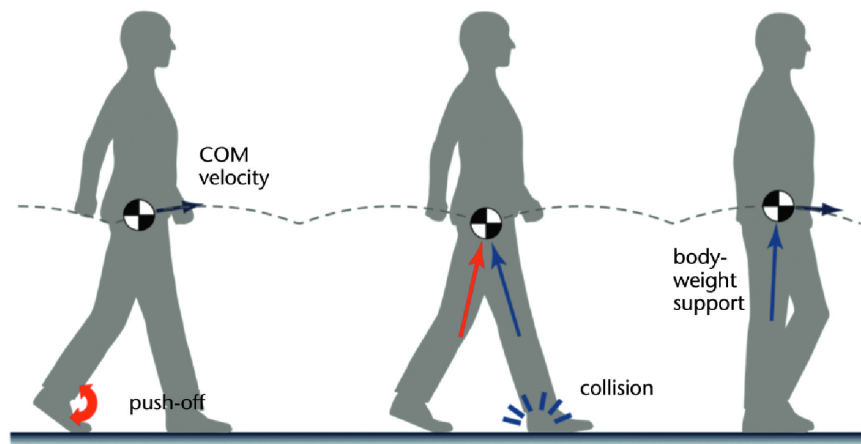


Figure 9.1: Process of the dynamic walking [70]

We compared the two abovementioned approaches and selected the model of an inverted pendulum as it allowed to study the effect of the human gait on the interaction process. This model is fairly simple to implement and is not demanding in terms of the computation power. It also helps to consider a number of important characteristics, such as the mass of the human body, its height, length of the legs,

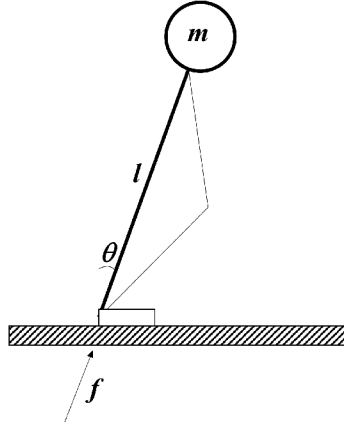


Figure 9.2: Model of an inverted pendulum with a fixed length [68]

the walking speed. The results of the assessment of both models are combined into the table. Inverted pendulum model can cover variations of body parameters that might have a significant impact of human-cart dynamics while pushing, pulling or turning the cart. From the perspective of human walking, there are two important parameters that affect the process of human gait significantly. One parameter is mass of the human body, because a body with the increased mass generates higher kinetic energy while walking. As a result, this energy effects human acceleration and forces that acts on the handlebar of the cart. Another important parameter is the length of the human legs, because it affects the length of possible maximum step as well as the amplitude of the human center of gravity (COG) oscillation. The length of the step together with the rate at which an individual changes the legs affects the overall speed of walking.

A mathematical model of inverted pendulum consists of equations that describe the dynamics of the system. The ground reaction force of walking gait model in terms of an inverted pendulum is determined by:

$$mg \cos \theta - ml \cos \ddot{\theta}^2 = f \quad (9.1)$$

where  $m$  is mass of the human body,  $g$  - gravity constant,  $\theta$  - reaction force angle,  $l$  - length of the leg,  $f$  - reaction force. Sometimes, the leg length changes during the walking cycle. The dynamic equation of model system is different from the previous model, as shown below:

$$mg \cos \theta + m\ddot{l} - ml \cos \ddot{\theta}^2 = f \quad (9.2)$$

The walking human model was implemented using the Python programming language. It is possible to adjust the mass of the human body, its height, length of the legs, the walking speed. Visualization of walking process with different model parameters is provided in the figure 9.3.

Another important factor that plays a great role in human - cart interaction is a mechanical impedance of the human arm. It describes the motion ability of the upper limb. This interaction imposes forces on the hand and can also destabilize

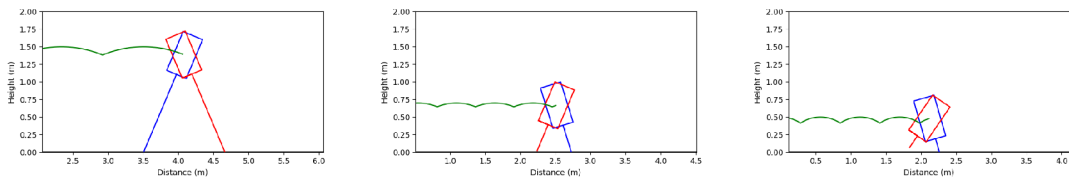


Figure 9.3: Examples of human walking with different model parameters

motion. Alternatively, humans have excellent capabilities to manipulate objects. This means that the central nervous system (CNS) is able to adapt to various task dynamics. For instance, one may experience difficulties opening a door for the first time due to an unknown friction. However, after many trials the appropriate force to be exerted is learned, and one opens the same door without any difficulty and even without thinking about it. This situation may be regarded as the impedance control [12] which can be described as an effective strategy of the nervous system to deal with the kinematic variability due to neuromuscular noise and environmental perturbations.

Biologically, muscle comes with two sections which are thick (myosin) filaments and thin (actin). This part is shown in figure 9.4. Myosin filaments slide against actin which tend to shorten the activated muscle. Neural activation signals are received when the muscle is activated. That signal consists of several spikes. The amount of force it produces depends on the frequency and magnitude of spikes.

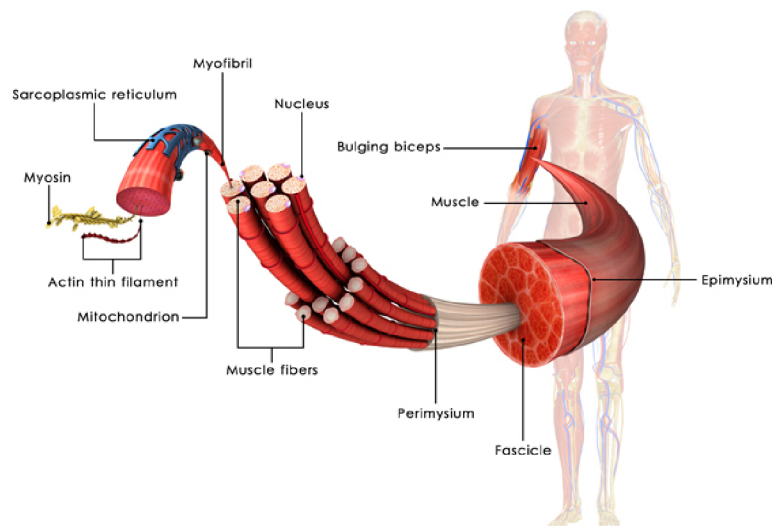


Figure 9.4: Myosin and actin filaments in a muscle [71]

In addition, muscle tension is counted on both muscle length and the velocity of its extension. Experiment was made by Burdet [72] to measure stiffness (K) and damping (B) for a cat's muscle. As a result, when the length is equal to half of

the initial length, the muscle cannot generate the force and the same is right for the velocity. However, the force increases as the muscle length or the velocity of its extension increases. Hence, the impedance of a single muscle changes with the force it generates.

From the perspective of biomechanics systems, Burde's [72] study introduced two types of muscle models which are the Maxwell model and the Voight model. As it can be seen from the figure 9.5, the Maxwell model consists of a spring in series with a damper while the Voight model has the spring in parallel with a damper. From the prospective of the input, it shows that the force step input test and the displacement step input test from the Voight model are more realistic if compared to the Maxwell model [73]. Even though the Voight model is more realistic, the limitation of both models is that none of them is capable of modeling the active contractile property of a muscle. In the following years, a number of researchers came up with a new modeling based on Voight model in order to predict the mechanical impedance of a human's upper limb. It can help us to rationalise and use the model of simulating the dynamics of upper limbs of the human operator.

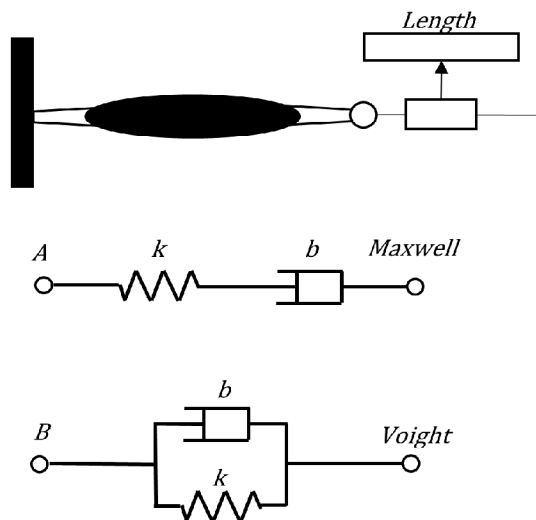


Figure 9.5: Maxwell (A) and Voight (B) muscle models

Mechanical impedance modeling is an important stage in order to determine the quantitative assessment of the system. Each element represents the function of the real human arm. In this section, various modalities are elaborated. It can be represented in two ways which are the structure model (see figure 9.6) and the mathematical model.

Previous studies used the mass-spring-damping (MSD) systems to a great extent in order to construct a mechanical impedance of human arm [73]-[74]. The mass-spring-damper model is shown in the figure 9.6. This is the second order dynamic system where  $m_e(t)$ ,  $b_e(t)$ , and  $k_e(t)$  are the impedance parameters which denote the mass, damping factor, and stiffness of the arm, respectively; and  $f_e(t)$  represents the force exerted to the arm. These researchers performed a number of experiments on

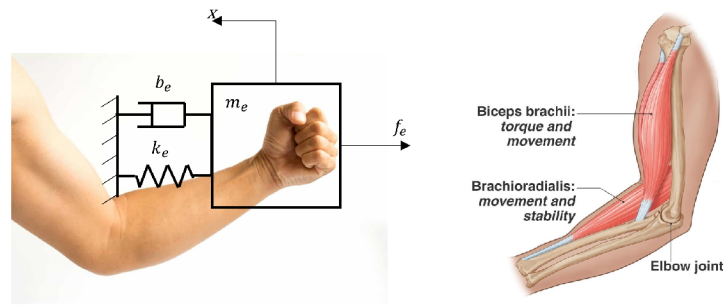


Figure 9.6: Mechanical impedance of the human arm. Structural model [73]. Arm illustration is adopted from [71]

mechanical impedance of a human arm. Several independent mathematical models are proposed for the representation of the human arm movement. Recently, the MSD model has been improved to investigate mechanical impedance during the movement of the arm [73]. The muscle activation was included as a dependent parameter [75]. However, this model was developed assuming that the system had simple joints and did not consider complex muscle mechanics and geometry because dealing with a muscle is not easy as its shape can be changing and irregular. As reported by Speich et al. [76] and Rahman et al. [77], a model with five parameters with additional spring and damper to better approximate the dynamics systems was developed. Then, Wang et al. [78] studied the mechanical impedance during maintained posture and reaching movements in order to analyze human impedance changes depending on the situation. Lagrangian approach is applied to develop the mathematical model of human arm during movement. Tanaka et al. [79] proposed an active-steering control method that uses human hand impedance properties.

## 9.2 Human Factors, Hazards and Limitations

The industrial cart manipulation is mainly performed by pulling backward and pushing forward with two hands. Pushing is preferable to pulling for several reasons. Firstly, operator's feet are often run over by the cart when pulling. It becomes even more dangerous in case of powered vehicles. If a person pulls while facing in the direction of travel, the arm is stretched behind the body, placing the shoulder and the back in a mechanically awkward position, increasing the risk of injury. Alternatively, pulling while walking backwards may be called a recipe for an accident, because the person is unable to view the path of travel. Possible poses of the human-operator during manipulation with industrial cart are shown in the figure 9.7.

The research of Lee [80] demonstrates that people can usually exert higher push forces than pull forces. In some situations, pulling may be the only viable means of movement, but such situations should be avoided wherever possible, and minimized when pulling is necessary. Because of the complex nature of body motion during pushing and pulling, no numerical standard has yet been developed that can be

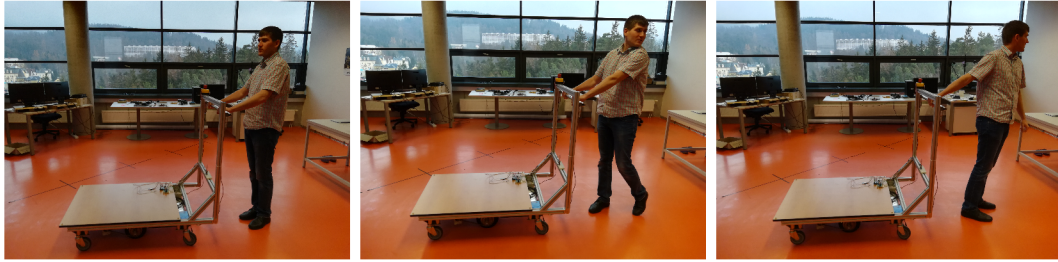


Figure 9.7: A few possible poses of the human operator during manipulation with the cart

directly applied in the industry. The amount of force that a worker can develop in case of translational and rotational motion depends on many factors. A sample list of factors is listed as follows:

- body weight and strength
- height of force application
- direction of force application
- distance of force application from the body
- different positions
- posture (bending forward or leaning backward)
- friction coefficient (amount of friction or grip between floors and shoes)
- duration and distance of push or pull

One of the earliest studies on the factors that influence manual handling capacity was conducted by Banerjee and Chattopadhyay [81] in 1959. In their study, the researchers found that the maximum force that a worker could exert while pushing or pulling a load was influenced by the load's weight, the angle at which it was applied, and the worker's body position. Other studies have also identified factors such as the worker's gender, age, and anthropometric dimensions as influencing manual handling capacity. More recent research works focused on the role of ergonomics and the design of the task and tools in improving manual handling capacity and reducing the risk of musculoskeletal disorders. They identified factors such as the height of the load, the grip size of the tools, and the presence of handles or grips as important considerations in manual handling tasks. Some examples of research on the role of ergonomics and the design of the task and tools in improving manual handling capacity and reducing the risk of musculoskeletal disorders include the following works, as stated in [82]: Lee et al. (1991) [83] investigated the effects of handle height on lower-back loading in cart pushing and pulling. Haisman et al. (1972) [84] examined the effects of different types of handles and grips on manual handling performance and the risk of injury for seven male volunteers. Jäger et al.

(1984) [85] analyzed the effects of different situations causing high postural stress during the transport of dustbins.

These studies also provided recommendations for the design of manual handling tasks and tools to improve manual handling capacity and reduce the risk of musculoskeletal disorders. The table 9.1 contains the upper force limits for a variety of pushing and pulling tasks. They indicate the amount of force that a worker should not overcome. It is important to note here that the forces in the tables are not the same as the weight of objects being pushed and pulled. This difference means that we cannot use these upper force limits as recommendations for limits for weights that can be pushed or pulled in the workplace.

The values in Table 9.1 show the upper limits of forces for horizontal pushing and pulling. These limits should not be exceeded in work situations. In fact, it is better and safer if pushing and pulling tasks require lower forces, particularly, if the task requires:

- pushing or pulling an object when the hands must be above the shoulder or below the waist level
- exerting a force for longer than 5 seconds
- exerting a force at an angle not directly in front of the body, e.g., not "straight on"

Higher forces (up to 675N or about 165 lbf or 75 Kgf) can be developed where a worker can support his body (or feet) against a firm structure.

Condition	Force limit(Newtons, lbf, kgf)**	Examples of Activities
A. Standing		
1. Whole body involved	225 N (50 lbf or 23 kgf)	Truck and cart handling. Moving equipment on wheels or casters.
2. Primary arm and shoulder muscles, arms fully extended	110 N (24 lbf or 11 kgf)	Leaning over an obstacle to move an object. Pushing an object at or above the shoulder height.
B. Kneeling		
	188 N (42 lbf or 21 kgf)	Removing or replacing a component from equipment while performing maintenance work. Handling in confined work areas such as tunnels or large conduits.
C. Seated		
	130 N (29 lbf or 13 kgf)	Operating a vertical lever, such as a floor shift on heavy equipment. Moving trays or a product on and off conveyors.

Table 9.1: Recommended Upper Force Limits for Horizontal Pushing and Pulling [6]

*\*\* Units of force are: Newton (N), kilogram-force (kgf), pound-force (lbf); 10N is about the same as 1 kgf or 2 lbf. The values in each unit system - Newtons, kilogram force and pound force, respectively - are provided in the table because they are used in the literature and while designing instruments, depending on the country of origin.*

Individual characteristics of the operator significantly affect emerging accidents and hazards. The developed system has to consider individual characteristics of a human operator and prevent the operator from exceeding the limits set by industrial and occupational safety guidelines.

### 9.3 Emotional feedback

The goal of this chapter is to describe the test methods to estimate operator's individual perception in response to the motion of the powered vehicle.

In the current study emotional feedback of the human operator is considered important and we had to find the method to evaluate subjective human emotions. One way to estimate the operator's feedback is to use the adjective measures in the rating scale method [93].

This method is used to measure how people feel about various stimuli such as sounds, colors or smells. Another application area of this method is ergonomics. It allows to evaluate emotions about the task environment, machine and robot motion.



The method is known as an evaluation tool based on several step-wise measures in which adjective pairs are located at the opposite poles. In the experiment, the person evaluates their emotions according to the adjective pairs. The goal of this measure is to find suitable impedance controller parameters that allow to perform comfort interaction based on subjective feeling.

Therefore, we selected six adjective pairs and a rating scale in order to perform human factor analysis. The rating scale is shown in the figure 9.8. The selected adjective pairs have the following statements:

1. **"comfortable — uncomfortable"**: This adjective pair should express the human operator feelings in terms of interaction comfort. It describes how precisely the dynamics of the powered cart follows the desired motion of the human operator.
2. **"reliable — unreliable"**: The adjective pair characterizes trust of the human operator in relation to the powered cart. It means that action of the powered cart fits to the expectations of the human operator.
3. **"controllable — uncontrollable"**: We work with the impedance controller for two degrees of freedom. A change or adaptation of the impedance controller parameters affects the ability of the human to control the system. This adjective pair should give the feedback about the controller settings.
4. **"pleasant — unpleasant"**: This adjective pair presents the motivation (willingness) of the human operator to use the powered cart.
5. **"satisfactory — unsatisfactory"**: Human estimation of the interaction task results are characterized by this adjective pair.
6. **"light — heavy"**: This adjective pair characterizes physical abilities of the human operator in the load handling.

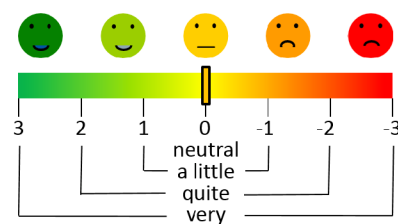


Figure 9.8: Rating scale for the emotional feedback of the human

The evaluation procedure was executed as follows. The operators expressed their feelings by choosing one of seven options in between the opposite poles in each adjective pair according to their impressions about the controller settings. Given the example of the procedure outcome, we could see the test sheet with the following answers, e.g.: "The controller's setting is not comfortable, a little reliable, not controllable, a little pleasant, very light". "Positive" feedback is defined as the mean

value located in the left position and "Negative" feedback is defined as the mean value located in the right part of the scale. In this subchapter we formed and analysed a list of parameters which are used to obtain emotional feedback from the human operator.

## 9.4 Physical feedback

"The thesis target is to reach the state where the operator manipulates the heavy loaded cart with minimal physical effort (pleasant and comfortable interaction). Iterative adjustment of controller parameters with continuous force measurement on the operator-cart interface and following recognition of the human-operator intention is expected."

---

doc. Ing. Petr Tůma, CSc.

This subchapter is devoted to the measurement methods of biological features and markers that help to define the health conditions of a person depending on the interaction between the human operator and the industrial cart. There are a few methods to choose from in this case. They are described below as follows. The Borg scale is used to measure an individual's level of physical exertion during exercise, while the Likert Scale is used to measure attitudes, opinions, or behaviors. Both scales are ordinal, meaning that they assign a numerical value to a person's response, but the interval between the values is not always equal. They are generally used to measure a person's subjective experience. However, the Borg scale is used specifically for measuring only once construct, physical exertion, while the Likert scale can be used for a wide range of topics. The Borg scale ranges from 6 to 20, while the Likert Scale typically ranges from strongly agree to strongly disagree. The advantages and disadvantages of both approaches are described in e.g. Chen et al. in 2002 [94], and Hartley and MacLean in 2006 [95]. We decided to unify the advantages and shortcomings of these approaches in the following chart 9.2 below:

Due to the fact that our goal was to find criteria for human interaction comfort in real-time we used a Borg scale [96] shown in the table 9.3 as a tool for operator's comfort measurement.

	<b>Advantages</b>	<b>Drawbacks</b>
<b>Borg Scale</b>	Widely used in exercise and sports science research. Simple and easy to use, making it accessible to a wide range of people. Can be used to monitor and adjust the intensity of exercise.	Limited to measuring physical exertion. Relies on subjective perception, affected by factors like fatigue, motivation, and pain.
<b>Likert Scale</b>	Can measure a wide range of attitudes, opinions, and behaviors. Widely used in research, facilitating data comparison across studies. Easy to use, accessible to a wide range of people.	Relies on subjective perception, influenced by factors like social desirability bias. Not always clear what the person is agreeing or disagreeing with, leading to confusion.

Table 9.2: Comparison of Likert and Borg Scales

Score	Description
6	
7	Very, very light
8	
9	Very light
10	
11	Fairly light
12	
13	Somewhat hard
14	
15	Hard
16	
17	Very hard
18	
19	Very, very hard
20	

Table 9.3: Borg scale (rate per exertion)

The Borg scale [96] was originally developed by the scientist Gunnar Borg who rated the scale from 6 to 20, which was basically built around a heart rate range. This scale correlates with a person's heart rate or how hard they feel they are working. We use the Borg scale in our experiments to evaluate biological markers of the human - cart interaction. The scales are shown in the table 9.3. In addition to the Borg scale, we used No.1 F4 IP68 Waterproof Smartband for the heart rate measurement. The device is shown in the figure 9.9.



Figure 9.9: No.1 F4 IP68 Waterproof Smartband

We are interested in such biomarkers as pulse, blood pressure, saturation and the number of steps made. The standard use of the band involves the connection to the mobile phone to read the statistical data through the bluetooth interface. The statistics it receives can be visualized in a certain application. The idea was to replace the mobile phone application backend with a custom program, so that it could receive the information on the condition of biological markers and forward this information to the high-level controller.

As a higher level controller a microcomputer Raspberry Pi, version 4 was used. An application called "GATTacker" was used as a tool to perform the task in order to intercept bluetooth packages and carry out the data analysis. As a result, the package structure was identified. This information allowed me to create a Python script which could connect to the smart band from the high-level controller over bluetooth. The script was able to read the pulse, blood pressure and blood oxygen saturation in real time. The tool chain described above allowed me to follow the biomarkers of a human operator during the interaction process with a powered industrial cart. To measure the pulse, blood pressure, and saturation the band used the sensor based on the photoplethysmogram principle.

A photoplethysmogram (PPG) is an optically obtained plethysmogram that can be used to detect blood volume changes in the microvascular bed of tissue. A PPG is often obtained by using a pulse oximeter which illuminates the skin and measures changes in light absorption [97]. A conventional pulse oximeter monitors the perfusion of blood to the dermis and subcutaneous tissue of the skin.

With each cardiac cycle, the heart pumps blood to the periphery. Even though this pressure pulse is somewhat damped by the time it reaches the skin, it is enough to distend the arteries and arterioles in the subcutaneous tissue. If the pulse oximeter is attached without compressing the skin, a pressure pulse can also be seen from the venous plexus, as a small secondary peak.

The change in volume caused by the pressure pulse is detected by illuminating the skin with the light from a light-emitting diode (LED) and then by measuring the amount of light either transmitted or reflected to a photodiode [98]. Because the blood flow to the skin can be modulated by multiple other physiological systems, the PPG can also be used to monitor breathing, hypovolemia, and other circulatory conditions [99]. Additionally, the shape of the PPG waveform differs from subject to subject, and varies with the location and manner in which the pulse oximeter is attached.

Smart band uses an accelerometer MC3413 to detect the number of steps. The parameters of the sensors are demonstrated in the data sheet [100].

In order to design the adaptive interaction controller we have to find a dependency between the emotional feedback of the human operator and a measurable physical equivalent. In the current research, we use the following physical measures per sample time period  $T_{sample} = 60s$ :

1. Mean and standard deviation of absolute interaction force value -  $mean(|F_{interaction}|)$  and  $SD(|F_{interaction}|)$
2. Mean and standard deviation of absolute interaction torque value -  $mean(|\tau_{interaction}|)$  and  $SD(|\tau_{interaction}|)$
3. Mean and standard deviation of absolute linear speed of the cart -  $mean(|v_{cart}|)$  and  $SD(|v_{cart}|)$
4. Mean and standard deviation of absolute angular speed of the cart -  $mean(|\omega_{cart}|)$  and  $SD(|\omega_{cart}|)$
5. Heart rate
6. Blood pressure
7. Oxygen saturation

In this subchapter we formed and analysed a list of parameters which are later used to obtain feedback about the physical well-being.

## List of variables

### Human operator simulation

$\mathbf{x}(t)$	Cart position during walking motion.
$\omega$	Angular frequency, $\omega = \frac{2\pi}{T}$ .

$v$	Linear velocity.
$T$	Period of the walking motion.
$w(t)$	Weight distribution over time.
$W$	Total weight.
$F_1, F_2$	Forces applied by the hands.
$k_1, k_2$	Force coefficients.
$v_{\text{hand}}, v_{\text{cart}}$	Velocities of the hand and cart, respectively.
$m$	Mass of the cart.
$M$	Mass of the human's upper body.
$\ddot{x}$	Acceleration of the cart.
$\theta$	Angular displacement.
$l$	Length parameter.
$I$	Moment of inertia of the upper body.

## 10 Human-cart interaction

### 10.1 Procedure description

This chapter describes the process of human – industrial power assisted cart interaction. The process of moving goods by a human operator with the help of the powered cart on the surface includes the interaction between the cart, the human operator and the environment.

The task of moving cargo can be divided into five stages [7]. The task scheme is shown in the figure 10.1. The first stage begins with the person's intention to carry out the act of moving goods using an industrial cart. The operators have some knowledge about the start and end points of the trajectory, the state of the environment. They can estimate the force needed to be applied in order to move the load and the powered cart from the start to the end points of the trajectory. They also may or may not have experience of interaction with a powered industrial cart.

The second stage is the initial impact. This stage starts the moment human hands touch a mobile cart. The cart is at rest at the point  $P_0$  taken as a point of origin. We take the time of the first touch as the task starting time in the system of a mobile cart. From the point of view of the cart, the force applied by the human is a stochastic variable, since the cart has no information about the real world (knowledge about the weight of the load, the type of surface, the position in space and the desires of a man). Operator's force is divided into rotational and translational components. Then, the desired dynamics of the interaction is set by the relevant impedance controllers. On the output of the impedance controller we obtain the desired linear and angular velocity. The obtained values become reference setpoints for the differential drive system. The motors run in order to reach the reference value and support the motion.

The third stage is the motion task. During this phase the process is about the accumulation of the interaction experience. Human-operator and cart find out the information about the response of the system (the change in the interaction force, acceleration, speed, distance, heart rate, oxygen saturation and blood pressure). In case of a mismatch of the expected response of the system obtained by a person during the first phase with the reaction of the real system, the operator estimates the correction of the applied force according to the new data and adapts to them.

The fourth phase is a positioning task. The operator performs the application of forces to the cart in order to stop the motion and reach the desired position. The fifth stage is the end of the interaction. This stage comes as soon as the person

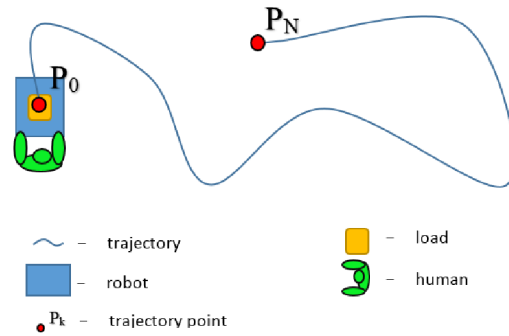


Figure 10.1: Moving cargo task

ceases to interact with the industrial cart. The point  $P_N$  is the end of the interaction and the endpoint of the path. The operator achieved the goal. The cart can perform the analysis of the completed tasks.

In the phase of the positioning task, the distances to the target and the actual traversed path are not equal. Over-reaching the target is influenced by the support of a power assistance system. In this case, the operator must perform additional manipulations to return to the target point. If power assistance is insufficient and cannot go beyond the total value of friction forces that resist to motion, then the distance to the target and the actual traversed path are equal, but the operator spends additional effort to overcome the friction forces.

## 10.2 Raw data analysis and feature detection

“Measurement is the first step that leads to control and eventually to improvement. If you can’t measure something, you can’t understand it. If you can’t understand it, you can’t control it. If you can’t control it, you can’t improve it.”

---

H. James Harrington

Figure 10.2 shows force sensors information when the human assistance ratio is bigger than the desired value and the mobile cart moves faster than the human-operator wants it to move. Periodic oscillations around -40/-50N in the middle of the curve demonstrate the human steps during the motion. Using this information we can estimate the motion rate, the human step time, the number of steps, the step length. Oscillations around zero in the beginning and at the end of the curve characterize the noise caused by the powered cart motion.

According to the measures defined in the chapter 9.4 we developed a few feature detection techniques to estimate them. In our application we detect human gait by



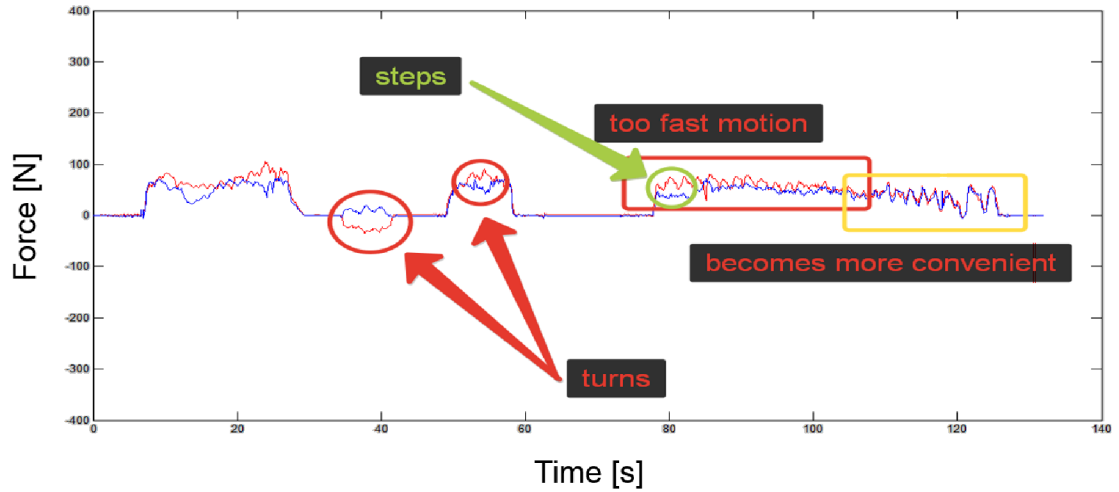


Figure 10.2: Raw data sample from pHRI handlebar

processing the filtered signal that comes from tensiometers located at the handle bar. At a later stage, the peak detection and error cancellation algorithm was applied to the signal. At the pipe output we received the information about the amount of steps per task, step time (mean+std), step length (mean+std). The example of the processed data is shown in the figure 10.3.

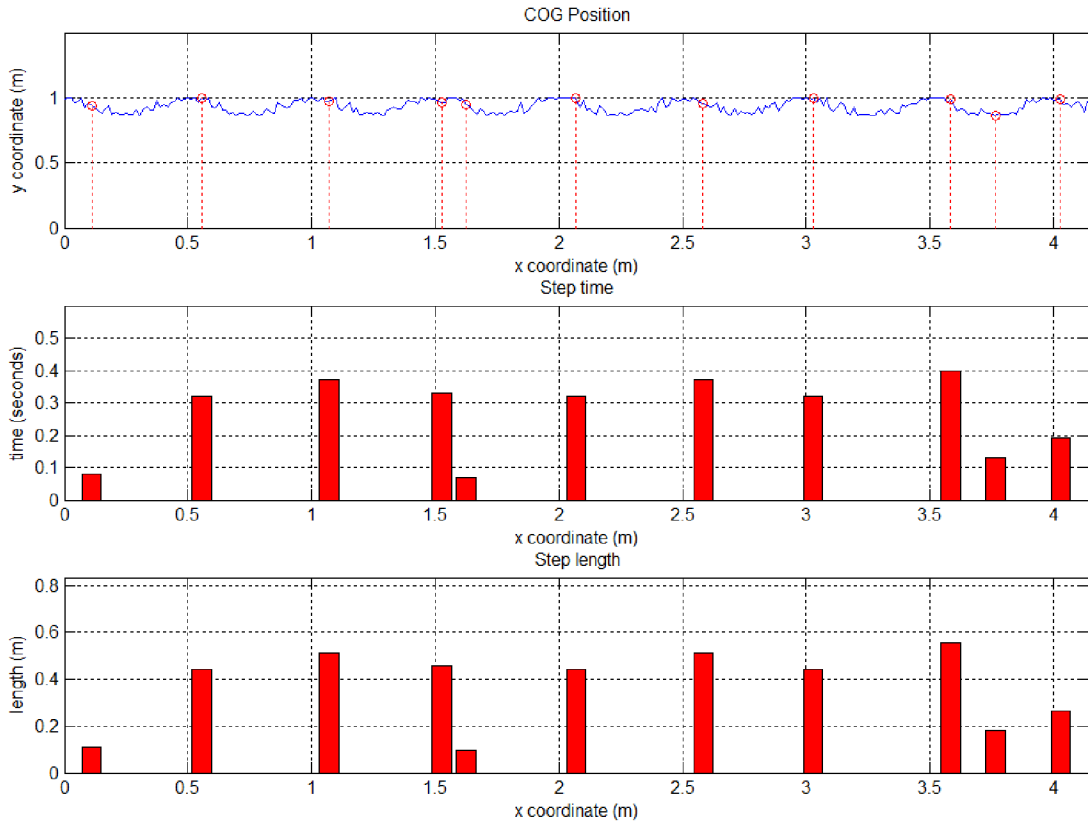


Figure 10.3: Human gait feature

The top line graph shows the fluctuations of the COG position. The red dotted line depicts the moment at which the gait (a single step) was identified with the use of feature detected technique. The middle histogram shows the time spent by the operator to make this step in seconds. The bottom graph illustrates the estimated step length in meters. This procedure of measuring the step, its time and length helps to understand the individuality of an operator, thus making it possible to identify operator's parameters and better adapt to their gait. The fluctuations of the center of gravity (COG) is used to estimate the step length of the human operator for enhanced adaptation of the mobile platform.

### 10.3 Effect of the impedance control

We conducted several experiments with various settings of the controller. In each experiment the operator cyclically performed a front and back motion with the powered cart. A gradual increase of the virtual inertia (mass=2, 5, 10, 18) is shown in the figure 10.4. As we can see, the operator's applied force required to transport the cargo is reducing (lines change from black to green). However, upon further reduction of the ratio (red line), there was a situation in which the momentum generated by the support system created uncomfortable interaction conditions and

operator had to make significant efforts to implement the desired motion.

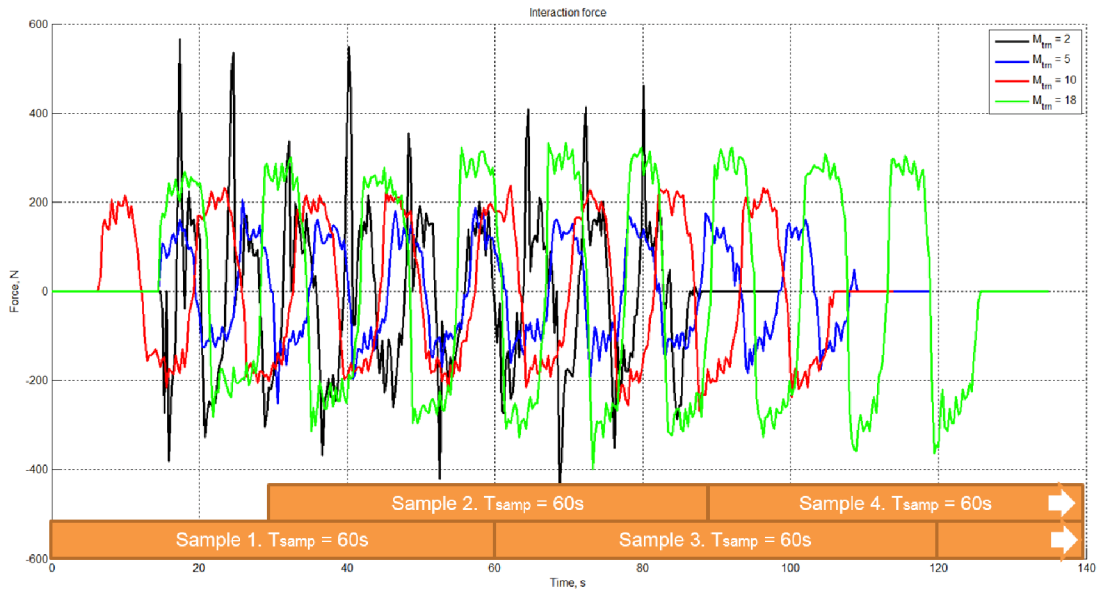


Figure 10.4: Change of interaction force with different settings of the impedance controller [54]

The graph shows the standard derivative of the absolute value of the interaction force using various settings of the impedance controller. We change the values of the impedance controller, i.e. its mass component (virtual mass). The time lapse of the sample is 60 seconds, the number of measurements is 120, which means we can generate 3 data samples.

In these cases when the mass component of the impedance control provides minimum or maximal value, the operator has to put a lot of effort to move the loaded trolley. If we consider both the standard derivative and the mean value it is noticeable that it requires a lot of effort from an operator. The reason for that was described in the figure 10.4 - the operator applies force which is transferred by the impedance controller into setpoints for the differential drive system. In case of small mass component, the task for the motor appears to be large. The engine works with a greater speed which means that the operator has to stop the trolley. On the contrary, if the operator stops the trolley abruptly, the engine gets a large task and start moving the trolley backwards, again, the operators have to stop it to prevent their feet from being run over.

In case of a large mass component, vice versa, the initial force is high, but the task for the engine is small, which means that the trolley does not help the operator to a desired extent. As a result, none of these modes of mass component seems to work well. The comfort of the human operator largely depends on the impedance controller settings. The cart is usually pulled or pushed with two hands. However, if the load is small (light), the cart could be handled with one hand or even with fingers. Each human hand has its inertial, damping and stiffness component (property) as described in the section 9.1. In the Figure 10.5, the change of the

standard deviation of interaction force is demonstrated with the sampling time of 60 seconds using various mass coefficients of the impedance controller. As it could be seen from the graph, the higher the mass parameter, the higher the force applied by the operator. However, if the mass coefficient is relatively small, operator applies significant force. It could be explained by the fact that the selected parameters provide more support than needed which results in additional efforts of the operator to complete the desired motion.

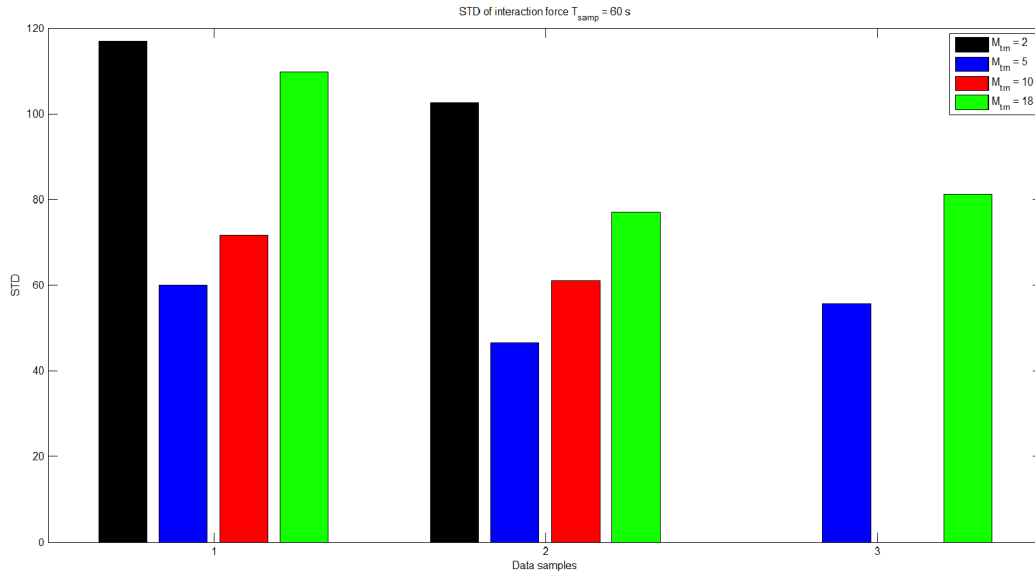


Figure 10.5: Change of interaction force with different settings of the impedance controller [54]  $T_{samp} = 60s$

The force standard deviation (Operator force change difference) takes larger values when the mass coefficients of the impedance controller are either too large, or too small. Significant fluctuations of the interaction force are not desirable as it leads to the discomfort of the human operator. However, it is visible from the graph that there are specific settings of the impedance controller that allow to reduce the range of fluctuations of the interaction force. These settings shown in blue lead to comfortable interaction between the operator and the platform. It confirms the findings from [77] and [36].

In the Figure 10.6 the change of the mean interaction force is demonstrated with sampling time of 60 seconds using various mass coefficients of the impedance controller. As it could be seen from the graph, the higher the mass parameter, the higher the force applied by the operator. However, if the mass coefficient is relatively small, operator still applies significant force. It could be explained similarly to the case with the standard deviation described above.

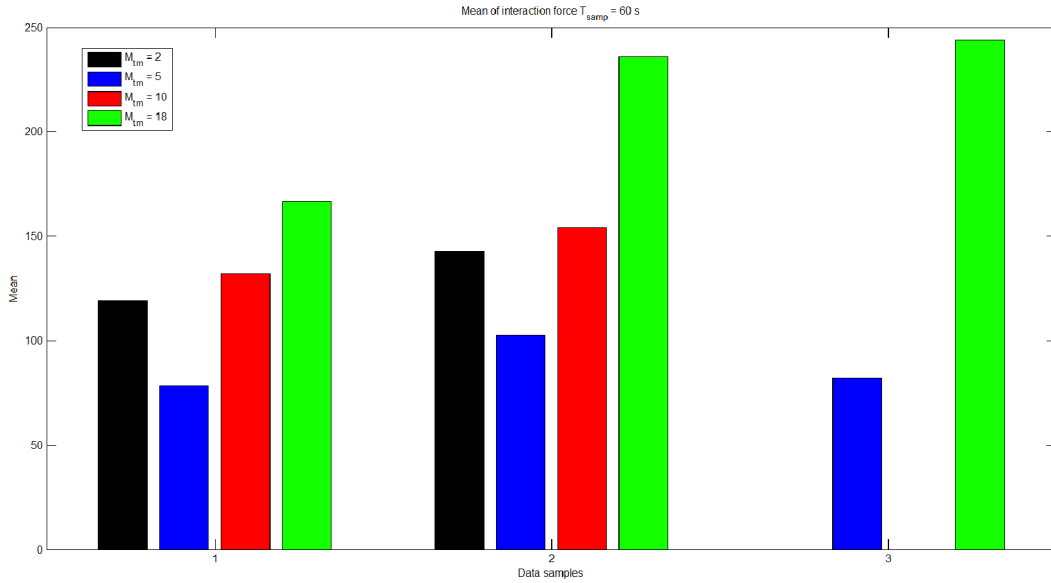


Figure 10.6: Change of interaction force with different settings of the impedance controller [54]  $T_{samp} = 60s$

The interaction force mean takes larger values when the mass coefficients of the impedance controller are either too large, or too small. Increase in the virtual mass (corresponding coefficient of impedance controller) leads to an increase in the applied force causing discomfort. On the other hand, decreasing virtual mass allows the operator to reduce effort. With small values of the mass coefficient but significant real mass (in our case, cart load should be over 50 kg), the operator needs to apply extra effort to implement the desired motion. It is visible from the graph that there are specific settings of the impedance controller that allow to reduce effort. These settings shown in blue lead to comfortable interaction between the operator and the platform. It confirms the findings from [77] and [26].

In the Figures 10.7 and 10.8 the change of the mean interaction force is demonstrated with sampling time of 30 seconds using various mass coefficients (2, 5, 10, 18) of the impedance controller. As it could be seen from the graph, the tendency is true for time period of 30 seconds as well. The higher the mass parameter, the more force is applied by the operator.

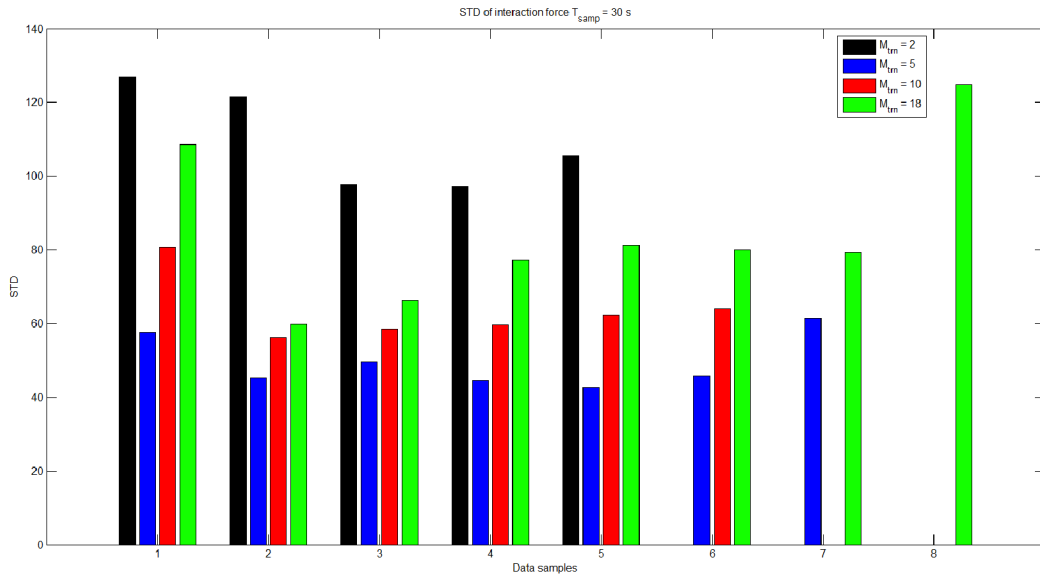


Figure 10.7: Change of interaction force with different settings of the impedance controller [54]  $T_{samp} = 30s$

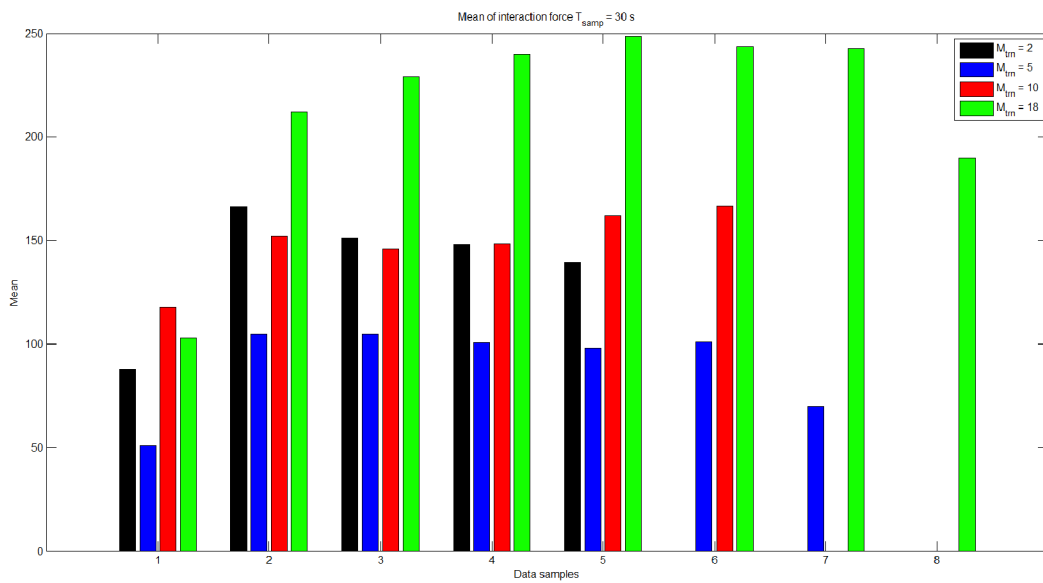


Figure 10.8: Change of interaction force with different settings of the impedance controller [54]  $T_{samp} = 30s$

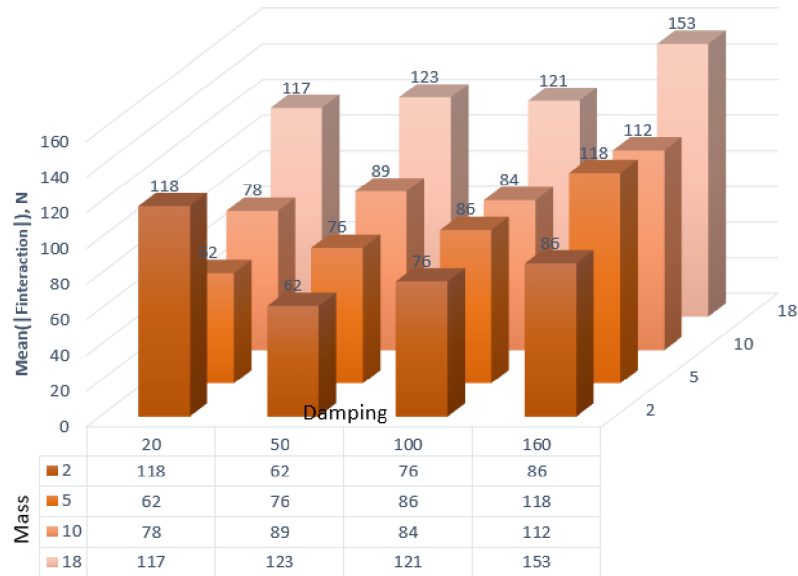


Figure 10.9: Mean value of absolute interaction force for different settings of impedance controller. Sample 1.  $T_{samp} = 60s$

In the Figure 10.9 the change of the mean value of interaction force module is demonstrated with the sampling time of 60 seconds using various mass and damping coefficients of the impedance controller. The interaction force values are shown in the table below the figure where the first row represents values of damping coefficient (20, 50, 100, 160) and the first column represents values of mass coefficient (2, 5, 10, 18). As it could be seen from the graph, the higher the mass parameter and damping parameters, the higher the average value of the module of the interaction force. If the damping and mass coefficients are too small, the operator applies a lot of effort to complete the desired motion as there is more assistance supplied than needed. For the first sample minimal value (62 N), the mean force module could be reached with combination of parameters mass=2 and damping=50, or mass=5 and damping=20.

For the second data sample shown in the figure 10.10 the minimal value of the mean force module (64 N) was reached with the combination of mass=5 and damping=20.

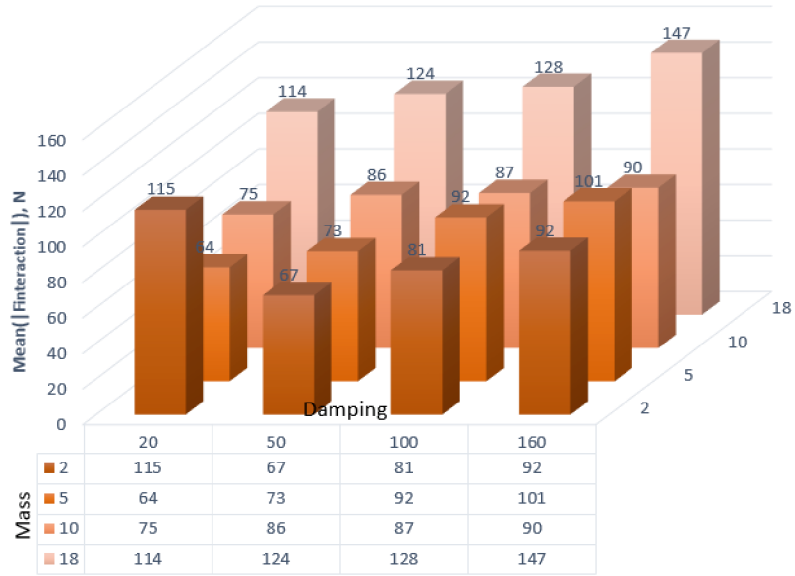


Figure 10.10: Mean value of absolute interaction force for different settings of impedance controller. Sample 2.  $T_{samp} = 60s$ .

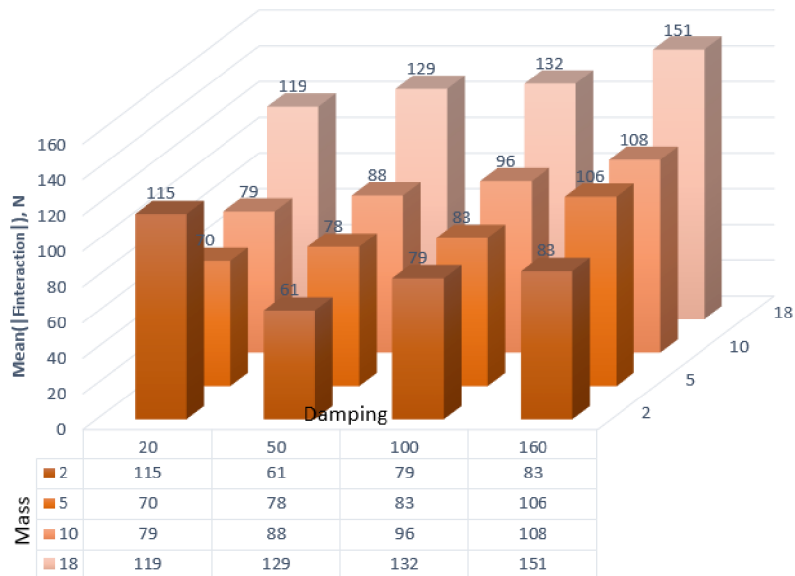


Figure 10.11: Mean value of absolute interaction force for different settings of impedance controller. Sample 3.  $T_{samp} = 60s$ .



The dataset collected from another operator concludes the same trend, see Figure 10.11. The minimal value of the mean force module (61 N) was reached with the combination of mass=2 and damping=50. In this subchapter we studied the effect of the impedance control parameters and learned how they affect the interaction process. It may be concluded that there is a specific setting for the impedance controller that changes for each individual operator. Therefore, the personalised approach is achieved, because each operator has a different setting of the impedance controller which they can consider as comfortable.

## 10.4 Experiment design

This chapter describes the experiments carried out using the mobile platform during the research project. In this chapter we would like to describe the set of performed experiments to measure the interaction parameters between the human operator and industrial cart. The goal of the experiments is to find the relationship between the subjective operator's estimation of the interaction process and the measured physical quantities.

The experiments were executed in the laboratories of the Institute for Nanomaterials, Advanced Technologies and Innovation. The coefficients of static and kinetic friction equal to 1 and 0.7 respectively, because of the fact that the floor material is concrete. Therefore, the laboratory area allowed to simulate material handling tasks related to warehouses, production area, offices and supermarkets.

The subject pool consisted of 5 human operators (three males and two females). Two male operators out of the pool had some experience driving powered vehicles. The other experiment members operated the vehicle for the first time. Both the experienced and inexperienced operators were needed to cover the variance of operator expectations from their interaction with the powered cart. The basic anthropometric data for the operators is presented in the table 10.1.



Figure 10.12: Operator's motion task

The participants had to push and pull a six wheeled powered cart on given trajectories. During the experiment, five types of trajectories depicted in the figure 10.13 were used, such as the linear path with the length of 7m in order to estimate the effect of the translational impedance controller parameters on human feelings during the transnational motion, circular path was used to verify the effect of the rotational impedance controller [101], eight-like trajectory to test the joint work of the controllers and trajectory with the complex shape similar to a real production

N	Parameter	Mean $\pm$ Standard Deviation
1	Age	$28 \pm 5.2$ [a]
2	Weight	$80 \pm 20.8$ [kg]
3	Height	$180 \pm 10.5$ [cm]
4	Legs Length	$90 \pm 12.5$ [cm]

Table 10.1: Operators parameters

scenario as shown in the figure 10.15. In the end of the experiment, human operators could evaluate their feelings of the collaboration on the free-run trajectory.



Figure 10.13: Trajectory setups

A set of barrels to simulate the different load was used. The set consisted of five 30 [l], two 50 [l] barrels and two metal pipes that weighted of 50kg each. All the barrels were filled with water. Their weight was measured before the experiment. As a result, it was possible to change the cart load in a range  $m_{load} \in [0; 340]$  kg. The load set is shown in the figure 10.14 which was changed and adjusted for each experiment and measured accordingly.



Figure 10.14: Load variation

In the current study, we performed the measurement of the emotional feedback. Methods from the section 9.3 were used to estimate the individual feelings of a particular operator. The subjective impressions were documented with questionnaires

and processed. In addition to the emotional feedback, the physical measures were obtained. The readings of the interaction process values were recorded (respectively translational and rotational components of position, speed, acceleration from wheel encoders; orientation, angular velocities and linear accelerations from IMU unit, motors currents from motors current sensors, interaction torque and force from tensiometers).

The developed system allowed to study the effect of different impedance controller settings on the interaction process. The parameter's values for translational and rotational impedance controller settings are combined in the table 10.2, where M is mass, J stands for the moment of inertia, Dtrn is the damping coefficient of the translational motion, Drot - damping coefficient of the rotational motion. The operator's feedback does not seem to cause instability of the platform as we have omitted the configurations that could possibly lead to the unstable platform support. It was carried out to ensure that the learning process could happen under any acceptable load of the platform and would be safe for the operator. Based on the parameter's values, the experimental test sets were generated. We evaluated the effects of the controller's settings on the operator's comfort. The results of the experiments were collected in the chapter 11.

<b>M</b>	<b>Dtrn</b>	<b>J</b>	<b>Drot</b>
2	20	1	10
5	50	4	20
10	100	8	50
18	160	18	160

Table 10.2: Tested impedance controller settings for translational and rotational motion

The linear 7m-long trajectory had the orthogonal lines to mark each meter so that it is suitable for the odometry calibration. Based on this trajectory, we can check if the internal calculated distance corresponds to the measured value. In addition, it is convenient to verify the rotational motion of the cart around its central axis. Trajectory layout including dimensions in cm is shown in the figure 10.16.

Circular trajectory shown in the figure 10.17 allows to evaluate human feelings during the time of turning the industrial trolley around some pivot point.

Another type of track was the 8-shape trajectory. This trajectory brings a significant benefit because it combines the linear and the rotary motions with certain patterns that could easily be detected in the measured data. The path with dimensions in cm is shown in the figure 10.18.

A free-run track 10.15 was designed to model typical logistics scenarios for material handling tasks in the shop floor or warehouse. It combines linear and rotary segments of different length. The detailed dimensions of the trajectory in cm are provided in the figure 10.19.



Figure 10.15: Predefined track. Setup for  $m_{load+cart} = 103[kg]$

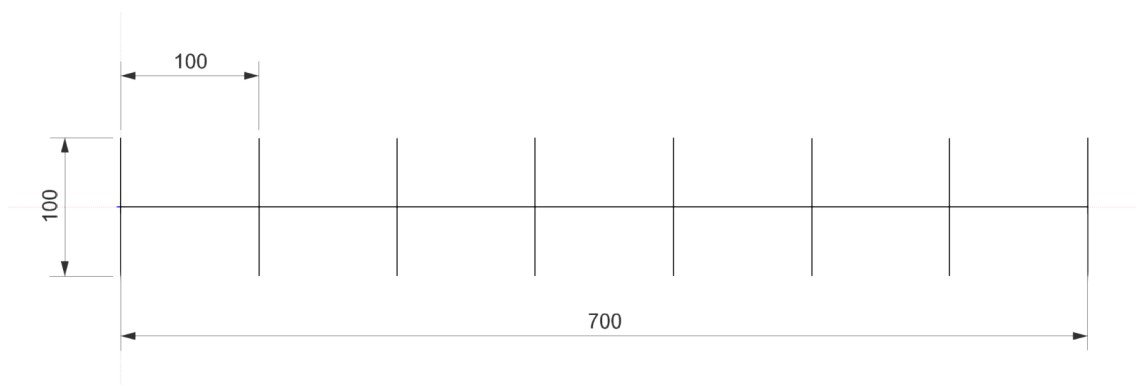


Figure 10.16: Linear track

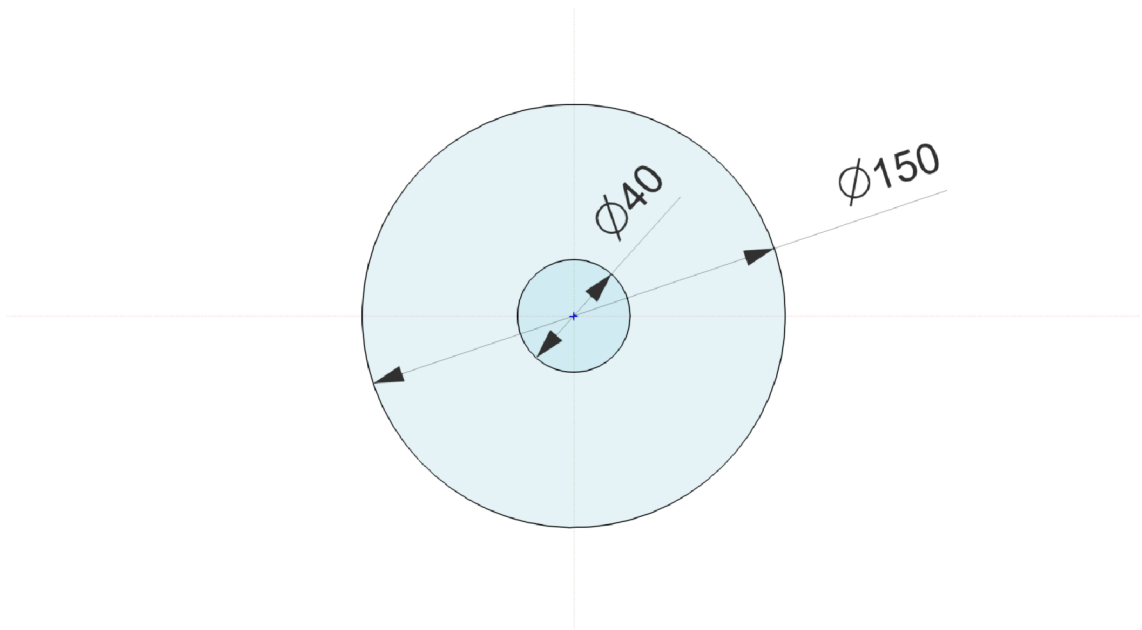


Figure 10.17: Circular track

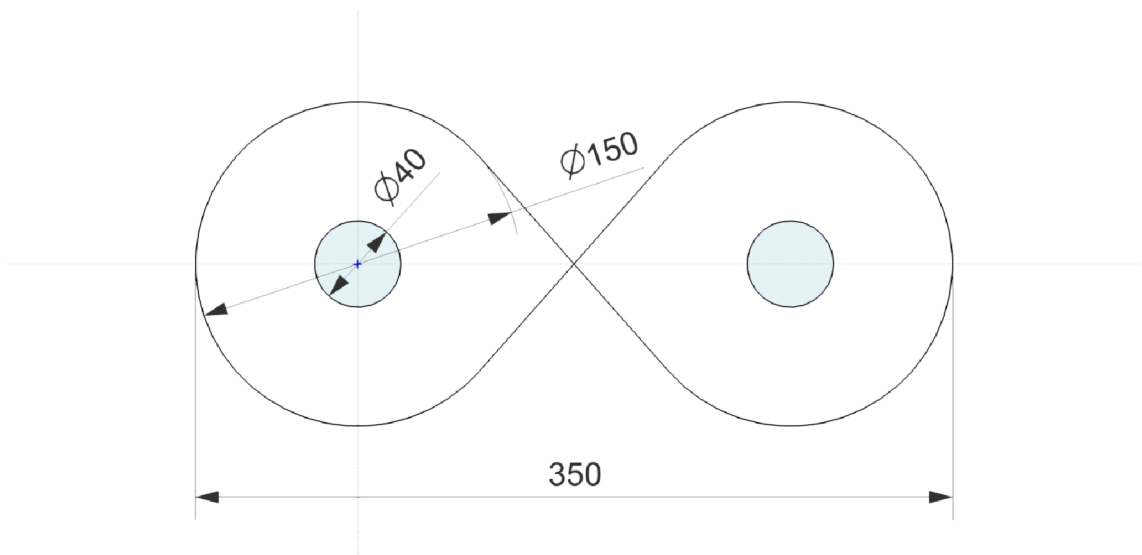


Figure 10.18: 8-like track

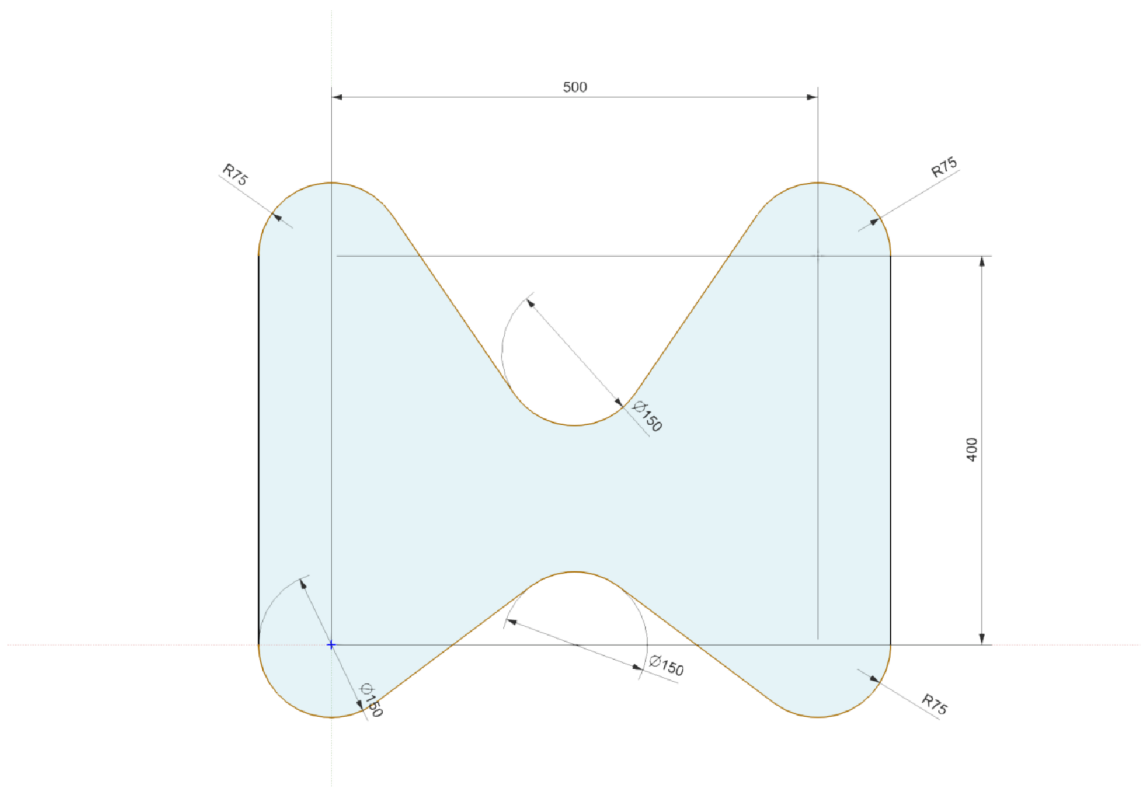


Figure 10.19: Free-run track

## 11 Evaluating comfort by means of the regression analysis

The regression analysis is a reliable method of identifying which variables impact operator's comfort, our topic of interest. The process of performing a regression allows us to confidently determine which factors matter the most, which factors can be ignored, and how these factors influence each other.

In order to describe the regression analysis in more detail, it is essential to comprehend the following terms:

1. **Dependent Variable or Predictor** is the main factor that we would like to understand and predict its future behaviour.
2. **Independent/Input Variables or Regressors** are the factors incorporated into the regression model which are assumed to influence the dependent variable according to the research hypotheses.

The multiple regression equation can be represented in the following form:

$$y = b_0 + b_1x_1 + b_2x_2 + \dots + b_nx_n + e \quad (11.1)$$

where  $b_i (i = 0, 1, 2, \dots, n)$  are the regression coefficients which denote the rate of change of the criterion variable with respect to the predictor variable. The coefficient  $b_0$  represents the intercept of the trend line with the  $y$  axis. In this chapter, the results of the regression analysis of data sets obtained from the experiments are described, such as the human operator feedback and physical measures. The data collected from the feedback surveys allows us to measure the human operator's feelings associated with various settings of the impedance control. We could also identify what variables influence those feelings. In the linear regression model 11.1, the sign of the coefficients  $b_1 \dots b_n$  indicates the direction of the relationship between the independent variable and the dependent variable. A positive coefficient implies that as the independent variable increases, the mean of the dependent variable tends to increase. Conversely, a negative coefficient indicates that as the independent variable increases, the mean of the dependent variable tends to decrease. It is important to note that the regression coefficients and their signs have no relation to the settings of the impedance controller.

The first analysis reflects on the effect of the impedance controller parameters on human comfort. We select operator's comfort as a dependent variable and param-

<i>Regression Statistics</i>	
Multiple R	0.632
R Square	0.400
Adjusted R Square	0.359
Standard Error	1.734
Observations	48

<i>ANOVA</i>					
	<i>df</i>	<i>SS</i>	<i>MS</i>	<i>F</i>	<i>Significance F</i>
Regression	3	88.090	29.363	9.771	4.65E-05
Residual	44	132.222	3.005		
Total	47	220.313			

	<i>Coefficients</i>	<i>Standard Error</i>	<i>t Stat</i>	<i>P-value</i>	<i>Lower 95%</i>	<i>Upper 95%</i>
Intercept	2.726	0.786	3.467	0.001	1.141	4.311
Mass	-0.172	0.04	-4.332	8.42E-05	-0.252	-0.092
Damping	-0.012	0.004	-3.248	0.002	-0.019	-0.004

Table 11.1: Regression analysis for comfort of the operator 1 using impedance controller coefficients

ters of the impedance controller as the independent variables. The analysis results are presented in the table 11.1.

If we look at the  $R^2$  (coefficient of determination) value <sup>1</sup>, we could conclude that for the 48 observations <sup>2</sup> almost 40% of change in the operator's comfort was likely caused by the impedance controller parameters. Significance value F is smaller than 0.05, so regression results are statistically significant. When we check the coefficients' values, we can see that we have a negative relationship between human comfort and the values of mass and dumping coefficients. In simple words, the increase of mass and dumping coefficient leads to the decrease of the operator's comfort for the analyzed data set. If we look at the P-value for the coefficients, we could say that P-values for mass and damping coefficients are lower than 0.05 that means these results are statistically significant, and as a result, both increasing coefficients affect operator's comfort in the negative way.

In the next step, we study the effect of independent variables, such as the mean value of the absolute interaction force and its standard deviation as well as the mean value and the standard deviation of the absolute linear velocity of the cart. The results are collected in the 11.2. When we analyze  $R^2$  for the 48 observations, nearly 78% of change in the operator's comfort is caused by the change of the interaction force and linear velocity of the cart. The significance value F is smaller than 0.05, so the regression results are statistically significant.

We can see that the mean and the standard deviation of absolute interaction force and the cart velocity has a significant effect on the operator's comfort, because

<sup>1</sup> $R^2=0$  indicates that the model equation 11.1 does not explain any of the variability of the response data around its mean and  $R^2=1$  indicates that the model explains all the variability of the response data around its mean.

<sup>2</sup>These observations come from evaluating the interaction process of a single operator, with specific mass and damping parameters of the impedance controller



<i>Regression Statistics</i>	
Multiple R	0.882
R Square	0.778
Adjusted R Square	0.757
Standard Error	1.067
Observations	48

<i>ANOVA</i>					
	<i>df</i>	<i>SS</i>	<i>MS</i>	<i>F</i>	<i>Significance F</i>
Regression	4	171.386	42.847	37.656	1.58E-13
Residual	43	48.926	1.138		
Total	47	220.313			

	<i>Coefficients</i>	<i>Standard Error</i>	<i>t Stat</i>	<i>P-value</i>	<i>Lower 95%</i>	<i>Upper 95%</i>
Intercept	4.272	0.979	4.363	7.91E-05	2.297	6.247
Mean Abs F	-0.031	0.011	-2.935	5.34E-05	-0.052	-0.01
Std Abs F	-0.014	0.005	-2.73	9.13E-03	-0.025	-0.004
Mean abs V	5.666	1.9	2.982	0.005	1.834	9.499
Std abs V	-5.419	1.497	-3.619	0.001	-8.438	-2.4

Table 11.2: Regression analysis for operator 1 comfort using mean value and standard deviation of interaction force and cart velocity

the P-value of each parameter is higher than 0.05. We apply the regression analysis to data sets of all the operators, and as a result, we could confirm that the interaction force and cart velocity have a significant effect on the operator's comfort, however for different operators the comfort state is reached with different impedance controller settings.

In the third step, we study the relationship between the operator's comfort and the biological markers, such as pulse, blood pressure, and oxygen saturation. The results were combined in the table 11.3. The value of  $R^2$  for the 48 observations, it could be concluded that approximately 81% of the change in the operator's comfort is caused by biological markers. The regression results are statistically significant, because the significance value F is smaller than 0.05. It could be observed that the heart rate and comfort of the human operator have an inverse relationship. It means that the human operator's heart rate is decreasing when the comfort zone is reached, while the heart rate is increasing when a lot of effort is applied to overcome the friction force or return the cart to a desired position if the target was overreached. The oxygen blood saturation and the Borg scale estimations have positive relation to the operator's comfort. If we look at the P-value for the coefficients we could say that only the P-value of oxygen blood saturation is lower than 0.05 that means the regression results are statistically significant only for this parameter.

The results of the regression analysis of the data set that includes all the participants are shown in the tables 11.4 - 11.6. The data set of all participants includes 240 observations. In the table 11.4 we analyze the effect of impedance controller parameter's change on comfort of different operators. The  $R^2$  for 240 observations equals to 0.332. It means that only 33.2% of the operator's comfort is caused by the

<i>Regression Statistics</i>	
Multiple R	0.9
R Square	0.81
Adjusted R Square	0.797
Standard Error	0.976
Observations	48

<i>ANOVA</i>					
	<i>df</i>	<i>SS</i>	<i>MS</i>	<i>F</i>	<i>Significance F</i>
Regression	3	178.378	59.46	62.39	6.87E-16
Residual	44	41.934	0.953		
Total	47	220.313			

	<i>Coefficients</i>	<i>Standard Error</i>	<i>t Stat</i>	<i>P-value</i>	<i>Lower 95%</i>	<i>Upper 95%</i>
Intercept	-123.766	48.772	-2.536	0.015	-222.061	-25.474
HR	-0.072	0.048	-1.49	0.143	-0.17	0.025
SPO2	1.3	0.482	2.696	0.01	0.329	2.273
Borg Scale	0.25	0.387	0.647	0.521	-0.529	1.03

Table 11.3: Regression analysis for operator 1 comfort using biological markers

change of the controller parameters. The regression results are statistically significant because the significance value F is smaller than 0.05. The relationship between the human comfort and the values of mass and dumping coefficients is negative. The P-value for the coefficients shows that the regression results are statistically significant.

<i>Regression Statistics</i>	
Multiple R	0.576
R Square	0.332
Adjusted R Square	0.324
Standard Error	1.727
Observations	240

<i>ANOVA</i>					
	<i>df</i>	<i>SS</i>	<i>MS</i>	<i>F</i>	<i>Significance F</i>
Regression	3	350.433	116.811	39.146	1.43E-20
Residual	236	704.217	2.98		
Total	239	1054.65			

	<i>Coefficients</i>	<i>Standard Error</i>	<i>t Stat</i>	<i>P-value</i>	<i>Lower 95%</i>	<i>Upper 95%</i>
Intercept	2.386	0.35	6.808	8.12E-11	1.695	3.075
Mass	-0.147	0.018	-8.258	1.06E-14	-0.181	-0.112
Damping	-0.011	0.002	-7.017	2.39E-11	-0.014	-0.008

Table 11.4: Regression analysis for comfort of all the operators using impedance controller coefficients

The result of the regression analysis for comfort of all the operators using the mean value and standard deviation of interaction force and cart velocity was collected in the table 11.5. For complete data set of all participants the 79% of change in the human comfort is caused by the mean value and standard deviation of the measured interaction force and the cart's velocity. The significance of the F value is less than 0.05 demonstrates statistically significant results. The P-value of all the

coefficients less than 0.05 shows that all the physical measures have an effect on the operator's comfort.

<i>Regression Statistics</i>						
Multiple R		0.87				
R Square		0.757				
Adjusted R Square		0.753				
Standard Error		1.044				
Observations		240				

<i>ANOVA</i>						
	<i>df</i>	<i>SS</i>	<i>MS</i>	<i>F</i>	<i>Significance F</i>	
Regression	4	798.702	199.675	183.333	4.98E-71	
Residual	235	255.948	1.089			
Total	239	1054.65				

	<i>Coefficients</i>	<i>Standard Error</i>	<i>t Stat</i>	<i>P-value</i>	<i>Lower 95%</i>	<i>Upper 95%</i>
Intercept	3.909	0.422	9.257	1.36E-17	3.077	4.741
Mean Abs F	-0.033	0.005	-6.945	3.67E-11	-0.042	-0.023
Std Abs F	-0.011	0.002	-4.888	1.88E-06	-0.016	-0.007
Mean Abs V	6.555	0.874	7.502	1.28E-12	4.833	8.276
Std Abs V	-5.79	0.696	-8.313	7.51E-15	-7.162	-4.418

Table 11.5: Regression analysis for comfort of all the operators using mean value and standard deviation of interaction force and cart velocity

Table 11.6 shows the effect of biological markers on the operator's comfort. The result of the regression analysis demonstrates that over 81% of the human comfort is caused by biological markers. The significance of the F value is less than 0.05 demonstrates statistically significant results. The P-values of the heart rate and oxygen blood saturation coefficients are less than 0.05. It shows that biological markers influence the operator's comfort.

<i>Regression Statistics</i>						
Multiple R		0.902				
R Square		0.814				
Adjusted R Square		0.811				
Standard Error		0.913				
Observations		240				

<i>ANOVA</i>						
	<i>df</i>	<i>SS</i>	<i>MS</i>	<i>F</i>	<i>Significance F</i>	
Regression	3	858.052	286.017	343.341	9.14E-86	
Residual	236	196.598	0.833			
Total	239	1054.65				

	<i>Coefficients</i>	<i>Standard Error</i>	<i>t Stat</i>	<i>P-value</i>	<i>Lower 95%</i>	<i>Upper 95%</i>
Intercept	-134.406	20.212	-6.65	2.02E-10	-174.225	-94.586
HR	-0.067	0.02	-3.278	0.001	-0.107	-0.027
SPO2	1.405	0.2	7.029	2.22E-11	1.011	1.799
Borg Scale	0.235	0.163	1.446	0.149	-0.085	0.556

Table 11.6: Regression analysis for comfort of all the operators using biological markers

When we evaluated the participants separately, the output of the regression

analysis was similar to the results demonstrated in tables 11.1 - 11.3. However, the analysis of data for all operators yields a different result. As it could be observed from the table 11.4, the  $R^2$  value is reduced by almost 7% in comparison to individual approach. It means the impedance controller settings that could be evaluated as comfortable are different from one operator to another. In fact, the dependency between the comfort, the mean and the standard values of the interaction force and the cart's velocity, as well as the biological markers remains the same. It allows us to conclude that the mean value and the standard deviation of the interaction force and the cart's velocity, the heart rate and the oxygen blood saturation could be used as sufficient references to generate the rewards which can be used by the developed reinforcement learning algorithm described in the following chapter.

## 12 Q-Learning for human-cart interaction

”When you first start off trying to solve a problem, the first solutions you come up with are very complex, and most people stop there. But if you keep going, and live with the problem and peel more layers of the onion off, you can often times arrive at some very elegant and simple solutions.”

---

Steve Jobs

This chapter describes the control algorithm developed for the robust and safe physical interaction between the human operator and the industrial cart. As demonstrated in the chapter 3, the impedance control is an essential component of the solution. It can be used as a part of the representation for the human operator dynamics. Additionally, it helps us to control the supporting effort of the mobile platform side during the collaboration. One of the possible physical collaboration scenarios is presented in the figure 12.1.

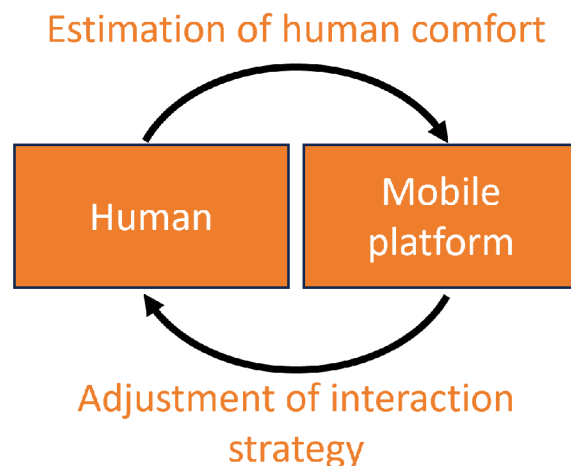


Figure 12.1: Physical collaboration scenario

While performing the task the human operators learn based on their estimations

and feelings. As a result, they adapt their arm impedance according to the required effort for the task. As shown in some field tasks [102], human operators generally combine two strategies to adapt their impedance to perturbations, thereby minimizing position error and energy consumption: 1) if perturbations are unpredictable, subjects increase their impedance through co-interaction; and 2) if perturbations are predictable, subjects learn a feed-forward command to offset the perturbation.

On the other hand, the mobile platform adjusts the interaction strategy by changing the impedance parameters. The change occurs according to the correlation between detected features and human feelings that was obtained in the chapter 11.

A Markov decision process (MDP) consists of the following items:

- $S$ , a set of states of the world.
- $A$ , a set of actions.
- $P : S \times S \times A \rightarrow [0, 1]$ , which specifies the dynamics. This is written as  $P(s'|s, a)$ , where  $\forall s \in S; \forall a \in A; \sum_{s' \in S} P(s'|s, a) = 1$ . In particular,  $P(s'|s, a)$  specifies the probability of transitioning to state  $s'$  given that the agent is in a state  $s$  and does action  $a$ .
- $R : S \times A \times S \rightarrow R$ , where  $R(s, a, s')$  gives the expected immediate reward from doing action  $a$  and transitioning to a state  $s'$  from the state  $s$ .

Both the dynamics and the rewards can be stochastic; there can be some randomness in the resulting state and reward, which is modeled by having a distribution over the resulting state and by giving the expected reward  $R$ . The outcomes are stochastic when they depend on random variables that are not modeled in the MDP.

A finite part of a Markov decision process can be depicted using a decision network as in Figure 12.2.

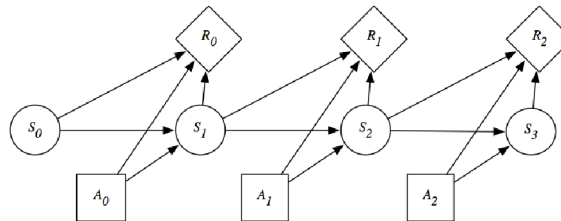


Figure 12.2: Decision network representing a finite part of an MDP [14]

In order to include human feelings in the control system we implemented a reinforcement learning algorithm. The textbook named "Reinforcement Learning: An Introduction" [18] provides the following definition to the reinforcement learning:

"Reinforcement Learning is an area of Machine Learning that can be considered both a set of problems and solution methods to these problems. It is concerned with finding the best possible behaviour strategy for an agent interacting with an

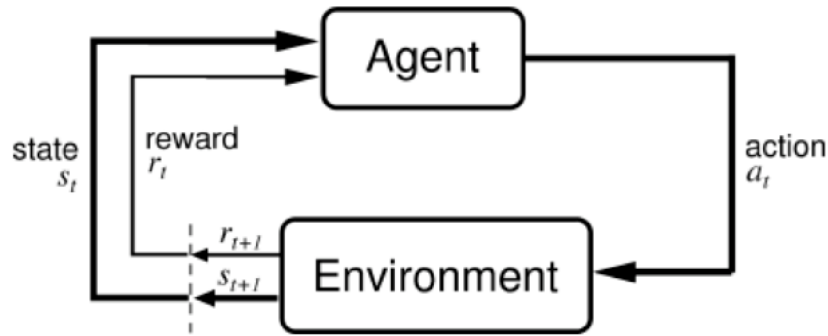


Figure 12.3: Reinforcement learning flow diagram [18]

environment. The underlying idea is that similarly to how humans and other animals learn by trial-and-error, so should also software agents be able to learn.”

Reinforcement Learning (RL) was originally inspired by the behavioural psychology. Similarly to how humans are taught that some actions are good and others are not by obtaining either a reward or a punishment, this class of algorithms reinforces desirable actions while discouraging the undesirable ones. This trial-and-error approach to learning is simulated by giving a numerical reward as a feedback on the performance of an algorithm. Thus, based on the result signal, a learning algorithm can evaluate and update its parameters based on how good or bad a set of actions were.

The following RL algorithms are built on the following main components and assumptions, as stated in [103] and [104]:

- **State.** Set  $S$  of states the agent and environment can be in.
- **Actions.** Set  $A$  of actions the agent can invoke. This set can be restricted depending on the current state.
- **Reward.**  $R$  is a function that provides numerical rewards for state transitions. It is used to estimate the quality of action  $a_t$  in state  $s_t$  based on the state change it causes.
- **State Variables.** The value map memorizes what outcomes an agent expects for given states
- **Policy.** A policy is a structure that maps states to actions. Roughly speaking, it defines what action to take in a specific state.
- **Model (Optional).** A model of the environment and agent predicts the new state  $s'$  when action  $a$  is invoked in states. The model can be probabilistic or unavailable.

The first task when designing a Q-Learning system is to define the environment. The environment consists of states, actions and rewards. It is assumed that the agent uses states and rewards as inputs and generates actions as outputs.

## 12.1 States

It is assumed that the number of possible states is finite. The agent could be in one fixed number of possible situations. In our case, we can think of each possible setting of the impedance controllers as of a state. The agent could be located at one state at a time. It means only one set of impedance controller settings could be selected and evaluated in one step. Each component of the impedance controller could switch among four states. According to the selected parameters of the impedance controllers shown in the table 10.2, the set of 256 system states was generated. It includes the states and the intervals between their set values to be used in the process of Q-learning. In this study, four parameters for each coefficient were used, resulting in a total of 256 possible combinations. This number of combinations is believed to be sufficient to demonstrate the learning process of the platform. However, it is important to note that this number is not limiting, as researchers must consider the trade-off between the flexibility of the settings and the time required for the learning process before determining the number of coefficients to be used.

**States[256] = generate**

M	Dtrn	J	Drot
2	20	1	10
5	50	4	20
10	100	8	50
18	160	18	160

Figure 12.4: Set of states

## 12.2 Actions

It is assumed that the number of possible actions is also finite. The agent always needs to choose from among a fixed number of possible actions as it was suggested by the results of the regression analysis obtained in chapter 11. Therefore, four parameters ( $M_{trn}$ ,  $D_{trn}$ ,  $M_{rot}$ ,  $D_{rot}$ ) were selected as adjustable variables. We define a set of possible actions in the following way: the agent could apply two actions (increase or decrease) per each of the four parameters and carry out an additional action "do nothing" when no change is required, see the figure 12.5. The change of inertial and dumping components of the impedance controller leads to the change in the cart dynamics.

## 12.3 Rewards

In order to help the agent in the learning process we created a condition based reward structure. The most important part is the reward definition for the state. The



$$\text{Actions}[9] = \{0, 1, 2, 3, 4, 5, 6, 7, 8\}$$

Figure 12.5: Set of actions

agent goal is always the same - to maximize its total rewards. In our case we mostly use negative rewards (i.e. punishments) for the settings that could be recognized as undesirable. The reason for the negative rewards is the following. Due to the fact that the agent goal is to maximize cumulative rewards, if we used positive rewards the agent could get stuck in switching between the first states and would accumulate a very large cumulative reward even if the comfortable impedance controller settings were not found. In case of negative rewards, the agent tries to minimize the punishment by searching for the most convenient set of impedance controller settings. The result will be the set of impedance controller settings convenient for the current operator.

The reward system works as follows, see figure 12.6. The agent checks if the interaction dynamics is positive by comparing the values of the mean and the standard deviation for both the current step *and* the previous step. Additionally, the agent checks if there is no emergency situation by analyzing the E-stop button state. The peaks of the interaction force have to be avoided as well. If a human operator thinks that the current settings are convenient for them, they might provide a positive feedback. In the end, we sum up the rewards for various criteria. If none of the criteria were met, the reward is set to be the negative one.

$$\text{Reward} = \sum \begin{cases} -1 & \text{If } \text{mean}(F_h) > \text{mean}(F_h)' \\ & \text{or } \text{STD}(F_h) > \text{STD}(F_h)' \\ -1 & \text{If } \text{mean}(T_h) > \text{mean}(T_h)' \\ & \text{or } \text{STD}(T_h) > \text{STD}(T_h)' \\ -10 & \text{If } \text{not\_aus} = \text{false} \\ +5 & \text{If } \text{fbd\_btn} = \text{true} \\ -2 & \text{If } \max(\text{abs}(F_h)) > 2.5 * \text{mean}(F_h) \\ -5 & \text{If } \max(\text{abs}(F_h)) > 2.5 * \text{mean}(F_h) \\ -5 & \text{If } \text{mean}(V_{\text{steps}}) \neq \text{mean}(V_{\text{cart}}) \\ -1 & \text{else} \end{cases}$$

Figure 12.6: Rewards

## 12.4 High-level control

The learning algorithm that is used in the context of this thesis is called Q-Learning, which is a model-free Temporal-Difference (TD) algorithm created within a PhD thesis of Watkins [103]. The further technical description is addressed in detail in [104]. TD learning methods combine the ideas behind Monte Carlo and dynamic programming methods. Therefore, a Q-Learning algorithm does not need a model

unlike Monte Carlo methods. Furthermore, TD methods update the state value directly after each step similar to the dynamic programming methods.

$$\underbrace{TD(s_t, a_t)}_{\text{temporal difference}} = \underbrace{r(s_t, a_t)}_{\text{reward}} + \underbrace{\gamma}_{\text{discount factor}} \cdot \underbrace{\max_a Q(s_{t+1}, a_{t+1})}_{\text{estimate of optimal future value}} - \underbrace{Q(s_t, a_t)}_{\text{old value}} \quad (12.1)$$

The discount factor is settled between 0 and 1. The purpose of the  $\gamma$  is to provide the mechanism to discount the future rewards. In other words, it allows to choose a better option, because the value of receiving a particular reward in the future is considered to be generally lower than receiving the same reward now. A discount factor of 1 makes the agent prioritize long-term rewards, while a discount factor of 0 makes the agent only consider immediate rewards. A common value for  $\gamma$  is 0.9.

Another important equation is the Bellman's equation 12.2. The Bellman equation demonstrates what Q-value has to be used as the value for the action that was taken in the previous step. The equation includes a learning rate parameter  $\alpha$  that defines how quickly Q-values are adjusted. The learning rate can take any value from 0 to 1, as the discount factor  $\gamma$  described above. The learning rate of 1 makes the agent update its Q-values completely based on the new information, while the learning rate of 0 makes the agent not update its Q-values at all. A common value for  $\alpha$  is 0.1. Both factors may help researchers to understand how the Q-table is updated to ensure that the learning agent keeps trying out new actions to learn from them and would not get trapped by "thinking" that the current process works perfectly well.

$$\underbrace{Q_{new}(s_t, a_t)}_{\text{new value}} = \underbrace{Q_{old}(s_t, a_t)}_{\text{old value}} + \underbrace{\alpha}_{\text{learning rate}} \cdot \underbrace{TD(s_t, a_t)}_{\text{temporal difference}} \quad (12.2)$$

Q-Learning works with MDPs only, because the values are calculated based on the current state. Therefore, each state instance must represent the entire configuration of the agent and environment. The basic Q-Learning update is defined by the equation 12.3:

$$\underbrace{Q(s_t, a_t)}_{\text{new value}} \leftarrow \underbrace{Q(s_t, a_t)}_{\text{old value}} + \underbrace{\alpha}_{\text{learning rate}} \cdot [\underbrace{r(s_t, a_t)}_{\text{reward}} + \underbrace{\gamma}_{\text{discount factor}} \cdot \underbrace{\max_a Q(s_{t+1}, a_{t+1})}_{\text{estimate of optimal future value}} - \underbrace{Q(s_t, a_t)}_{\text{old value}}] \quad (12.3)$$

where  $Q(s_t, a_t)$  represents the value for a cell in the Q-matrix that demonstrates the choice of action  $a$ , from a state  $s$  at current time  $t$ , and  $r(s_t, a_t)$  is the reward received for the choice of action  $a$ , from state  $s$ .

The following figure presents the specific form of the MDP implemented in the current application of 256 states, where blue circles represent states, and black lines represent actions or transitions between the states.

The diagram shown in the figure 12.7 presents the process of Q-Learning. The process begins by initializing the Q-Table. This table represents the agent's policy

on how to behave in the environment. In the next step the action for the current step has to be selected. There are two available options. One option is to choose the action with the highest Q-Value. Another option is to take a random action in order to explore the environment. The common strategy for resolution of the trade-off between exploration and exploitation is the Epsilon-Greedy algorithm.

In the framework of this algorithm, for each step within an episode, we set our exploration rate threshold to a random number between 0 and 1. This is used to determine whether our agent explores or exploits the environment in this time-step.

If the threshold is greater than the exploration rate, which is initially set to 1, then the agent exploits the environment and selects the action that has the highest Q-value in the Q-table for the current state. If, on the other hand, the threshold is less than or equal to the exploration rate, then the agent explores the environment, and samples an action randomly.

As soon as the action is selected, the agent performs the action. When the action is performed, the agent receives a reward. Based on the received reward and the information about the current state, the TD is updated. While the Q-Value for the current state is updated using the information about the current state, TD value and the Bellman's equation 12.2 and the agent switches to the next step.

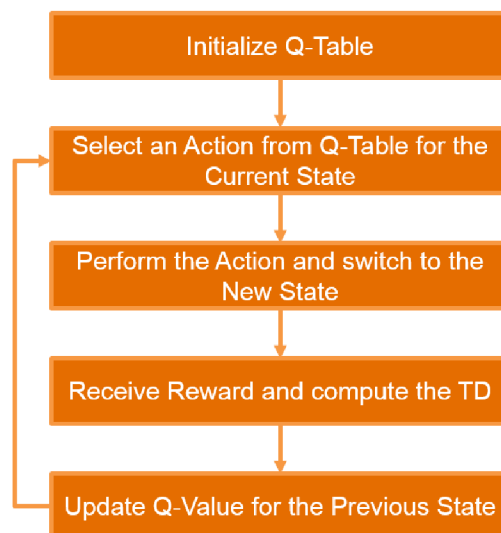


Figure 12.7: Q-learning process diagram

The diagram of the Q-Learning process could be presented in the shape of a pseudo-code shown in the table 12.1.

The Q-Learning algorithm was implemented inside the high-level controller which is Raspberry Pi 4 in our case. Python language was used in the implementation process. The information about the process values (interaction forces, odometry) is supplied to a high-level controller from a low-level controller by means of the serial port. Using the same link information about the actual impedance controller, the parameters are provided to the low-level controller. The protocol uses a

---

*Q*-learning: Learn function  $Q : \mathcal{X} \times \mathcal{A} \rightarrow \mathbb{R}$

---

**Require:**  
States  $\mathcal{X} = \{1, \dots, n_x\}$   
Actions  $\mathcal{A} = \{1, \dots, n_a\}$ ,  $A : \mathcal{X} \Rightarrow \mathcal{A}$   
Reward function  $R : \mathcal{X} \times \mathcal{A} \rightarrow \mathbb{R}$   
Black-box (probabilistic) transition function  $T : \mathcal{X} \times \mathcal{A} \rightarrow \mathcal{X}$   
Learning rate  $\alpha \in [0, 1]$ , typically  $\alpha = 0.1$   
Discounting factor  $\gamma \in [0, 1]$

**procedure** QLEARNING( $\mathcal{X}$ ,  $A$ ,  $R$ ,  $T$ ,  $\alpha$ ,  $\gamma$ )  
Initialize  $Q : \mathcal{X} \times \mathcal{A} \rightarrow \mathbb{R}$  arbitrarily  
**while**  $Q$  is not converged **do**  
Start in state  $s \in \mathcal{X}$   
**while**  $s$  is not terminal **do**  
Calculate  $\pi$  according to  $Q$  and exploration strategy (e.g.  $\pi(x) \leftarrow \arg \max_a Q(x, a)$ )  
 $a \leftarrow \pi(s)$   
 $r \leftarrow R(s, a)$  ▷ Receive the reward  
 $s' \leftarrow T(s, a)$  ▷ Receive the new state  
 $Q(s', a) \leftarrow (1 - \alpha) \cdot Q(s, a) + \alpha \cdot (r + \gamma \cdot \max_{a'} Q(s', a'))$   
**return**  $Q$

---

Table 12.1: Learn function of the Q-Learning algorithm presented in a pseudo-code

cyclic redundancy check (CRC) data check. The data of biological markers is read from a smart band using a bluetooth low energy (BLE) protocol. The console output of the learning process is shown in the figure 12.8. The information consists of the current episode number, the number of the step inside the episode, the selected action, the obtained reward, and the new set of impedance controller parameters to be tested.

The graphic visualization of the Q-table values during the learning process is provided in the figure 12.9. The yellow color represents the areas with the high rating and the blue color represents the areas with low rating. As we start the interaction process, the values in the Q-Table are equal to one another. However, as soon as the algorithm takes action, the system state is changed and the corresponding value in the Q-table is updated according to the reward information. The quality and the speed of the RL process partially depends on the teacher. If a human operator uses a user button to give a positive feedback or the E-stop button to give a negative feedback, it could significantly speed up the learning process.

When we observe the Q-Learning dynamics by considering the Q-Table changes in time, the following information could be extracted. The Q-Table is visualized by means of color map (heat map). In the first figure of the set of six (see figure 12.9) it is shown that in the first moments of the learning process, the Q-Values are quite similar to each other. A significant area of the color map is colored in yellow. However, with time the color map obtains darker spots by receiving the negative feedback about the impedance controller settings. In the long run, it is depicted that the major area of the color map is covered in dark blue and green colors that demonstrate a negative effect of the impedance controller setting on the interaction

```

Episode 36
Step 189
Current action Mdown
State_num 0
New state [2, 20, 1, 10]
Reward -1
Episode 36
Step 190
Current action Jup
State_num 4
New state [2, 20, 4, 10]
Reward -1
Episode 36
Step 191
Current action Drup
State_num 5
New state [2, 20, 4, 20]
Reward -1
Episode 36
Step 192
Current action Dtdown
State_num 0
New state [2, 20, 1, 10]
Reward -1
Episode 36

```

Figure 12.8: Console output of the learning process

process. Only a tiny yellow line is presented in the color map. This line represents the impedance controller settings that fully respond to the intention of the human operator. It is possible to obtain the impedance controller settings by selecting the state that corresponds to the maximum value of the Q-Table.

By observing and learning from the operator's behavior, a mobile platform can adapt its own behavior to match that of the operator. This can improve the platform's performance in the presence of disturbances and its ability to recover from errors, as the platform will be able to respond in a similar way to the operator. This mobile platform can learn to predict and avoid dangerous situations, such as collisions with obstacles or other vehicles.

There are several scientific criteria that are used to determine if a mobile platform is robust and safe. These criteria are typically based on the performance of the platform in various scenarios, such as its ability to withstand external disturbances and its ability to recover from errors. Here are a few examples of scientific criteria that are commonly used to evaluate the robustness and safety of mobile platforms:

*Performance in the presence of disturbances* assesses the platform's ability to remain stable and perform its intended function in the presence of external disturbances, such as vibrations, noise, or changes in environmental conditions. *Recovery*

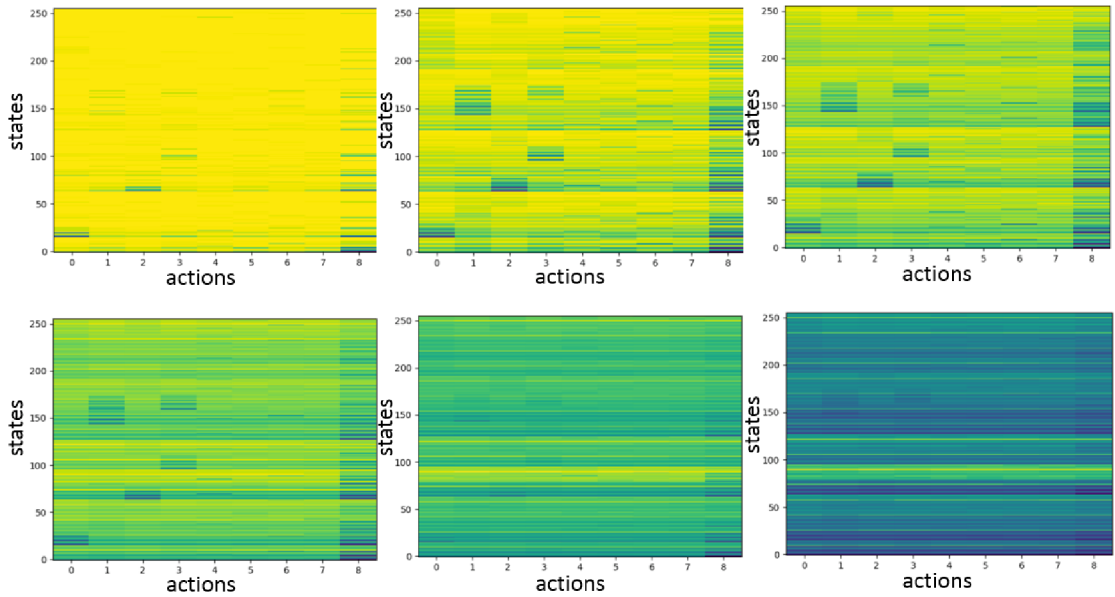


Figure 12.9: Dynamic change of the Q-value during the learning process

*from errors* evaluates the platform’s ability to recover from unexpected events, such as sensor failures or actuator malfunctions. *Safety* assesses the platform’s ability to prevent accidents and minimize the potential for injury or damage. *Passivity* evaluates the platform’s ability to be controlled by an external force, ensuring stability of the system. *Efficiency* assesses the platform’s ability to perform its intended function with minimal energy consumption or other resources.

It is worth pointing out that these criteria have been developed and studied by a number of engineers and scientists over time, and are formalized in various research papers and industry standards. For example, such organisations as IEEE <sup>1</sup> and ISO <sup>2</sup> have developed standards for mobile robots and AGVs (Automated Guided Vehicles) safety and performance. The specific criteria and standards used to evaluate the robustness and safety of a mobile platform depends on the specific application and environment in which the platform is used. Having specified these criteria, we believe that the current mobile platform can be robust and safe due to the following list of reasons: 1. the maximum speed is restricted to prevent dangerous situations and unexpected behavior; 2. an emergency stop button (E-stop) has been implemented to ensure additional safety; 3. moreover, the main power switch is available to control the power supply to the system; 4. to further prevent dangerous situations, an interlock has been implemented to avoid instant changes in direction at high velocity setpoints. The system is also designed to slow down, but not accelerate in the opposite direction without reaching a low speed to prevent sudden changes in direction.

<sup>1</sup>Institute of Electrical and Electronics Engineers

<sup>2</sup>International Organisation for Standardisation

## 13 Conclusion

“Perfection is achieved, not when there is nothing more to add, but when there is nothing left to take away.”

---

Antoine de Saint Exupery

In the course of this work we have systematized the existing theory in the field of PHRI related to human in-the-loop study while designing, developing, and interacting with the powered mobile platform to evaluate the operator’s comfort. Both the mathematical and the experimental models of the industrial power assisted cart were developed. An extensive amount of work was performed in powered mobile platform programming and control system implementation. Therefore, artificial intelligence (AI) methods were employed to adjust the controller settings in order to achieve such controller settings in which an operator can manipulate a heavy loaded industrial cart with minimum physical effort and ultimate comfort.

The objectives mentioned in the first part of the thesis were completed as follows:

1. The state of art information in the area of physical human-robot interaction was collected up to 2022 and a promising fully adaptable algorithm was developed to deliver a new human-powered cart interaction control technique which goes in line with state-of-art research and practical investigations.
2. A mathematical description for dynamics and kinematics of the human – cart physical interaction model was prepared.
3. An experimental model of an industrial cart was developed, assembled and described in the framework of this thesis.
4. A set of experiments including real people and modelled operators were performed and the human feedback during the interaction process was evaluated.
5. The dynamic characteristics were analysed in order to search for criteria that directly or indirectly determine a physical feeling of human comfort and operator’s expectations during the interaction with IPAC.
6. Human estimation criteria that characterize the satisfaction and comfort from the human-powered cart interaction process were synthesised.

7. Based on these synthesised criteria, the human – powered cart interaction control algorithm was developed using AI methods (Q-learning).
8. The performance of the proposed solution for the developed industrial cart was tested and verified.

The dissertation contributed the following theoretical input into the field of technical cybernetics - the use of Q-learning algorithm in adjusting controller settings so that the mobile platform could successfully and effectively adapt to the unique gait and tasks of any operator it assists. To comply with this task, the models from Chapters 8-11 were derived and the model could be used in the future to estimate the quality of control with the help of Markov processes. Markov processes are utilized to make decisions on regulating the impedance control settings.

The work brings significant contribution to the area of PHRI by the developed workflow that includes the experimental platform development, the experiment design and the evaluation of the results using the regression analysis and the development of adaptive impedance controller that is suitable to perform collaborative tasks. The personality-oriented scheme presented in this work results in efficient physical interaction that responds to the intentions of the human-operator, as well as it enhances the user comfort during the material handling process.

This work also brings a contribution to the area of the raw data analysis and feature detection. We tested the interaction with different loads and on various types of trajectories such as 7m-long strait drive, circular, the 8-like shape trajectory, a complex predefined path, and a free ride. All the experiments were performed in the indoor environment.

The control system with the impedance controllers of rotational and translational motion was implemented in the experimental platform. It allowed to support the human operator during the linear drive and turns. It helped to obtain the dynamics relevant to the material handling task. The analysis of the interaction characteristics allowed us to identify the physical measures, emotional feedback as well as biological markers which were used as additional sources of information to improve the human-cart interaction.

We evaluated the effects of the controllers' settings on the operator's comfort and developed a system of automatic adjustment and tuning of the parameters. One of the AI methods was applied to the developed powered industrial cart. The method called Q-learning belongs to the area of reinforcement learning (RL). It allows the powered cart to learn the desired intention of the human operator by means of obtaining rewards for certain settings of impedance controllers. Consequently, it was possible to find out the set of settings that refers to the highest comfort level and sufficient performance for a particular operator. The RL algorithm was implemented in the microcomputer Raspberry Pi using Python language. This controller was called a high-level controller. The low-level control was implemented in the microprocessor ATmega2560 (Arduino board). It includes the mathematical description of the cart's dynamics and kinematics, as well as impedance controllers for the translational and rotational motion of the cart and the PID controller for the powered wheels.



In addition, the applications for the load cell control and configuration software, C-Sharp based hardware extension libraries for Raspberry Pi and Matlab were developed. They allow to run a real-time target-based simulation using math apparatus of Matlab in combination with the low-cost embedded sensors and drives. More information could be found in appendix to this research work.

The results obtained from the current research suggest a few promising implications for the future work. In particular, the number of involved experienced and inexperienced human operators (males and females) could be increased. It would allow to extend the number of observations used to assess the interaction process and evaluate operator's comfort to estimate the correlation (dependency) between operator's comfort and the impedance controller's settings. Furthermore, a combination of the results with industrial PHRI scenarios, where human comfort is set as a significant measure, allows to optimize operator's tasks and logistic processes in plant simulation. These optimized tasks and processes could be applied in a real factory, which could bring a significant value to the end customer in the form of a drastic reduction of sick leave requests caused by transportation hazards.

Lastly, I would like to express my gratitude to the people who supported me during the research and acknowledged the importance of my work. I am pleased that my research made a contribution to the future development of human-robot co-existence and cooperation.

## 14 Internship

I am grateful to the TUL International Office for granting me with an opportunity to develop my skills and do my internship in the Linz Center of Mechatronics GmbH at the Department of Sensors & Communication. This Austrian company is located in the Since Park of Johannes-Kepler University in Linz. The LCM team has comprehensive experience in tendering for EU projects and other international project plans. The project proposals for the following national programmes and structural funds were submitted: European Technology Platforms: Initiative to support international networking; Joint Technology Initiatives: public-private partnership to support transnational research collaboration in selected technological fields; Future and Emerging Technologies Art. 185-Initiativen, etc. Some of the results obtained from these projects have since been successfully brought onto the market.



Figure 14.1: Linz Center of Mechatronics GmbH

As an intern, I participated in several research and commercial projects related to the indoor navigation applications and human motion detection. By working with outstanding professionals I developed a cross-platform application that allowed to add a network interface to any USB (UART) device (USB - Universal Serial Bus). I wrote some documentation including API (Application Programming Interface) description and created an application sample, which was a significant part of the work.

I was delighted to help modify and optimize UART(Universal Asynchronous

Receiver-Transmitter) data transfer protocol in order to use DMA (Direct Memory Access).

In the framework of another project, I was designing and implementing the software for MEMS (Microelectromechanical systems) sensors reading. In addition, I was among the developers to create a software program for MEMS data visualization. At a later stage of the project we improved and extended the MEMS sensor library.

Implementing the algorithm for human motion detection was a project that helped me to learn a lot. I transmitted features activation information to a base station. Last but not least, I was able to design and implement a wireless network sniffer to debug the indoor positioning systems (IPS) shown in the figure 14.2.

It was a priceless experience as it helped me to take my knowledge and skills to a new level. I acquired competences in the areas of indoor navigation and digital signal processing in the field of human motion detection. The internship deepened my knowledge of python multi tasking and C++ in the field of embedded systems.

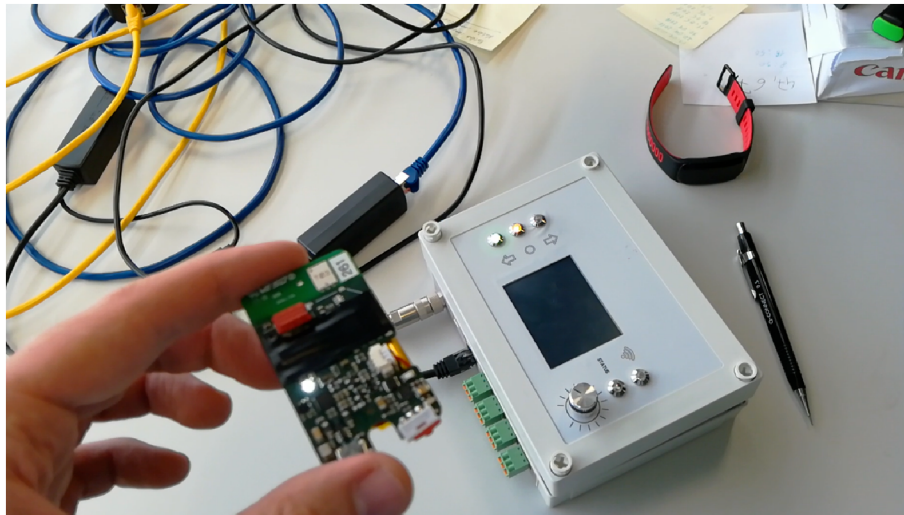


Figure 14.2: Developed indoor positioning system

## 15 Publications

1. KOCHUBEY, Dmitry; TUMA, Petr. Industrial Cart Power Assistance on Undefined Path. In: Proceedings of the 11th PErvasive Technologies Related to Assistive Environments Conference. Corfu, Greece: Association for Computing Machinery, 2018, pp. 108–109. PETRA '18. ISBN 9781450363907. Available from DOI: 10.1145/3197768.3203174.
2. KOCHUBEY, Dmitry; TUMA, Petr. Human Comfort and Skill Evaluation During Interaction with PAMV. In: Proceedings of the 10th International Conference on PErvasive Technologies Related to Assistive Environments. Island of Rhodes, Greece: Association for Computing Machinery, 2017, pp. 250–251. PETRA '17. ISBN 9781450352277. Available from DOI: 10.1145/3056540.3076213.
3. KOCHUBEY, Dmitry. IMPROVING HUMAN-ROBOT PHYSICAL INTERACTION COMFORT IN MATERIAL HANDLING TASKS USING a SMART PLATFORM. ACC Journal, 2023, 29(1), pp. 23–33. Available from DOI: 10.15240/tul/004/2023-1-002

## References

- [1] LU, Yuqian et al. Outlook on human-centric manufacturing towards Industry 5.0. *Journal of Manufacturing Systems*. 2022, vol. 62, pp. 612–627. ISSN 0278-6125. Available from DOI: <https://doi.org/10.1016/j.jmsy.2022.02.001>.
- [2] FANG, Cheng et al. Human Modeling in Physical Human-Robot Interaction: A Brief Survey. *IEEE Robotics and Automation Letters*. 2023, vol. 8, no. 9, pp. 5799–5806. Available from DOI: [10.1109/LRA.2023.3296349](https://doi.org/10.1109/LRA.2023.3296349).
- [3] YANG, Chenguang, Jing LUO, and Ning WANG. *Human-in-the-Loop Learning and Control for Robot Teleoperation*. 125 London Wall, London EC2Y 5AS, United Kingdom; 525 B Street, Suite 1650, San Diego, CA 92101, United States; 50 Hampshire Street, 5th Floor, Cambridge, MA 02139, United States; The Boulevard, Langford Lane, Kidlington, Oxford OX5 1GB, United Kingdom: Academic Press, an imprint of Elsevier, 2023. ISBN 978-0-323-95143-2. Available also from: <https://www.elsevier.com/books-and-journals>.
- [4] THE EUROPEAN COMMISSION. *Eurostat: Stats finder A-Z*. 2023. Available also from: <https://ec.europa.eu/eurostat/web/main/data/stats-finder-a-z>.
- [5] BUSCH, Baptiste et al. Postural Optimization for an Ergonomic Human-Robot Interaction. In: BICCHI, A and OKAMURA, A (eds.). *2017 IEEE/RSJ INTERNATIONAL CONFERENCE ON INTELLIGENT ROBOTS AND SYSTEMS (IROS)*. IEEE; RSJ; IEEE Robot & Automat Soc; IEEE IES; SICE; New Technol Fdn, 2017, pp. 2778–2785. IEEE International Conference on Intelligent Robots and Systems. ISBN 978-1-5386-2682-5. ISSN 2153-0858. IEEE/RSJ International Conference on Intelligent Robots and Systems (IROS), Vancouver, CANADA, SEP 24-28, 2017.
- [6] COMPANY, T.E.K. *Kodak's Ergonomic Design for People at Work*. Wiley, 2003. ISBN 9780471418634. Available also from: <https://books.google.cz/books?id=139RAAAAMAAJ>.
- [7] DARCOR IN COOPERATION WITH ERGOWEB. The ergonomics of manual material handling. Pushing and pulling tasks. *Darcor*. 2014, no. 37(4), pp. 1–28.
- [8] GARG, Arun et al. Psychophysical basis for maximum pushing and pulling forces: A review and recommendations. *International journal of industrial ergonomics*. 2014, pp. 281–291.

- [9] HOOZEMANS, Marco et al. Low-back and shoulder complaints among workers with pushing and pulling tasks. *Scandinavian journal of work, environment & health*. 2002, vol. 28, pp. 293–303. Available from DOI: [10.5271/sjweh.678](https://doi.org/10.5271/sjweh.678).
- [10] FRYMOYER, JW et al. Epidemiologic studies of low-back pain. *Spine*. 1980, vol. 5, no. 5, pp. 419–423. ISSN 0362-2436. Available from DOI: [10.1097/00007632-198009000-00005](https://doi.org/10.1097/00007632-198009000-00005).
- [11] CHAFFIN, DON B. Manual Materials Handling and the Biomechanical Basis for Prevention of Low-Back Pain in Industry—An Overview. *American Industrial Hygiene Association Journal*. 1987, vol. 48, no. 12, pp. 989–996. Available from DOI: [10.1080/15298668791385967](https://doi.org/10.1080/15298668791385967). PMID: 2963515.
- [12] HOGAN, N. Impedance Control: an Approach to Manipulation: Part I-III. *SME Journal of Dynamic Systems, Measurement, and Control*. 1985, vol. 107, pp. 1–24.
- [13] LYNCH, Kevin M. and Frank C. PARK. *Modern Robotics Mechanics, Planning, and Control*. Cambridge, UK: Cambridge University Press, 2017. ISBN 978-1107156302.
- [14] *Decision Processes*. 2018. Available also from: [https://artint.info/html/ArtInt%5C\\_224.html](https://artint.info/html/ArtInt%5C_224.html).
- [15] TAHIROVIC, Adnan and Gianantonio MAGNANI. *SpringerBriefs in Control, Automation and Robotics*. Passivity-Based Model Predictive Control for Mobile Vehicle Motion Planning. Springer, 2013. Available from DOI: [10.1007/978-1-4471-5049-7\\_5](https://doi.org/10.1007/978-1-4471-5049-7_5).
- [16] CRESWELL, John W. *Research Design: Qualitative, Quantitative, and Mixed Methods Approaches*. 4th. SAGE Publications, 2017. ISBN 978-1506386706.
- [17] FEIL-SEIFER, David and MATARIĆ, Maja J. (eds.). *Research Methods in Human-Robot Interaction*. Morgan & Claypool Publishers, 2019. ISBN 978-1627057999.
- [18] SUTTON, Richard S. and Andrew G. BARTO. *Reinforcement Learning: An Introduction*. Second. Cambridge, Massachusetts and London, England: The MIT Press, 2018. ISBN 9780262039246.
- [19] HARKNESS, Elaine et al. Mechanical and psychosocial factors predict new onset shoulder pain: A prospective cohort study of newly employed workers. *Occupational and environmental medicine*. 2003, vol. 60, pp. 850–7.
- [20] ABEL, E. and T. FRANK. The design of attendant propelled wheelchairs. *Prosthetics and Orthotics International*. 1991, vol. 15, pp. 38–45.
- [21] SNOOK, George A. The father of sports medicine. *The American Journal of Sports Medicine*. 1978, vol. 6, no. 3, pp. 128–131. Available from DOI: [10.1177/036354657800600306](https://doi.org/10.1177/036354657800600306). PMID: 350061.
- [22] KUMAR, S., Y. NARAYAN, and C. BACCHUS. Symmetric and asymmetric two-handed. *Hum Factors*. 1995, no. 37 (4), pp. 854–865.

- [23] WEB OF SCIENCE. *Core collection: Physical human-robot interaction*. 2023. Available also from: <https://www.webofscience.com/wos/woscc/analyze-results/25493a6f-3b07-44f6-8672-43c020d2fbe3-bbd16c74>.
- [24] DINH, Khoi Hoang et al. Adaptation and Transfer of Robot Motion Policies for Close Proximity Human-Robot Interaction. *FRONTIERS IN ROBOTICS AND AI*. 2019, vol. 6. ISSN 2296-9144. Available from DOI: [10.3389/frobt.2019.00069](https://doi.org/10.3389/frobt.2019.00069).
- [25] WANG, Jianhua et al. Linear Trajectory Planning for Material Handling Robot. In: *2019 9TH IEEE ANNUAL INTERNATIONAL CONFERENCE ON CYBER TECHNOLOGY IN AUTOMATION, CONTROL, AND INTELLIGENT SYSTEMS (IEEE-CYBER 2019)*. IEEE; RA, 2019, pp. 323–328. IEEE Annual International Conference on Cyber Technology in Automation Control and Intelligent Systems. ISBN 978-1-7281-0770-7. ISSN 2379-7711. 9th IEEE Annual International Conference on Cyber Technology in Automation, Control, and Intelligent Systems (IEEE-CYBER), Suzhou, PEOPLES R CHINA, JUL 29-AUG 02, 2019.
- [26] MULLER, Florian et al. Human-Robot Interaction with Redundant Robots Using Force-Field-Dependent Variable Impedance Control. In: *2017 IEEE 5TH INTERNATIONAL SYMPOSIUM ON ROBOTICS AND INTELLIGENT SENSORS (IRIS)*. IEEE; IEEE Ottawa Sect; IEEE RAS Malaysia Chapter; Joint Chapter Robot & Automat Soc & Control Syst Soc; Joint Chapter Computat Intelligence & Syst Man & Cybernet Soc; Instrumentat & Measurement Soc Chapter, 2017, pp. 166–172. ISBN 978-1-5386-1342-9. 5th IEEE International Symposium on Robotics and Intelligent Sensors (IEEE IRIS), Ottawa, CANADA, OCT 05-07, 2017.
- [27] KANG, Gitae et al. Variable Admittance Control of Robot Manipulators Based on Human Intention. *IEEE-ASME TRANSACTIONS ON MECHATRONICS*. 2019, vol. 24, no. 3, pp. 1023–1032. ISSN 1083-4435. Available from DOI: [10.1109/TMECH.2019.2910237](https://doi.org/10.1109/TMECH.2019.2910237).
- [28] CAPDEPUY, Philippe et al. Improving Human-Robot Physical Interaction with Inverse Kinematics Learning. In: TAPUS, A et al. (eds.). *SOCIAL ROBOTICS (ICSR 2015)*. 2015, vol. 9388, pp. 103–112. Lecture Notes in Artificial Intelligence. ISBN 978-3-319-25554-5; 978-3-319-25553-8. ISSN 0302-9743. Available from DOI: [10.1007/978-3-319-25554-5\\_11](https://doi.org/10.1007/978-3-319-25554-5_11). 7th International Conference on Social Robotics (ICSR), Paris, FRANCE, OCT 26-30, 2015.
- [29] HERRERA, D. et al. Human-Robot Interaction: Legible Behavior Rules in Passing and Crossing Events. *IEEE LATIN AMERICA TRANSACTIONS*. 2016, vol. 14, no. 6, SI, pp. 2644–2650. ISSN 1548-0992. Available from DOI: [10.1109/TLA.2016.7555232](https://doi.org/10.1109/TLA.2016.7555232).
- [30] MACLEAN, Karon E. and Antonio FRISOLI. Introduction to Journal of Human-Robot Interaction Special Issue on Haptics in HRI: Cooperation and Communication. *JOURNAL OF HUMAN-ROBOT INTERACTION*. 2015,

vol. 4, no. 1, SI, pp. 1+. ISSN 2163-0364. Available from DOI: [10.5898/JHRI.4.1.MacLean](https://doi.org/10.5898/JHRI.4.1.MacLean).

- [31] OLTEAN, Stelian-Emilian. Mobile Robot Platform with Arduino Uno and Raspberry Pi for Autonomous Navigation. In: MOLDOVAN, L and GLIGOR, A (eds.). *12TH INTERNATIONAL CONFERENCE INTERDISCIPLINARITY IN ENGINEERING (INTER-ENG 2018)*. 2019, vol. 32, pp. 572–577. Procedia Manufacturing. ISSN 2351-9789. Available from DOI: [10.1016/j.promfg.2019.02.254](https://doi.org/10.1016/j.promfg.2019.02.254). 12th International Conference Interdisciplinarity in Engineering (INTER-ENG), Tirgu Mures, ROMANIA, OCT 04-05, 2018.
- [32] SNOOK, Stover H. and Vincent M. CIRIELLO. The design of manual handling tasks: revised tables of maximum acceptable weights and forces. *Ergonomics*. 1991, vol. 34, no. 9, pp. 1197–1213. Available from DOI: [10.1080/00140139108964855](https://doi.org/10.1080/00140139108964855). PMID: 1743178.
- [33] CIRIELLO, V. M. et al. Distributions of manual materials handling task. *International Journal of Industrial Ergonomics*. 1999, no. 24, pp. 379–388.
- [34] CIRIELLO, V.M., R.W. MCGORRY, and S.E. MARTIN. Maximum acceptable horizontal and vertical forces of dynamic pushing on high and low coefficient of friction floors. *International Journal of Industrial Ergonomics*. 2001, no. 27, pp. 1–8.
- [35] NAGAMI, A., T. MURAKAMI, and K. OHNISHI. *Industrial Electronics Society, 2003. IECON '03. The 29th Annual Conference of the IEEE. A Power-Assistant Platform Taking Environmental Disturbance into Account*. 2000.
- [36] ALMEIDA, F., A.LOPES, and P. ABREU. *Force-Impedance Control: a new control strategy of robotic manipulators*. 1999.
- [37] SHARIFI, M., S. BEHZADIPOUR, and G. VOSSOUGH. Nonlinear model reference adaptive impedance control for human–robot interactions. *Control Engineering Practice*. 2014, no. 32, pp. 9–27.
- [38] MIYAZAWA, T., S. KATSURA, and K. OHNISHI. *A Power-Assisted Wheelchair Taking Running Environment into Account*. 2003. No. 2.
- [39] DUCHAINE, V. and C. GOSSELI. General Model of Human-Robot Cooperation Using a Novel Velocity Based Variable Impedance Control. *IEEE/WHC*. 2007, pp. 1–24.
- [40] WIDDOWSON, Christopher et al. VR Environment for the Study of Collocated Interaction Between Small UAVs and Humans. In: CHEN, J (ed.). *ADVANCES IN HUMAN FACTORS IN ROBOTS AND UNMANNED SYSTEMS*. 2018, vol. 595, pp. 348–355. Advances in Intelligent Systems and Computing. ISBN 978-3-319-60384-1; 978-3-319-60383-4. ISSN 2194-5357. Available from DOI: [10.1007/978-3-319-60384-1\\_33](https://doi.org/10.1007/978-3-319-60384-1_33). AHFE International Conference on Human Factors in Robots and Unmanned Systems, Los Angeles, CA, JUL 17-21, 2017.



- [41] LIU, Yang, Xinyang LI, and Chenguang YANG. Design of a Control Platform for Mobile Robot with SSVEP-BCI System. In: *PROCEEDINGS OF THE IEEE 2019 9TH INTERNATIONAL CONFERENCE ON CYBERNETICS AND INTELLIGENT SYSTEMS (CIS) ROBOTICS, AUTOMATION AND MECHATRONICS (RAM) (CIS & RAM 2019)*. IEEE, 2019, pp. 198–203. ISBN 978-1-7281-3458-1. 9th IEEE International Conference on Cybernetics and Intelligent Systems (CIS) / IEEE Conference on Robotics, Automation and Mechatronics (RAM), Bangkok, THAILAND, NOV 18-20, 2019.
- [42] SILVA, L. A., L.A. RODRIGUES, and B.J. CARDOSO. Methodology for rating three phase induction motors to drive vehicles used by collectors of recyclable materials. *Brazilian Symposium on Intelligent Automation*. 2011, no. 3, pp. 1346–1351.
- [43] SILVA, L. A. et al. Design and Implementation of a Low-Cost Robotic Load Carrier. *IEEE International Conference on Robotics and Automation*. 2014, no. 3, pp. 2731–2737.
- [44] TERASHIMA, K. et al. Auto-Tuning Control of Power Assist System Based on The Estimation of Operator’s Skill Level for Forward and Backward Driving of Omni-Directional Wheelchair. *IEEE/RSJ International Conference on Intelligent Robots and Systems (IROS)*. 2010, no. 37(4), pp. 6046–6051.
- [45] KOURO, Samir et al. Model Predictive Control—A simple and powerful method to control power converters. *IEEE Transactions on Industrial Electronics*. 2009, vol. 56, no. 6, pp. 1826–1838. Available from DOI: [10.1109/tie.2008.2008349](https://doi.org/10.1109/tie.2008.2008349).
- [46] BLAYA, Joaquín A. and Hugh M. HERR. Adaptive control of a variable-impedance ankle-foot orthosis to assist drop-foot gait. *IEEE Transactions on Neural Systems and Rehabilitation Engineering*. 2004, vol. 12, no. 1, pp. 24–31. Available from DOI: [10.1109/tnsre.2003.823266](https://doi.org/10.1109/tnsre.2003.823266).
- [47] BELTRAN, Brice, Tarek AHMED-ALI, and Mohamed BENBOUZID. Sliding mode Power control of Variable-Speed wind energy Conversion Systems. *IEEE Transactions on Energy Conversion*. 2008, vol. 23, no. 2, pp. 551–558. Available from DOI: [10.1109/tec.2007.914163](https://doi.org/10.1109/tec.2007.914163).
- [48] DAYAN, Peter and Bernard W. BALLEINE. Reward, motivation, and reinforcement learning. *Neuron*. 2002, vol. 36, no. 2, pp. 285–298. Available from DOI: [10.1016/s0896-6273\(02\)00963-7](https://doi.org/10.1016/s0896-6273(02)00963-7).
- [49] GUO, Yi, David HILL, and Youyi WANG. Nonlinear decentralized control of large-scale power systems. *Automatica*. 2000, vol. 36, no. 9, pp. 1275–1289. Available from DOI: [10.1016/s0005-1098\(00\)00038-8](https://doi.org/10.1016/s0005-1098(00)00038-8).
- [50] GUERRERO, Josep M. et al. Decentralized control for parallel operation of distributed generation inverters using resistive output impedance. *IEEE Transactions on Industrial Electronics*. 2007, vol. 54, no. 2, pp. 994–1004. Available from DOI: [10.1109/tie.2007.892621](https://doi.org/10.1109/tie.2007.892621).

- [51] SCIARRETTA, Antonio, Michael BACK, and Lino GUZZELLA. Optimal control of parallel hybrid electric vehicles. *IEEE Transactions on Control Systems and Technology*. 2004, vol. 12, no. 3, pp. 352–363. Available from DOI: [10.1109/tcst.2004.824312](https://doi.org/10.1109/tcst.2004.824312).
- [52] KIGUCHI, Kazuo, Tomokazu TANAKA, and Toshio FUKUDA. Neuro-Fuzzy control of a robotic exoskeleton with EMG signals. *IEEE Transactions on Fuzzy Systems*. 2004, vol. 12, no. 4, pp. 481–490. Available from DOI: [10.1109/tfuzz.2004.832525](https://doi.org/10.1109/tfuzz.2004.832525).
- [53] POZO, Esteban, Nikunj Kumar PATEL, and Frank SCHRÖDEL. Collaborative Robotic Environment for Educational Training in Industry 5.0 Using an Open Lab Approach. *IFAC-PapersOnLine*. 2022, vol. 55, no. 17, pp. 314–319. ISSN 2405-8963. Available from DOI: <https://doi.org/10.1016/j.ifacol.2022.09.298>. 13th IFAC Symposium on Advances in Control Education ACE 2022.
- [54] KOCHUBEY, Dmitry and Petr TUMA. Human Comfort and Skill Evaluation During Interaction with PAMV. In: *Proceedings of the 10th International Conference on Pervasive Technologies Related to Assistive Environments*. Island of Rhodes, Greece: Association for Computing Machinery, 2017, pp. 250–251. PETRA '17. ISBN 9781450352277. Available from DOI: [10.1145/3056540.3076213](https://doi.org/10.1145/3056540.3076213).
- [55] *HX711 24-Bit Analog-to-Digital Converter (ADC) for Weigh Scales*. AVIA SEMICONDUCTOR, 2014. No. HX711. Rev. 1.0.
- [56] *AS5045 12-Bit Programmable Magnetic Rotary Position Sensor*. AMS, 2017. No. AS5045. v2-01.
- [57] *HMC5983 3-Axis Digital Compass IC*. Honeywell, 2012. No. HMC5983. 900425.
- [58] *MPU-6000/MPU-6050 Register Map and Descriptions*. InvenSense, 2013. No. MPU6050. Revision 4.2.
- [59] OKAMURA, Allison M. Haptic Dimensions of Human-Robot Interaction. *J. Hum.-Robot Interact.* 2018, vol. 7, no. 1. Available from DOI: [10.1145/3209768](https://doi.org/10.1145/3209768).
- [60] GIORDANO, Marcello et al. Mid-Air Haptics for Control Interfaces. In: *Extended Abstracts of the 2018 CHI Conference on Human Factors in Computing Systems*. Montreal QC, Canada: Association for Computing Machinery, 2018, pp. 1–8. CHI EA '18. ISBN 9781450356213. Available from DOI: [10.1145/3170427.3170625](https://doi.org/10.1145/3170427.3170625).
- [61] KATSURA, Seiichiro and Kouhei OHNISHI. Advanced Motion Control for Wheelchair in Unknown Environment. In: *2006 IEEE International Conference on Systems, Man and Cybernetics*. 2006, vol. 6, pp. 4926–4931. Available from DOI: [10.1109/ICSMC.2006.385086](https://doi.org/10.1109/ICSMC.2006.385086).
- [62] MOOG, Robert A. Voltage controlled electronic music modules. *Journal of the Audio Engineering Society*. 1964, vol. 13, no. 3, pp. 200–206. Available also from: <https://www.aes.org/e-lib/browse.cfm?elib=1204>.

- [63] HERR, Hugh M. Exoskeletons and orthoses: classification, design challenges and future directions. *Journal of Neuroengineering and Rehabilitation*. 2009, vol. 6, no. 1. Available from DOI: [10.1186/1743-0003-6-21](https://doi.org/10.1186/1743-0003-6-21).
- [64] MARSHAK, Alan H. A unique current-controlled negative resistance generator. *IEEE Transactions on Communication and Electronics*. 1964, vol. 83, no. 71, pp. 182–184. Available from DOI: [10.1109/tcome.1964.6539337](https://doi.org/10.1109/tcome.1964.6539337).
- [65] SARTORI, Emanuela. Hybrid transformers. *IEEE Transactions on Parts, Materials and Packaging*. 1968, vol. 4, no. 3, pp. 59–66. Available from DOI: [10.1109/tpmp.1968.1135893](https://doi.org/10.1109/tpmp.1968.1135893).
- [66] PETROV, B. M. and Y. V. YUCHANOV. Inverse scattering problem for an impedance cylinder of arbitrary cross section. *Radel*. 1980, vol. 23, pp. 78–81. Available also from: <http://ui.adsabs.harvard.edu/abs/1980Radel..23R..78P/abstract>.
- [67] CHALMERS, B.J. and Anshul AGARWAL. Importance of direct- and quadrature-axis damper impedances in starting performance of salient-pole motors. *Proceedings of the Institution of Electrical Engineers*. 1966, vol. 113, no. 4, p. 663. Available from DOI: [10.1049/piee.1966.0107](https://doi.org/10.1049/piee.1966.0107).
- [68] OMER, Aiman et al. Study of Bipedal Robot Walking Motion in Low Gravity: Investigation and Analysis. *International Journal of Advanced Robotic Systems*. 2014, vol. 11, no. 45, p. 123. Available from DOI: [10.5772/58731](https://doi.org/10.5772/58731). Regular Paper.
- [69] SAUNDERS, J., Verne INMAN, and Howard EBERHART. Major determinants in normal and pathological gait. *The Journal of bone and joint surgery. American volume*. 1953, pp. 543–58. Available from DOI: [10.2106/00004623-195335030-00003](https://doi.org/10.2106/00004623-195335030-00003).
- [70] KUO, Arthur D. and J. Maxwell DONELAN. Dynamic Principles of Gait and Their Clinical Implications. *Physical Therapy*. 2010, vol. 90, no. 2, pp. 157–174. ISSN 0031-9023. Available from DOI: [10.2522/ptj.20090125](https://doi.org/10.2522/ptj.20090125).
- [71] MARTINI, F., M.J. TIMMONS, and R.B. TALLITSCH. *Human Anatomy*. Pearson Benjamin Cummings, 2012. ISBN 9780321688156. Available also from: <https://books.google.cz/books?id=loaWbwAACAAJ>.
- [72] BURDET, E. et al. How are internal models of unstable tasks formed? In: *The 26th Annual International Conference of the IEEE Engineering in Medicine and Biology Society*. 2004, vol. 2, pp. 4491–4494.
- [73] CHOUDHURY, T. T. et al. Modeling of Human Arm Movement: A Study on Daily Movement. In: *2013 Fifth International Conference on Computational Intelligence, Modelling and Simulation*. 2013, pp. 63–68.
- [74] ARTEMIADIS, P. K. et al. Human arm impedance: Characterization and modeling in 3D space. In: *2010 IEEE/RSJ International Conference on Intelligent Robots and Systems*. 2010, pp. 3103–3108.

- [75] TEE, K P et al. A model of force and impedance in human arm movements. *Biological cybernetics*. 2004, vol. 90, pp. 368–375.
- [76] SPEICH, John, Liang SHAO, and Michael GOLDFARB. Modeling the human hand as it interacts with a telemanipulation system. *Mechatronics*. 2005, vol. 15, pp. 1127–1142. Available from DOI: [10.1016/j.mechatronics.2005.06.001](https://doi.org/10.1016/j.mechatronics.2005.06.001).
- [77] RAHMAN, M. M., R. IKEURA, and K. MIZUTANI. Investigating the impedance characteristic of human arm for development of robots to cooperate with human operators. In: *IEEE SMC'99 Conference Proceedings. 1999 IEEE International Conference on Systems, Man, and Cybernetics (Cat. No.99CH37028)*. 1999, vol. 2, 676–681 vol.2.
- [78] WANG, S et al. *Biomedical Engineering and Informatics (BMEI), 2011 4th International Conference*. Vol. 3. IEEE, 2011.
- [79] TANAKA, Y. et al. Active-steering control system based on human hand impedance properties. In: *2010 IEEE International Conference on Systems, Man and Cybernetics*. 2010, pp. 1697–1702.
- [80] LEE, K.S. et al. Effect of handle height on lower-back. *Applied Ergonomic*. 1991, no. 2(2), pp. 117–123.
- [81] SACHCHIDANANDA, BANERJEE, ACHARYA KESHAB NARAYAN, and CHATTOPADHYAY DHURJATI PROSAD. Studies on energy expenditure of rickshaw pullers. *Indian Journal of Physiology and Pharmacology*. 1959, vol. 3, pp. 147–60.
- [82] TODD and ANDREW. CURRENT TRENDS IN RESEARCH FOCUSED ON PUSHING AND PULLING. 2005.
- [83] LEE, Kwan S. et al. Effect of handle height on lower-back loading in cart pushing and pulling. *Applied Ergonomics*. 1991, vol. 22, no. 2, pp. 117–123. Available from DOI: [10.1016/0003-6870\(91\)90310-e](https://doi.org/10.1016/0003-6870(91)90310-e).
- [84] HAISMAN, M. F., Fred R. WINSMANN, and Rachel GOLDMAN. Energy cost of pushing loaded handcarts. *Journal of Applied Physiology*. 1972, vol. 33, no. 2, pp. 181–183. Available from DOI: [10.1152/jappl.1972.33.2.181](https://doi.org/10.1152/jappl.1972.33.2.181).
- [85] JÄGER, Matthias, Alwin LUTTMANN, and Wolfgang LAURIG. The load on the spine during the transport of dustbins. *Applied Ergonomics*. 1984, vol. 15, no. 2, pp. 91–98. Available from DOI: [10.1016/0003-6870\(84\)90278-3](https://doi.org/10.1016/0003-6870(84)90278-3).
- [86] CHOTIPRAYANAKUL, Pholchai et al. A Haptic base human robot interaction approach for robotic grit blasting. *Proceedings of the ... ISARC*. 2008. Available from DOI: [10.22260/isarc2008/0022](https://doi.org/10.22260/isarc2008/0022).
- [87] BREAZEAL, Cynthia. Function Meets Style: Insights from Emotion Theory Applied to HRI. *IEEE Transactions on Systems, Man and Cybernetics*. 2004, vol. 34, no. 2, pp. 187–194. Available from DOI: [10.1109/tsmcc.2004.826270](https://doi.org/10.1109/tsmcc.2004.826270).

- [88] GRECZEK, Jillian et al. Socially assistive robotics for personalized education for children. *Human-Robot Interaction*. 2014. Available also from: <http://robotics.usc.edu/publications/media/uploads/pubs/socially-assistive-robotics.pdf>.
- [89] DAUTENHAHN, Kerstin. Socially intelligent robots: dimensions of human-robot interaction. *Philosophical Transactions of the Royal Society B*. 2007, vol. 362, no. 1480, pp. 679–704. Available from DOI: [10.1098/rstb.2006.2004](https://doi.org/10.1098/rstb.2006.2004).
- [90] BRÖHL, Christina et al. Human-Robot Collaboration Acceptance Model: development and comparison for Germany, Japan, China and the USA. *International Journal of Social Robotics*. 2019, vol. 11, no. 5, pp. 709–726. Available from DOI: [10.1007/s12369-019-00593-0](https://doi.org/10.1007/s12369-019-00593-0).
- [91] MOUBAYED, Sàmer Al et al. *Multimodal Feedback from Robots and Agents in a Storytelling Experiment*. 2008. Available also from: <https://hal.science/hal-03164370>.
- [92] BOUDOIN, Pierre et al. Towards multimodal human-robot interaction in large scale virtual environment. *Proceedings of the 3rd ACM/IEEE International Conference on Human Robot Interaction*. 2008. Available from DOI: [10.1145/1349822.1349869](https://doi.org/10.1145/1349822.1349869).
- [93] HARNISS, Mark et al. The behavioral and emotional rating scale. *Journal of Psychoeducational Assessment*. 1999, vol. 17, no. 1, pp. 4–14. Available from DOI: [10.1177/073428299901700101](https://doi.org/10.1177/073428299901700101).
- [94] CHEN, Michael, Xitao FAN, and S. T. MOE. Criterion-related validity of the Borg ratings of perceived exertion scale in healthy individuals: a meta-analysis. *Journal of Sports Sciences*. 2002, vol. 20, no. 11, pp. 873–899. Available from DOI: [10.1080/026404102320761787](https://doi.org/10.1080/026404102320761787).
- [95] HARTLEY, Sigan L. and William E. MACLEAN. A review of the reliability and validity of Likert-type scales for people with intellectual disability. *Journal of Intellectual Disability Research*. 2006, vol. 50, no. 11, pp. 813–827. Available from DOI: [10.1111/j.1365-2788.2006.00844.x](https://doi.org/10.1111/j.1365-2788.2006.00844.x).
- [96] BORG, Gunnar A.V. Psychophysical bases of perceived exertion. *Medicine and science in sports and exercise*. 1982, no. 14(5), pp. 377–381.
- [97] ALIAN, Aymen and Kirk SHELLEY. Photoplethysmography: Analysis of the Pulse Oximeter Waveform. 2014, pp. 165–178. ISBN 978-1-4614-8556-8. Available from DOI: [10.1007/978-1-4614-8557-5\\_19](https://doi.org/10.1007/978-1-4614-8557-5_19).
- [98] AGUILAR PELAEZ, Eduardo and Esther VILLEGAS. LED power reduction trade-offs for ambulatory pulse oximetry. *Conference proceedings : ... Annual International Conference of the IEEE Engineering in Medicine and Biology Society. IEEE Engineering in Medicine and Biology Society. Conference*. 2007, vol. 2007, pp. 2296–9. Available from DOI: [10.1109/IEMBS.2007.4352784](https://doi.org/10.1109/IEMBS.2007.4352784).

- [99] REISNER, Andrew et al. Reisner A, Shaltis PA, McCombie D, Asada HH. Utility of the photoplethysmogram in circulatory monitoring. *Anesthesiology*. 2008, vol. 108, pp. 950–8. Available from DOI: [10.1097/ALN.0b013e31816c89e1](https://doi.org/10.1097/ALN.0b013e31816c89e1).
- [100] *MC3413 3-Axis Accelerometer Preliminary Datasheet*. mCube, 2014. No. MC3413. Revision 1.7.
- [101] KOCHUBEY, Dmitry and Petr TUMA. Industrial Cart Power Assistance on Undefined Path. In: *Proceedings of the 11th PErvasive Technologies Related to Assistive Environments Conference*. Corfu, Greece: Association for Computing Machinery, 2018, pp. 108–109. PETRA '18. ISBN 9781450363907. Available from DOI: [10.1145/3197768.3203174](https://doi.org/10.1145/3197768.3203174).
- [102] STULP, F. et al. Reinforcement learning of impedance control in stochastic force fields. In: *2011 IEEE International Conference on Development and Learning (ICDL)*. 2011, vol. 2, pp. 1–6.
- [103] WATKINS, Christopher. Learning From Delayed Rewards. 1989.
- [104] WATKINS Christopher; Dayan, Peter. Technical Note Q-Learning. 1992, pp. 279–292.
- [105] BANERJEE, S. and D.P. CHATTOPADHYAY. Studies on energy expenditure of rickshaw pullers. *Indian Journal of Physiology and Pharmacology*. 1959, no. 3, pp. 147–160.
- [106] HAISMAN, M.F., F.R. WINSMANN, and R.F. GOLDMAN. Energy cost of pushing loaded handcarts. *Journal of Applied Physiology*. 1972, no. 33, pp. 181–183.
- [107] JB, Saunders, Inman VT, and Eberhart HD. The major determinants in normal and pathological gait. *J Bone Joint Surg Am*. 1953, no. 35, pp. 543–558.
- [108] VAN DER BEEK, A.J. et al. Gender differences in exerted forces and physiological load during pushing and pulling of wheeled cages by postal workers. *Ergonomics*. 2000, vol. 43, no. 2, pp. 269–281. Available from DOI: [10.1080/001401300184602](https://doi.org/10.1080/001401300184602). cited By 44.
- [109] MATARIĆ, M. and P. DARIO. Haptic feedback in human-robot interaction. *IEEE Transactions on Robotics and Automation*. 1994, vol. 10, no. 6, pp. 788–797.
- [110] KANDA, T. and H. ISHIGURO. Social and emotional interactions with robots. *Interaction Studies*. 2007, vol. 8, no. 1, pp. 73–87.
- [111] ARKIN, R.C. and B.J. GROSZ. A formal model of the interaction of ethical constraints and robot behavior. *Robotics and autonomous systems*. 1994, vol. 12, no. 3-4, pp. 181–204.
- [112] DAUTENHAHN, K. Human-robot interaction: An interdisciplinary challenge. *Journal of Physiology-Paris*. 2007, vol. 101, no. 2-3, pp. 147–152.

- [113] BELPAEME, T. Multimodal interaction in human-robot systems. *IEEE Transactions on Systems, Man, and Cybernetics, Part C (Applications and Reviews)*. 2012, vol. 42, no. 4, pp. 533–539.
- [114] HOWARD, A. Affective and social interactions with robots. *Interaction Studies*. 2007, vol. 8, no. 1, pp. 73–87.
- [115] JÄGER, M., A. LUTTMANN, and W. LAURIG. The load on the spine during the transport of dustbins. *Applied Ergonomics*. 1984, no. 15, pp. 91–98.
- [116] SCHIBYE, B. et al. Mechanical load on the low back and shoulders during pushing and pulling of two-wheeled waste containers compared with lifting and carrying of bags and bins. *Clinical Biomechanics*. 2001, no. 16, pp. 549–559.
- [117] OHNISHI, Akihiro, Masato TAKANOKURA, and Atsushi SUGAMA. Evaluation of Interhandle Distance During Pushing and Pulling of a Four-Caster Cart for Upper Limb Exertion. *Safety and Health at Work*. 2016, vol. 7. Available from DOI: [10.1016/j.shaw.2016.01.005](https://doi.org/10.1016/j.shaw.2016.01.005).
- [118] SWAMYNATHAN, Manohar. Step 6 – Deep and Reinforcement Learning. In: *Mastering Machine Learning with Python in Six Steps: A Practical Implementation Guide to Predictive Data Analytics Using Python*. Berkeley, CA: Apress, 2017, pp. 297–344. ISBN 978-1-4842-2866-1. Available from DOI: [10.1007/978-1-4842-2866-1\\_6](https://doi.org/10.1007/978-1-4842-2866-1_6).
- [119] RIENER, Robert et al. Human-centered rehabilitation robotics. In: 2005, vol. 2005, pp. 319–322. ISBN 0-7803-9003-2. Available from DOI: [10.1109/ICORR.2005.1501110](https://doi.org/10.1109/ICORR.2005.1501110).
- [120] SCHMIDTLER, Jonas and Klaus BENGLER. Fast or Accurate? – Performance Measurements for Physical Human-robot Collaborations. *Procedia Manufacturing*. 2015, vol. 3, pp. 1387–1394. ISSN 2351-9789. Available from DOI: <https://doi.org/10.1016/j.promfg.2015.07.298>. 6th International Conference on Applied Human Factors and Ergonomics (AHFE 2015) and the Affiliated Conferences, AHFE 2015.
- [121] KÖPF, Florian et al. Inverse Reinforcement Learning for Identification in Linear-Quadratic Dynamic Games. *IFAC-PapersOnLine*. 2017, vol. 50, no. 1, pp. 14902–14908. ISSN 2405-8963. Available from DOI: <https://doi.org/10.1016/j.ifacol.2017.08.2537>. 20th IFAC World Congress.
- [122] LI, Y. et al. A Framework of Human–Robot Coordination Based on Game Theory and Policy Iteration. *IEEE Transactions on Robotics*. 2016, vol. 32, no. 6, pp. 1408–1418.
- [123] K. TERASHIMA T. Miyoshi, J. Urbano and H. KITAGAWA. Frequency shape control of omni-directional wheelchair to increase user’s comfort. *IEEE International Conference on Robotics and Automation*. 2004, no. 3, pp. 3119–3124.

- [124] D. KOCHUBEY, P.Tuma. Human Comfort and Skill Evaluation During Interaction with PAMV. *Pervasive Technologies Related to Assistive Environments*. 2017, no. 3, pp. 1346–1351.
- [125] FURUTA, K. Control of Pendulum: From Super Mechano-System to Human Adaptive Mechatronics. *Proceedings of the 42nd IEEE Conference on Decision and Control*. 2003, no. 3, pp. 1498–1507.
- [126] L. S. BEALS, Jr. The Human Operator as a Link in Closed-Loop Control Systems. *American Institute of Electrical Engineers: Electrical Engineering*. 1952, no. 71, pp. 319–324.
- [127] KITAGAWA, H. et al. Fuzzy Power Assist Control System for Omni-Directional Transport Wheelchair. *IEEE/RSJ International Conference on Intelligent Robots and Systems*. 2004, no. 1, pp. 1580–1585.
- [128] MALDONADO, B. et al. Stiffness-based Tuning of an Adaptive Impedance Controller for Robot-assisted Rehabilitation of Upper Limbs. *Institute of Electrical and Electronics Engineers*. 2015, no. 71, pp. 319–324.
- [129] KAZEROONI, H. Human-robot interaction via the transfer of power and information signals part I : dynamics and control analysis. *Proceedings of IEEE International Conference on Robotics and Automation*. 1989, no. 71, pp. 1632–1642.
- [130] CHUGO, D. et al. An Assistive Wheelchair based on concept of Passive Robotics. *Industrial Electronics Society IECON*. 2013, no. 71, pp. 8253–8258.
- [131] DIN, ENISO. *10218-2.: Robots and Robotic Devices–Safety Requirements For Industrial Robots–Part 2: Robot Systems and Integration*. Beuth Verlag GmbH, Berlin, 2012.
- [132] SUTTON, Richard S. and Andrew G. BARTO. *Reinforcement Learning: An Introduction*. Cambridge, MA, USA: A Bradford Book, 2018. ISBN 0262039249.
- [133] PLÍVA, Zdeněk et al. *Guidelines for Writing Bachelor or Master Thesis*. 2nd ed. Liberec: Technical University of Liberec, Faculty of Mechatronics, 2019. ISBN 978-80-7494-456-7. Available from DOI: [10.15240/tul/002/978-80-7494-456-7](https://doi.org/10.15240/tul/002/978-80-7494-456-7).
- [134] PLÍVA, Zdeněk et al. *Metodika zpracování bakalářských a diplomových prací*. 3rd ed. Liberec: TU v Liberci, 2019. ISBN 978-80-7494-455-0. Available from DOI: [10.15240/tul/002/978-80-7494-455-0](https://doi.org/10.15240/tul/002/978-80-7494-455-0).
- [135] SATRAPA, Pavel. *Balík tul pro LaTeX verze 2.0*. Verze 2.0. Liberec: TUL, 2022. Available also from: <http://www.nti.tul.cz/~satrapa/vyuka/latex-tul/>.
- [136] ČSN ISO 690: *Informace a dokumentace – Pravidla pro bibliografické odkazy a citace informačních zdrojů*. 1st ed. Praha: Úřad pro technickou normalizaci, metrologii a státní zkušebnictví, 2011. Třídící znak 01 0197.



- [137] FIRSTOVÁ, Zdeňka. *Podrobný návod, jak citovat literaturu a prameny, s českými příklady* [online]. Plzeň: ZČU, 2011 [visited on 2022-09-10]. Available from: <https://www.iso690.zcu.cz>.
- [138] MENDELEY. *Mendeley - Reference Management Software & Researcher Network* [online]. 2022. [visited on 2022-09-10]. Available from: <https://www.mendeley.com/>.
- [139] CLARIVATE. *EndNote* [EndNote] [online]. 2022. [visited on 2022-09-10]. Available from: <https://endnote.com/>.
- [140] ZOTERO. *Zotero / Your personal research assistant* [online]. 2022. [visited on 2022-09-10]. Available from: <https://www.zotero.org/>.
- [141] CITACE.PRO. *Citace PRO* [online]. 2022. [visited on 2022-09-10]. Available from: <http://citacepro.com/>.
- [142] JABREF. *JabRef* [online]. 2022. [visited on 2022-09-10]. Available from: <http://www.jabref.org>.
- [143] HOFTICH, Michal. *biblatex-iso690 – BibL<sup>A</sup>T<sub>E</sub>X style for ISO 690 standard* [online]. [visited on 2022-09-10]. Available from: <https://ctan.org/pkg/biblatex-iso690>.
- [144] SATRAPA, Pavel. *LaTeX pro pragmatiky*. TUL a CESNET, 2011. Available also from: <http://www.nti.tul.cz/~satrapa/docs/latex/>.

## A Appendix

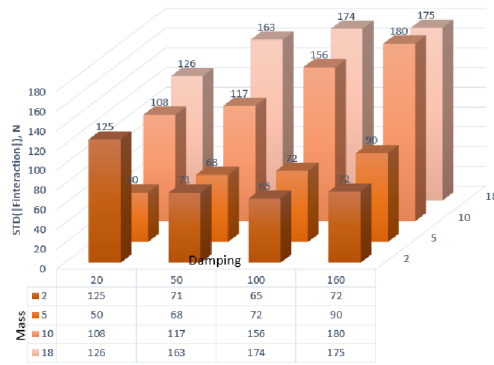


Figure A.1: Standard deviation of absolute interaction force for different settings of impedance controller. Sample 1.

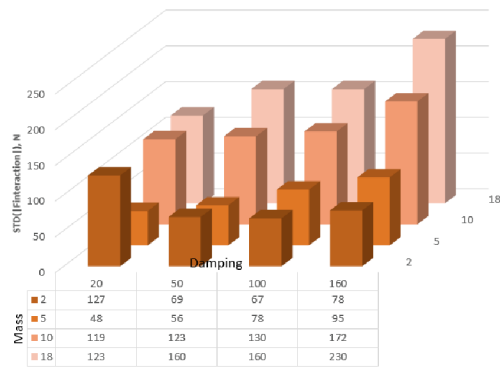


Figure A.2: Standard deviation of absolute interaction force for different settings of impedance controller. Sample 2.

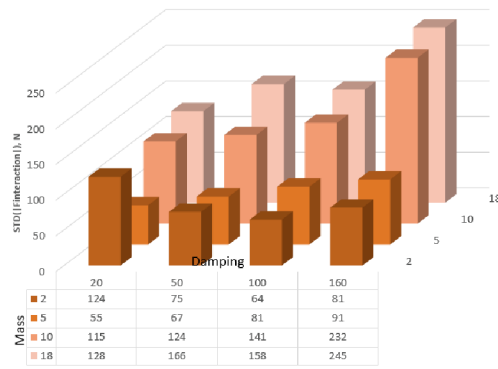


Figure A.3: Standard deviation of absolute interaction force for different settings of impedance controller. Sample 3.

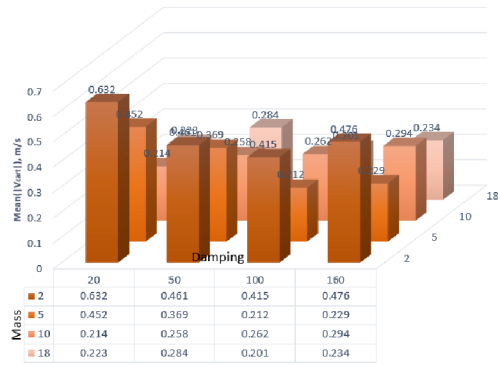


Figure A.4: Mean value of absolute cart velocity for different settings of impedance controller. Sample 1.

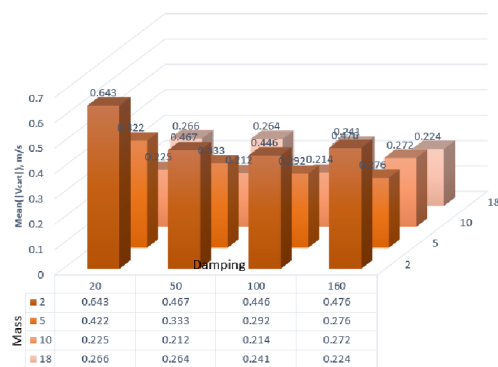


Figure A.5: Mean value of absolute cart velocity for different settings of impedance controller. Sample 2.

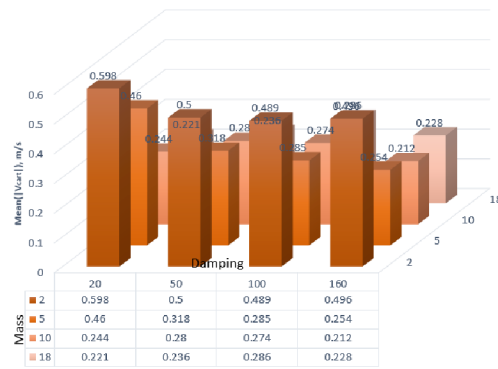


Figure A.6: Mean value of absolute cart velocity for different settings of impedance controller. Sample 3.

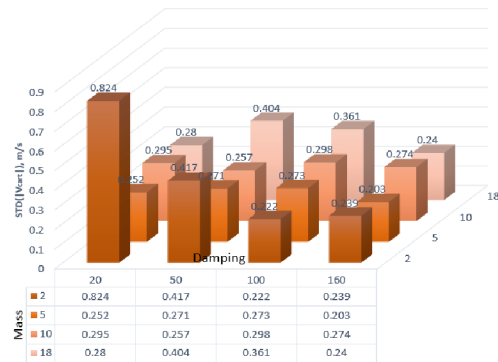


Figure A.7: Mean value of absolute cart velocity for different settings of impedance controller. Sample 1.

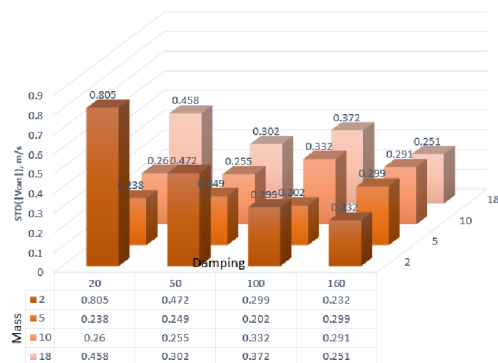


Figure A.8: Mean value of absolute cart velocity for different settings of impedance controller. Sample 2.

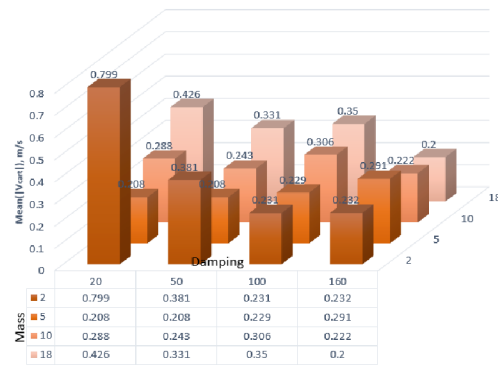


Figure A.9: Mean value of absolute cart velocity for different settings of impedance controller. Sample 3.

## B Mathematical Modeling of an Industrial Cart

In the dynamic realm of industrial automation, the design and control of mobile platforms play an important role in achieving efficient and seamless material transportation. The accurate representation of these systems through mathematical models is necessary to analyze their behavior, predicting their performance, and ultimately optimizing their operation. This chapter describes the development of a comprehensive mathematical model for an industrial cart. We aim to provide a framework to understand cart's dynamics, control strategies, and system optimization.

Using the results from the chapter 7 we selected specific configuration commonly found in heavily-loaded industrial carts. This configuration prominently features two powered wheels and four casters, which serve as the primary components of the cart. This carefully designed arrangement is important as it enables the cart to achieve optimal mobility and stability during its operational tasks. By taking advantage of the power coming from the two powered wheels, the cart can efficiently move in both forward and backward directions, allowing for controlled and precise movement. Complementing the powered wheels, the four casters play a significant role in providing essential support and facilitating smooth steering of the cart. Together, this configuration forms the foundation of the current research.

Due to the complexity of the system caused by several factor shown below we explain the model step-by-step in the set of subchapters.

- Various friction types.
- Wheel spin dynamics.
- Wheel suspension.
- Load distribution.

### B.1 Caster wheel

The mathematical description of a caster wheel can be quite complex due to its swiveling action and the dependence on various factors such as the geometry of the caster, the friction properties of the wheel and the surface, and the velocity and direction of movement of the vehicle. A caster wheel is generally designed to align itself in the direction of movement due to the offset between the point about which

it swivels and the center of the wheel. This self-aligning torque depends on factors such as the velocity of the vehicle, the load on the wheel, and the friction properties of the wheel and the surface.

In a simplified 2D planar model, the kinematics of the caster wheel can be described by the following equations:

$$\frac{dx}{dt} = v_c \cdot \cos(\theta_c) \quad (\text{B.1})$$

$$\frac{dy}{dt} = v_c \cdot \sin(\theta_c) \quad (\text{B.2})$$

$$\frac{d\theta_c}{dt} = w_c \quad (\text{B.3})$$

where  $\theta_c$  - the angle formed by the caster wheel's direction makes with the x-axis (the reference line);  $v_c$  - the velocity of the caster wheel;  $w_c$  - the angular velocity of the caster wheel.

In addition, we need to consider self-aligning torque that aims to minimize the angle  $\theta_c$ .

$$\frac{dw_c}{dt} = -k \cdot \theta_c - d \cdot w_c \quad (\text{B.4})$$

where  $k$  is a spring constant that represents the self-aligning torque and  $d$  is a damping constant that represents the resistance to the change in the wheel's direction.

Continuous differential equation B.4 could be written in the discrete form using a simple forward Euler method, because it gives a sufficient precision for a simple model, which is the damped harmonic oscillator in our case. For more complex models we can use more advanced techniques, such as the Runge-Kutta method.

$$w_c[n+1] = w_c[n] + dt \cdot (-k \cdot \theta_c[n] - d \cdot w_c[n]) \quad (\text{B.5})$$

where  $dt$  is the time step for the discretisation,  $n$  is the current time step, and  $n+1$  is the next time step.  $k$  and  $d$  are the spring constant and the damping constant, respectively,  $w_c$  is the angular velocity of the caster wheel, and  $\theta_c$  is the angle of the caster wheel.

The equation to adjust the angle  $\theta_c$  could be written as:

$$\theta_c[n+1] = \theta_c[n] + dt \cdot w_c[n] \quad (\text{B.6})$$

Therefore, we used these equations to simulate the behaviour of caster wheels.

## B.2 Numerical methods for solving ordinary differential equations (ODEs)

Numerical methods are widely used to solve ordinary differential equations (ODEs) when analytical solutions are not available or difficult to obtain. Two of the most commonly used methods among the others are the Euler's method and the Runge-Kutta method.

The Euler's method is the simplest method for numerical integration of ODEs. It works by using the derivative at the current point to estimate the value of the function at the next point. The formula for the forward Euler method is:

$$y[n + 1] = y[n] + h \cdot f(t[n], y[n]) \quad (\text{B.7})$$

where  $h$  is the step size,  $f(t[n], y[n])$  is the derivative of  $y$  with respect to  $t$  at the point  $(t[n], y[n])$ .

While the Euler's method is straightforward and easy to implement, it is only first-order accurate, meaning that the error per step is proportional to the square of the step size. This can lead to significant inaccuracies for larger step sizes or more complex functions.

The Runge-Kutta method is a more sophisticated method for numerical integration that provides greater accuracy. The most common form is the 4th order Runge-Kutta method, which takes four estimates of the derivative at various points within the step size, and combines them to produce a more accurate estimate of the function at the next point.

The formulas for the 4th order Runge-Kutta method are depicted in [B.8-B.12](#).

$$k1 = h \cdot f(t[n], y[n]) \quad (\text{B.8})$$

$$k2 = h \cdot f\left(t[n] + \frac{h}{2}, y[n] + \frac{k1}{2}\right) \quad (\text{B.9})$$

$$k3 = h \cdot f\left(t[n] + \frac{h}{2}, y[n] + \frac{k2}{2}\right) \quad (\text{B.10})$$

$$k4 = h \cdot f(t[n] + h, y[n] + k3) \quad (\text{B.11})$$

$$y[n + 1] = y[n] + (k1 + 2 \cdot k2 + 2 \cdot k3 + k4)/6 \quad (\text{B.12})$$

where  $k1$ ,  $k2$ ,  $k3$ , and  $k4$  are intermediate variables that are used to compute the estimate of the derivative of the function at different points within the step. These four estimates are then combined to compute a more accurate estimate of the derivative of the function over the step, which is used to update the value of the function at the next step.

- **k1** is the estimate of the derivative at the beginning of the step. It is computed in the same way as in the Euler's method, using the derivative of the function at the current point.
- **k2** is an estimate of the derivative at the midpoint of the step, it uses the derivative of the function at the point estimated by  $k1$ .
- **k3** is another estimate of the derivative at the midpoint of the step, but this time it uses the derivative of the function at the point estimated by  $k2$ .



- **k4** is an estimate of the derivative at the end of the step, it uses the derivative of the function at the point estimated by k3.

In summary, the main difference between the Euler method and the Runge-Kutta method is a trade-off between computational complexity and accuracy. The Euler method is simpler and faster, but less accurate, while the Runge-Kutta method is more accurate, but also more computationally intensive.

## B.3 Direct current motor model

The industrial cart designed in this thesis is using DC motors for its movement. A DC motor converts direct current electrical energy into mechanical energy. In this chapter we show the mathematical model for a DC motor. The core idea is based on Newton's second law of motion and Kirchhoff's voltage law.

The DC motor is characterized by the following set of parameters:

- V: input voltage to the motor.
- I: current flowing through the motor.
- R: resistance of the motor.
- L: inductance of the motor.
- $w$ : angular velocity of the motor shaft.
- J: moment of inertia of the rotor.
- B: viscous damping coefficient.
- K: a constant that relates the input current and output torque, and also relates the back-emf and speed of the motor, sometimes split into  $K_t$  (torque constant) and  $K_e$  (back-emf constant).

Electrical equation (Kirchhoff's voltage law):

$$V = L \frac{dI}{dt} + RI + K\omega \quad (\text{B.13})$$

This equation states that the input voltage (V) to the motor is equal to the sum of the voltage drop across the inductor ( $L \cdot (\frac{dI}{dt})$ ), the voltage drop across the resistor (RI), and the back-emf (K).

Mechanical equation (Newton's second law):

$$\tau = J \frac{d\omega}{dt} + B\omega \quad (\text{B.14})$$

This equation states that the torque ( $\tau$ ) produced by the motor is equal to the sum of the torque due to inertia ( $J \cdot (\frac{d\omega}{dt})$ ) and the torque due to damping ( $B \cdot \omega$ ).

It is common to combine these two equations into a state-space form for control design, B.15-B.16:

$$\frac{dI}{dt} = \frac{1}{L}(V - RI - K\omega) \quad (\text{B.15})$$

$$\frac{d\omega}{dt} = \frac{1}{J}(KI - B\omega) \quad (\text{B.16})$$

These are the fundamental equations that describe a DC motor's dynamics. The precise values of R, L, K, J, and B depend on the specific motor's design. Note that these equations are a simplification; real motors have many other effects such as magnetic saturation, non-linear friction, and thermal effects that are not captured in these equations.

Applying forward Euler discretisation to the state-space equations, we obtain:  
The discretised electrical equation:

$$I[k + 1] = I[k] + T \cdot \frac{1}{L} \cdot (V[k] - R \cdot I[k] - K \cdot \omega[k]) \quad (\text{B.17})$$

The discretized mechanical equation:

$$\omega[k + 1] = \omega[k] + T \cdot \frac{1}{J} \cdot (K \cdot I[k] - B \cdot \omega[k]) \quad (\text{B.18})$$

where  $I[k]$  and  $w[k]$  are the current and angular velocity at the k-th discrete-time instant, respectively.  $V[k]$  is the input voltage at the k-th discrete-time step. The code obtained for this specific case can be demonstrated upon request.

## B.4 Powered wheel

In this subchapter we describe mathematical model of a wheel connected to a DC motor via a chain belt. This model typically involves several aspects, including the motor characteristics, the gear ratio of the chain belt, the radius of the wheel, and the load on the wheel.

For this mathematical model we make the following assumptions:

- The chain belt and gear mechanism is 100% efficient (this is usually not the case in reality due to friction, slippage, etc.).
- The radius of the wheel is  $r$  and the load on the wheel is  $F$  (which opposes the movement).
- The gear ratio is  $n$  (number of teeth on the wheel gear divided by the number of teeth on the motor gear).
- The torque output of the motor is  $T_m$ , which depends on the current flowing through the motor and the characteristics of the motor. The angular velocity of the motor is  $w_m$ .

The torque on the wheel can be calculated as:

$$T_w = n \cdot T_m \quad (\text{B.19})$$

The force exerted by the wheel on the ground, which propels the vehicle forward, can be determined as:

$$F_w = \frac{T_w}{r} \quad (\text{B.20})$$

If there is a load on the wheel, we could assume that it opposes the movement. Therefore, the net force can be calculated as follows:

$$F_n = F_w - F \quad (\text{B.21})$$

The angular velocity of the wheel is determined by the gear ratio and the motor's angular velocity:

$$\omega_w = \frac{\omega_m}{n} \quad (\text{B.22})$$

The linear velocity can be obtained by using the angular velocity of the wheel:

$$v = \omega_w \cdot r \quad (\text{B.23})$$

We use this mathematical description from this subchapter to simulate the behaviour of the powered wheels of the industrial cart, the torque generated by powered wheels, its corresponding force, angular and linear velocity of the powered wheel.

## B.5 Wheel suspension

The spring suspension system for a wheel can be modeled using Hooke's Law and Newton's Second Law of Motion. Let's assume that the wheel is connected to a single spring that is attached to a fixed point above it. When the wheel moves up or down, the spring exerts a force that opposes the motion and tries to bring the wheel back to its equilibrium position.

The mathematical description of the spring suspension system is provided below.

The Hooke's law states that the force exerted by a spring is directly proportional to the displacement from its equilibrium position. Mathematically, it can be expressed as:

$$F = -kx \quad (\text{B.24})$$

where  $F$  is the force exerted by the spring,  $k$  is the spring constant (stiffness),  $x$  is the displacement from the equilibrium position. The negative sign indicates that the force exerted by the spring is in the opposite direction to the displacement.

Newton's second Law states that the net force acting on an object is equal to the mass of the object multiplied by its acceleration. In the case of the wheel, the net force is the sum of the force exerted by the spring and any other external forces acting on the wheel. Mathematically, it can be expressed as:

$$F_{\text{net}} = ma \quad (\text{B.25})$$

where  $F_{\text{net}}$  is the net force acting on the wheel,  $m$  is the mass of the wheel,  $a$  is the acceleration of the wheel. By combining the Hooke's law and Newton's second law, we can write the equation of motion for the spring suspension system:

$$ma = -kx \quad (\text{B.26})$$

This equation relates the acceleration of the wheel to the displacement from the equilibrium position and the spring constant.

Solving this second-order ordinary differential equation yields the motion of the wheel as a function of time. As the result, the accelerations and displacements depend on the specific initial conditions and the properties of the system (mass, spring constant, etc.).

## B.6 Load distribution

When it comes to designing carts or analyzing their stability, understanding load distribution on the wheels is of utmost importance. The distribution of weight determines how the load is supported and impacts the performance and safety of the cart. By employing the principles of static equilibrium, engineers and designers can calculate the load distribution on cart wheels based on the position of the load.

In the static equilibrium state, a cart is assumed to be at rest with no net force acting on it. This means that the forces applied to the cart must be balanced to maintain stability. If we consider a cart with two wheels — one at the front and another at the rear — the load distribution between these wheels can be determined.

To begin the analysis, the total weight of the cart and load needs to be known. This weight, denoted as  $W$ , represents the force that needs to be supported by the wheels. The next step involves identifying the position of the load with respect to the front and rear wheels. These distances, denoted as  $x_1$  and  $x_2$  respectively, are measured from the front wheel.

Once these parameters are established, the load distribution can be calculated using the formulas derived from the static equilibrium principles. The key concept is that the reaction forces exerted by the wheels, referred to as  $R_1$  and  $R_2$ , must balance the total weight of the cart and load.

To calculate the reaction force at the front wheel ( $R_1$ ), the following formula is used:

$$R_1 = \frac{W \cdot x_2}{x_1 + x_2} \quad (\text{B.27})$$

This formula takes into account the position of the load and the total weight. It distributes the load between the wheels based on their distances from the load. The closer the front wheel is to the load (smaller  $x_2$  compared to  $x_1$ ), the larger the reaction force  $R_1$  it experiences.

Similarly, the reaction force at the rear wheel ( $R_2$ ) can be calculated using the formula:

$$R_2 = \frac{W \cdot x_1}{x_1 + x_2} \quad (\text{B.28})$$

This formula follows the same logic as the previous one but considers the position of the load in relation to the rear wheel.

It is important to note here that these formulas assume ideal conditions, such as a level surface, identical and equally capable wheels, and the absence of other external forces or factors affecting load distribution. In real-world scenarios, however, various factors, such as uneven terrain, wheel characteristics, and dynamic loads, may require additional consideration to obtain a more accurate analysis.

By employing the principles of static equilibrium and utilizing these formulas, engineers and designers can gain insights into load distribution on cart wheels based on the position of the load. This knowledge is crucial to ensure stability, optimize performance, and maintain safety in cart design and operation.

In conclusion, load distribution on cart wheels is a notable aspect to consider in cart design. To understand the principles of static equilibrium and employ appropriate formulas, we determined the load distribution between the wheels based on the position of the load. This information enables us to design a cart which is stable, efficient, and capable of safely carrying its intended loads.

## B.7 Friction simulation

This chapter provides an in-depth understanding of friction and its role in the functioning and efficiency of industrial carts. We discuss the different types of friction forces that come into play in industrial carts. These may include static friction (when the cart is at rest), kinetic or dynamic friction (when the cart is in motion), rolling friction, and sliding friction. In addition, we explain how friction affects the motion of industrial carts. The process of how static friction needs to be overcome to set the cart in motion, and how kinetic friction influences the speed and acceleration of the cart is also addressed in this subsection. The following formulas are used to calculate friction B.29 and B.30 and the corresponding coefficients for static and kinetic frictions are depicted in tables B.1 and B.2. These coefficients can be selected to adjust to the environmental parameters of the simulation model.

For static friction:

$$F_{\text{static}} = \mu_{\text{static}} \cdot N \quad (\text{B.29})$$

For kinetic friction:

$$F_{\text{kinetic}} = \mu_{\text{kinetic}} \cdot N \quad (\text{B.30})$$

Table B.1: Coefficients of Friction for Material Handling Surfaces

Surface Combination	Dry Condition	Wet/Oily Condition
Steel on Steel	0.5 - 0.8	0.15 - 0.3
Steel on Concrete	0.6 - 0.8	0.1 - 0.3
Rubber on Concrete	0.6 - 1.0	0.3 - 0.6
Wood on Wood	0.25 - 0.5	0.1 - 0.2
Plastic on Plastic	0.2 - 0.4	0.1 - 0.2
Rubber on Asphalt	0.7 - 0.9	0.4 - 0.6

Table B.2: Coefficients of Friction for Material Handling Surfaces

Surface Combination	Static Friction	Dynamic Friction	Rolling Friction	Sliding Friction
Steel on Steel	0.8	0.6	0.05	0.6
Steel on Concrete	0.7	0.5	0.04	0.5
Rubber on Concrete	1.0	0.8	0.02	0.8
Wood on Wood	0.5	0.4	0.06	0.4
Plastic on Plastic	0.4	0.3	0.08	0.3
Rubber on Asphalt	0.9	0.7	0.03	0.7

## B.8 Kinematics

Let's assume that the cart moves in a 2D plane ( $x, y$ ) and is controlled by the angular velocity of its two powered wheels. We can define the following variables:

$x$  and  $y$ : the position of the cart in the plane  
 $\theta$ : the orientation of the cart with respect to the  $x$ -axis  
 $v_l$  and  $v_r$ : the linear velocities of the left and right powered wheels, respectively  
 $R$ : the distance between the two powered wheels

The kinematic equations that describe the motion of the cart are:

$$v_c = (v_l + v_r)/2 \quad (\text{B.31})$$

( $v_c$  - the average linear velocity of the two powered wheels)

$$\omega_c = (v_r - v_l)/R \quad (\text{B.32})$$

( $\omega_c$  - the angular velocity of the cart)

$$\dot{x} = v_c \cdot \cos(\theta) \quad (\text{B.33})$$

$$\dot{y} = v_c \cdot \sin(\theta) \quad (\text{B.34})$$

$$\dot{\theta} = \omega_c \quad (\text{B.35})$$

Using these formulas we obtained the linear speed of the cart and its angular velocity, as well as its position and orientation in the 2D plane.

## B.9 Dynamics

To describe the dynamics of the cart, we need to consider the forces acting on it. Let's assume that the cart is subject to the following forces:

$F_l$  and  $F_r$ : the forces exerted by the left and right powered wheels, respectively  
 $F_c$ : the force exerted by the caster wheels

We can then write the following equations of motion for the cart:

$$m \cdot \ddot{x} = F_l \cdot \cos(\theta) + F_r \cdot \cos(\theta) + F_c \cdot \cos(\phi) \quad (\text{B.36})$$

$$m \cdot \ddot{y} = F_l \cdot \sin(\theta) + F_r \cdot \sin(\theta) + F_c \cdot \sin(\phi) \quad (\text{B.37})$$

$$I \cdot \ddot{\theta} = (F_r - F_l) \cdot R \quad (\text{B.38})$$

where  $m$  is the mass of the cart,  $I$  is the moment of inertia of the cart about its center of mass, and  $\phi$  is the angle between the direction of motion and the direction of the force exerted by the caster wheels.

The above equations can be solved numerically to simulate the motion of the cart in time. We should note here that the forces  $F_l$ ,  $F_r$ , and  $F_c$  depend on the control inputs (i.e., the angular velocities of the powered wheels), as well as on the friction coefficients between the wheels and the ground, and on the geometry of the cart.

Let's assume that each of the powered wheels is driven by a DC motor. The dynamics of a DC motor can be described by the following equations:

$$V = R_m \cdot i + L_m \cdot \frac{di}{dt} + V_e \quad (\text{B.39})$$

$$T_m = k_t \cdot i \quad (\text{B.40})$$

where  $V$  is the applied voltage,  $R_m$  is the motor resistance,  $L_m$  is the motor inductance,  $i$  is the motor current,  $di/dt$  is the time derivative of the current,  $V_e$  is the back electromotive force,  $T_m$  is the motor torque, and  $k_t$  is the torque constant.

The back electromotive force can be modeled as:

$$V_e = k_e \cdot \omega \quad (\text{B.41})$$

where  $\omega$  is the angular velocity of the motor and  $k_e$  is the motor's back electromotive force constant.

Assuming that the motor torque is transmitted to the powered wheel through a gear train with gear ratio  $G$ , we can write:

$$T_w = T_m \cdot G \quad (\text{B.42})$$

where  $T_w$  is the torque applied to the powered wheel.

Finally, we can relate the torque applied to the powered wheel to the force exerted on the ground by the wheel through the following equation:

$$T_w = F_w \cdot r_w \quad (\text{B.43})$$

where  $F_w$  is the force exerted on the ground by the wheel, and  $r_w$  is the radius of the wheel.

Putting it all together, we can write the equations that describe the dynamics of the powered wheels as:

$$V_l = R_m \cdot i_l + L_m \cdot \frac{di_l}{dt} + k_e \cdot \omega_l \quad (\text{B.44})$$

$$V_r = R_m \cdot i_r + L_m \cdot \frac{di_r}{dt} + k_e \cdot \omega_r \quad (\text{B.45})$$

$$T_l = k_t \cdot i_l \quad (\text{B.46})$$

$$T_r = k_t \cdot i_r \quad (\text{B.47})$$

$$T_{lw} = T_l \cdot G \quad (\text{B.48})$$

$$T_{rw} = T_r \cdot G \quad (\text{B.49})$$

$$F_{lw} = \frac{T_{lw}}{r_w} \quad (\text{B.50})$$

$$F_{rw} = \frac{T_{rw}}{r_w} \quad (\text{B.51})$$

where  $V_l$  and  $V_r$  are the voltages applied to the left and right motors, respectively,  $i_l$  and  $i_r$  are the currents through the left and right motors,  $\omega_l$  and  $\omega_r$  are the angular velocities of the left and right motors,  $T_{lw}$  and  $T_{rw}$  are the torques applied to the left and right powered wheels,  $F_{lw}$  and  $F_{rw}$  are the forces exerted on the ground by the left and right powered wheels, and  $r_w$  is the radius of the powered wheels.



## List of variables

### Caster wheel

$x$	Horizontal position of the caster wheel in the 2D plane
$y$	Vertical position of the caster wheel in the 2D plane
$\theta_c$	Orientation or angular position of the caster wheel
$v_c$	Linear velocity of the caster wheel
$w_c$	Angular velocity or rotational speed of the caster wheel
$\frac{dw_c}{dt}$	Rate of change of angular velocity with respect to time
$k$	Proportional constant affecting the self-aligning torque
$d$	Damping coefficient affecting the angular velocity

### Numerical methods

$y$	Dependent variable
$h$	Step size or time increment
$f(t, y)$	Function representing the rate of change of $y$ with respect to $t$
$t$	Independent variable or time
$k1$	First intermediate variable in the 4th order Runge-Kutta method
$k2$	Second intermediate variable in the 4th order Runge-Kutta method
$k3$	Third intermediate variable in the 4th order Runge-Kutta method
$k4$	Fourth intermediate variable in the 4th order Runge-Kutta method

### DC motor model

$V$	Applied voltage across the DC motor terminals
$L$	Inductance of the motor winding
$\frac{dI}{dt}$	Rate of change of armature current with respect to time
$R$	Resistance of the motor winding
$I$	Armature current (current flowing through the motor winding)
$K$	Motor constant related to back electromotive force (back EMF)
$\omega$	Angular velocity of the motor shaft
$\tau$	Torque generated by the motor
$J$	Moment of inertia of the motor's rotor
$\frac{d\omega}{dt}$	Rate of change of angular velocity with respect to time
$B$	Viscous damping coefficient in the mechanical system
$T$	Sampling or time step for discretisation

### Powered wheel chapter

$T_w$	Torque exerted by the wheel
$n$	Gear ratio
$T_m$	Torque generated by the motor
$F_w$	Force exerted by the wheel on the ground
$r$	Radius of the wheel

$F_n$	Net force accounting for external load
$F$	Load force opposing wheel movement
$\omega_w$	Angular velocity of the wheel
$\omega_m$	Angular velocity of the motor
$v$	Linear velocity of the wheel

### Wheel suspension

$F$	Spring force in the suspension system
$k$	Suspension spring constant
$x$	Displacement of the wheel from its equilibrium position
$F_{\text{net}}$	Net force acting on the wheel-suspension system
$m$	Mass of the vehicle wheel
$a$	Acceleration of the wheel in the suspension system

### Friction simulation

$F_{\text{static}}$	Static frictional force
$\mu_{\text{static}}$	Coefficient of static friction
$N$	Normal force exerted on the object
$F_{\text{kinetic}}$	Kinetic (or sliding) frictional force
$\mu_{\text{kinetic}}$	Coefficient of kinetic friction

### Cart kinematics

$v_c$	Average linear velocity of the two powered wheels
$v_l$	Linear velocity of the left powered wheel
$v_r$	Linear velocity of the right powered wheel
$\omega_c$	Angular velocity of the cart
$R$	Radius from the center of the cart to a powered wheel
$\dot{x}$	Cart velocity in the direction of x axis
$\dot{y}$	Cart velocity in the direction of y axis
$\dot{\theta}$	Rate of change of the orientation of the cart (Angular velocity of the cart)
$\theta$	Orientation or angular position of the cart

### Cart dynamics

$m$	Mass of the cart
$\ddot{x}$	Acceleration of the cart in the horizontal direction
$\ddot{y}$	Acceleration of the cart in the vertical direction
$\ddot{\theta}$	Angular acceleration of the cart
$I$	Moment of inertia of the cart
$R$	Radius from the center of the cart to a powered wheel
$F_l$	Force applied to the cart from the left wheel
$F_r$	Force applied to the cart from the right wheel

$F_c$	Force applied to the cart from the caster wheel
$\theta$	Angle representing the orientation of the cart
$\phi$	Angle representing the orientation of the caster wheel
$V$	Voltage applied to the DC motor
$R_m$	Motor resistance
$i$	Current flowing through the motor
$L_m$	Motor inductance
$\frac{di}{dt}$	Rate of change of current
$V_e$	Back electromotive force (EMF)
$T_m$	Motor torque
$k_t$	Motor torque constant
$k_e$	Motor back EMF constant
$\omega$	Angular velocity of the motor
$G$	Gear ratio
$T_w$	Torque applied to the powered wheel
$F_w$	Force exerted on the ground by the wheel
$r_w$	Radius of the wheel
$V_l$	Voltage applied to the left wheel motor
$V_r$	Voltage applied to the right wheel motor
$i_l$	Current flowing through the left wheel motor
$i_r$	Current flowing through the right wheel motor
$\omega_l$	Angular velocity of the left wheel
$\omega_r$	Angular velocity of the right wheel
$T_l$	Torque generated by the left wheel motor
$T_r$	Torque generated by the right wheel motor
$T_{lw}$	Torque applied to the left powered wheel
$T_{rw}$	Torque applied to the right powered wheel
$F_{lw}$	Force exerted on the ground by the left powered wheel
$F_{rw}$	Force exerted on the ground by the right powered wheel